IMPACTORS FOR AEROSOL MEASUREMENTS: DEVELOPMENTS AND SAMPLING BIASES

Thesis by

Pratim Biswas

In Partial Fulfillment of the Requirements

for the degree of

Doctor of Philosophy

California Institute of Technology

Pasadena, California

1985

(submitted October 29, 1984)

ACKNOWLEDGEMENTS

I would like to thank my advisor, Dr. Richard C. Flagan, for his encouragement, support, and guidance throughout this work. His timely suggestions and innumerable ideas were extremely helpful. I would also like to thank the other members of my Committee: Drs. John Seinfeld, Glen Cass, C.E. Brennen, and R.H. Sabersky.

Financial support was primarily provided by the Environmental Protection Agency, under grant EPA-R-809010101.

No experimental work at Keck Laboratories has probably been done without the assistance of Elton and his band of men. Mine is no exception. I thank : Elton Daly, Joe Fontana, Rich Eastvedt, and Leonard Montengro. The invaluable help of Rayma Harrison and Gunilla Hastrup in retrieving obscure references is appreciated. The assistance of Melinda Hendrix-Werts, Elaine Granger, Joan Mathews, and Sandy Brooks is gratefully acknowledged. Thanks are also due to Theresa Fall and Nancy Tomer for their help in drafting.

I have benefited in numerable ways by my association with fellow graduate students. Connie Senior and M.K. Alam had useful suggestions and their experience to guide me. Carol Jones was a great help in the laboratory. Whenever I had any computer related problems (software or hardware), Dale Warren was the expert who always had an

Acknowledgements (contd.)

answer. Jin Jwang Wu, with her digitized giggles and laughter, often provided 'inbetween experiments' entertainment. Dennis Lyn has been a great office mate. Residing in the basement of Keck Labs has been an excellent experience and lot of fun. Thanks to : Imad Hannoun, Liyuan Liang, Ellen Johnson, Andy Hong, Diane Austin, Jim Viking Skjelbreia, Sue Larson, Peter Goodwin, Ted Russell, Jeff Zee, Costas Synolakis, Daniel Jacob, Jed Waldman, Brian Wong, Yiannis, Kit Yin, Panos, and all others.

Education is a process that has no end. However, the earning of the 'Doctorate degree' marks an end to the process of 'formal education'. I dedicate this thesis to my father, Dr. A.B. Biswas; my mother, Mrs. Anjali Biswas; and my brother, Dr. Gautam Biswas; who by their encouragement and love, have guided me through it all.

ABSTRACT

This work is subdivided into four parts. The first part consists of characterizing high jet velocity impactors, developing their scaling criteria to facilitate instrument design and prediction of impactor performance under conditions where no calibration data are available.

The second part discusses the problem of distortion of size distributions by aerosol sampling instruments because of particle size changes occurring due to vapor or condensable phase transport to and from the particles. The severity of the problem is demonstrated both theoretically and experimentally for a few commonly used aerosol sampling instruments.

The third part is the development of a 'Particle Trap Impactor' working on the virtual impaction principle. The inherent problems of bounce and re-entrainment in conventional impactors is minimized, without the addition of substrates such as grease, in these impactors. The result of operating the unit at high temperature is also discussed.

The final part is the calculation of the scavenging rate of particles due to differential impaction. The results are used to determine upperbounds on the number concentration of particles entering the impactor to minimize biasing the measurements.

TABLE OF CONTENTS

Table of Contents (Continued)

LIST OF TABLES

LIST OF FIGURES

CHAPTER 1

INTRODUCTION

1.1 Motivation

Combustion sources and many other high temperature industrial processes generate large quantities of submicron particles. These particles provide a large surface for condensation of vapors (1,2). Hence, they can be enriched with volatile and toxic species. Although they are only a few percent of the particle mass generated in coal combustion, they may account for as much as one-fifth of the aerosol emitted to the atmosphere (3). These particles are more difficult to remove than the larger ones. It is, therefore, very important to know the size distribution of the aerosol generated by these processes to enable design of effective particulate control devices.

The cascade impactor is an instrument that has the ability to sample and collect particles with size segregation. They consist of a series of stages, each having a converging nozzle through which an aerosol flows normal to a collecting surface. Particles too large to follow the gas streamlines deposit on the collecting surface. Smaller particles proceed to the lower stages with decreasing nozzle diameters (increasing gas velocities) and are progressively collected with higher efficiencies.

Conventional cascade impactors (operating in the incompressible flow limit and at ambient conditions) have been used to obtain reliable aerosol size distributions. They have been well characterized (4), and can measure size

distribution of particles down to 0.3 micron in diameter. A few other impactors, using high velocity jets, have been developed to classify particles down to 0.05 micron in diameter. Very few calibration data are, however, available for such instruments. An understanding of the scaling laws is necessary if such impactors are to be reliably used at conditions other than those for which calibration data are available.

Antibounce coatings (such as grease) cannot be used for high temperature measurements, thus reducing the reliability of data obtained from impactors used under such conditions. Inherent problems of bounce and re-entrainment, and the need to use impactors at high temperatures, led to the development of the virtual impactor (5). However, plumbing and flow control complications make such multistage impactors impractical.

1.2 Objective

This work aims at developing instruments which can classify particles down to a few-hundredths of a micron, and can also be used to obtain size distribution data at high temperatures. The presentation of this work is outlined briefly.

Chapter 2 aims at developing the necessary scaling and design criteria for high velocity inertial impactors which can classify submicron aerosols. Chapter 3 describes

problems in the use of aerosol size measurement devices due to vapor (or volatile constituent) transport to and from the particles leading to size changes within the instruments.

The development of a particle trap virtual impactor is described in Chapter 4. The results of testing the device under ambient conditions and its advantages over conventional impactors are demonstrated. The use of the 'Particle Trap' impactor at high temperature is outlined in Chapter 5. The problem of coagulation of particles in the impingement region of the impactor by differential impaction is described in Chapter 6. Chapter 7 summarizes the entire work and lists the major conclusions.

References

(1) Flagan, R.C.; Friedlander, S.K.: Fine Particle Formation in Pulverized Coal Combustion, A Review, pp 1-25, Recent Developments in Aerosol Science, D. Shaw, Editor, Wiley, New York (1978).

(2) Neville, M.; Quann, R.; Haynes, B.S.; Sarofim, A.F.: Factors Governing the Surface Enrichment of Fly Ash in Volatile Trace Species. Presented at the ACS/IEC Winter Symposium on Aerosols, Tucson, Arizona (1981).

(3) Ensor, D.S.; Cowen, S.; Hooper, R.; Markowski, G.; Scheck, R.; Farrell, G.D.; Burham, J.: Evaluation of the George Neal No. 3 Electrostatic Precipitator, EPRI Report No. EPRI-FP-1145 (1979).

(4) Marple, V.A.: Fundamental Study of Inertial Impactors, Ph.D. Thesis, Univ. of Minnesota (1970).

(5) Hounam, R.F.; Sherwood, R.J.: Ind. Hyg. J., Mar-Apr, 122-131 (1965).

CHAPTER 2

HIGH VELOCITY INERTIAL IMPACTORS

2.1 Introduction

The efficiency with which particles of diameter d will be collected on a given stage of a cascade impactor is a function of the impaction parameter or Stokes number:

$$\text{St or } \psi = \frac{\rho_p U d^2}{18 \mu D} C \tag{2.1}$$

where ρ_p is the particle density, U is the jet velocity, μ is the dynamic viscosity, D is the width or diameter of the jet and C is the Cunningham slip correction factor, i.e.,

$$C = 1 + \frac{2\lambda}{d} [1.257 + 0.4 \exp(-0.55\, d/\lambda)] \tag{2.2}$$

where λ is the mean free path.

The Reynolds number of the impactor jet, the ratio of the jet-to-plate spacing, S, to the jet width or diameter D, and the impactor geometry also influence the collection efficiency. Within a limited range of jet Reynolds numbers

$$500 \lesssim \text{Re}(= \frac{\rho U D}{\mu}) \lesssim 3000$$

for incompressible jet flows (Mach number $M = U/a < 0.3$), and for length ratios in the range

$$0.5 < S/D < 5 ,$$

the collection efficiency is a function of the impaction parameter alone (1-3), i.e.,

$$\eta = \eta(\psi) . \tag{2.3}$$

Impactors which satisfy these criteria and operate at atmospheric pressure are generally capable of classifying particles larger than a few tenths of a micron in diameter.

Smaller particles can be classified if impactor stages are operated at reduced pressures so the particles begin to slip relative to the gas. If the jet Mach number is below about 0.3, the particle drag coefficient is constant throughout the impaction region, and the scaling criteria described above are still valid.

Impactors in which the pressure is reduced by flow through a critical orifice so that the low pressure stages may be operated in the incompressible flow regime have been constructed (4,5). Particle size cuts as small as 0.05 microns have been achieved in these multiple jet impactors. The pumping requirements for such instruments are, however, so large that their use has been limited.

Particles as small as 0.05 micron diameter have been classified in compact instruments having modest pumping requirements but in which jet velocities have been increased to or near the sonic limit. In the instrument developed by Hering, et al. (6,7) the pressure is initially reduced by passing the aerosol through a critical orifice. The pressure is further reduced by the high velocity flow through the low pressure stages. Pilat, et al. (8) reported an instrument in which substantial pressure reduction is achieved without the use of a critical orifice. This pressure drop must be accompanied by compressible flow through the jets of some of the impactor stages. Although the latter instrument has not been fully calibrated, the

size cuts estimated by microscopic analysis of the collected particles are about a factor of two larger than was estimated by using the incompressible flow scaling criteria (8). The former instrument has been calibrated, but only for one inlet pressure and temperature (P = 745 mm Hg. and T = 295 K). Nonetheless, this instrument has been used to obtain size resolved aerosol composition data in land based studies at elevations as high as 2300 m msl (mean sea level) (9) and in aircraft sampling at elevations from 2600 to 3000 m msl (10). The sizes of particles collected on the high velocity stages in these experiments are uncertain due to the reduction in the inlet pressure. Similarly, use of the impactor at higher temperatures or in gases other than air also presents problems in data interpretation.

An understanding of the scaling laws for high velocity impaction is needed if high velocity impactors are to be reliably used at conditions other than those for which calibration data are available. Israel and Rosner (11) have recently defined a generalized impaction parameter which takes into account variations in the particle drag coefficient due to particle Reynolds number effects (non-Stokesian flow) or fluid property variations. A perturbation method calculation of the velocity gradient at the stagnation point was used to incorporate a correction for flow compressibility up to a free stream Mach number of 0.4 into the generalized Stokes number. High pressure drop

impactors may be operated with sonic jet velocities (Mach number, M = 1), well beyond the limits of the perturbation solution. Flagan (12) suggested a somewhat simpler approach which is an approximation to the use of the generalized Stokes number. Noting that particle drag is most important close to the impaction substrate, it was suggested that the impaction parameter be calculated in terms of the jet velocity and gas viscosity and mean free path corresponding to the stagnation conditions. Although few calibration data were available for high velocity impaction stages, the 50 % cutoff Stokes number, St_{50}, appeared to be independent of the jet Mach number when St was computed in terms of the fluid properties at the upstream stagnation conditions.

An experimental study of the aerosol fractionation characteristics of high velocity impactor stages was undertaken in order to elucidate scaling criteria suitable either for the design of new instruments or for the prediction of the performance of existing instruments when they are operated at conditions other than those for which calibration data are available. Since the performance of an impaction stage depends on the pressure at which it is operated and, therefore, on the pressure drops through all of the upstream stages, the relationship between the pressure drop and the flow rate through an impactor stage has also been examined. On the basis of the results of the experimental study, sample calculations have been performed

to examine the following two cases of compressible flow impactor operations:

(i) operation of a conventional impactor at flow rates large enough that compressibility becomes important; and

(ii) operation of a low pressure impactor which incorporates choked (sonic velocity) stages at inlet pressures and temperatures other than those for which calibration data are available.

2.2 Experimental Method

The impactor used in the present study is based upon the design of Marple and co-workers (1,2). Extensive theoretical and experimental investigations of the performance of this impactor in the limit of low jet Mach numbers have been conducted, providing data for comparison with the results of the present high velocity impaction experiments (1-3). A single stage impactor in which the jet-to-plate spacing and jet nozzle diameter can be varied was constructed (see Figure 2.1). A filter downstream of the impaction stage collects those particles which bypass the impaction plate. The entire system is sealed with O-rings to allow operation at elevated or reduced pressures. Pressure taps and feed-through for internal pressure measurements are also provided.

Calibration aerosols were generated by atomizing solutions of sodium fluorescein with a constant liquid feed

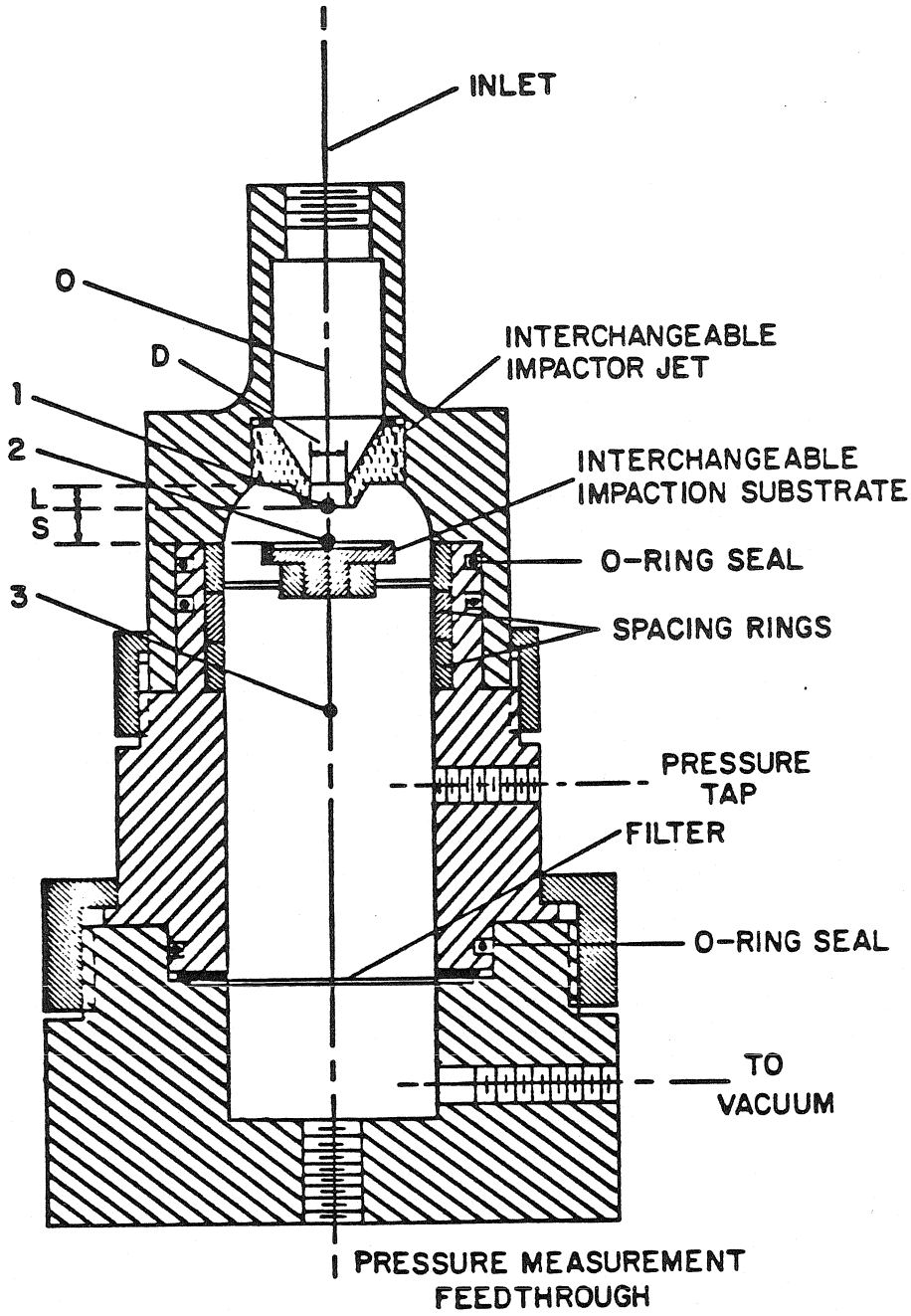

Figure 2.1 Sectional view of the single stage impactor. Numbers indicate reference locations for fluid property evaluation.

rate atomizer (13). The aerosol was neutralized by using a Kr^{85} decharger and then dried in a silica gel diffusion column. The dried aerosol was then classified with a TSI model 3071 electrostatic classifier to produce a monodisperse calibration aerosol. The electrostatic classifier was calibrated by transmission electron microscopy of samples collected with a thermal precipitator. Impaction experiments were conducted with glass cover slips greased with Apiezon-L as impaction substrates. The quantities of sodium fluorescein collected on the impaction substrate and on the glass fiber filter were determined by fluorometric analysis with an Aminco-Bowman spectrophotofluorometer of extracts prepared according to the procedure of Hering, et al. (6,7).

Stagnation pressures upstream and downstream of the impaction stage (points 0 and 3 in Figure 2.1, respectively) were measured. A pressure tap 0.36 mm in diameter at the center of a flat plate the same size as the impaction substrate was used to measure the stagnation pressure on the impaction plate (point 2 in Figure 2.1). The flow rate through various impactor nozzles was measured as a function of pressure ratio and the upstream stagnation pressure in order that the pressure ratio-flow rate relationships could be elucidated.

2.3 Calibration Results

The jet velocity may be estimated by using the isentropic flow relationships and assuming that the pressure at the jet outlet, P_1, is equal to that downstream of the impaction plate, P_3. The jet velocity increases with decreasing pressure ratio, $r = P_3/P_0$, where P_0 is the stagnation pressure upstream of the impaction stage, until the sonic limit is reached at

$$r = r^* = \left(\frac{2}{\gamma+1}\right)^{\frac{\gamma}{\gamma-1}} \qquad (2.4)$$

Further reductions below this critical pressure ratio have no effect on the jet velocity since the flow is choked. The flow in the jet impingement region may, however, continue to change for $r < r^*$. For this reason, we shall characterize the impactor performance in terms of the pressure ratio, r, instead of the jet Mach number. The jet velocity is

$$V = \begin{cases} \sqrt{\frac{2\gamma}{\gamma-1} RT_0 \left(1 - r^{\frac{\gamma-1}{\gamma}}\right)} & : \; r > r^* \\ \sqrt{\frac{2\gamma}{\gamma+1} RT_0} & : \; r \leq r^* \end{cases} \qquad (2.5)$$

where $\gamma = C_p/C_v$ is the ratio of the specific heats for the gas, R is the gas constant, and T_0 is the upstream stagnation temperature.

Flagan (12) reported that the pressure at the center of the impaction plate of a high velocity impactor

with a small jet-to-plate spacing (S/D = 0.5) was very nearly the same as the upstream stagnation pressure for pressure ratios larger than r^* and decreased to about 83 % of the upstream stagnation pressure at r = 0.2. Figure 2.2 shows the ratio P_2/P_0 as a function of r for three values of the jet-to-plate spacing. As the ratio S/D is increased, the decrease in P_2/P_0 with decreasing r for choked flow becomes more pronounced. Hence, the suggestion (12) that the gas properties be evaluated at the upstream stagnation conditions becomes questionable for impactors with large values of S/D.

The flow rate through a converging nozzle is conveniently represented in terms of the dimensionless mass flow rate

$$\tilde{m} = \frac{\dot{m}\sqrt{RT_0}}{A P_0} \tag{2.6}$$

where $\dot{m}$ is the mass flow rate and A is the nozzle throat area. The dimensionless mass flow rates for a number of jet diameters and for a jet-to-plate spacing of S/D = 2.5 are shown in Figure 2.3. The isentropic nozzle flow rate

$$\tilde{m}_s = \begin{cases} r^{1/\gamma}\sqrt{\frac{2\gamma}{\gamma-1}\left(1 - r^{\frac{\gamma-1}{\gamma}}\right)} & : \quad r > r^* \\ \left(\frac{2}{\gamma+1}\right)^{\frac{1}{\gamma-1}}\sqrt{\frac{2\gamma}{\gamma+1}} & : \quad r \leq r^* \end{cases} \tag{2.7}$$

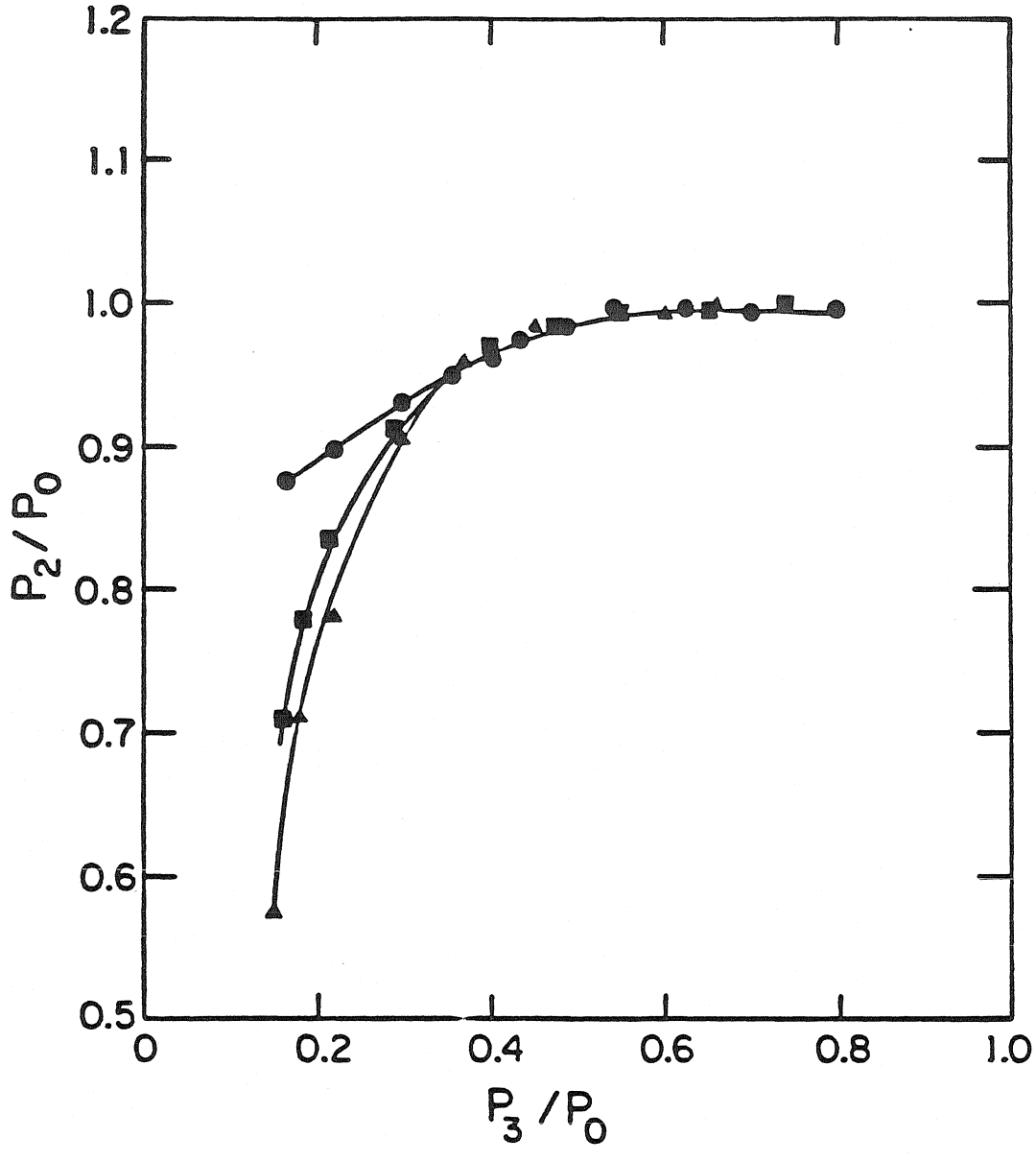

Figure 2.2 Variation of the measured pressure at the center of the impaction plate with overall pressure ratio for various ratios of jet-plate spacing to jet diameter.
● S/D = 0.8, ■ S/D = 1.2, ▲ S/D = 2.5

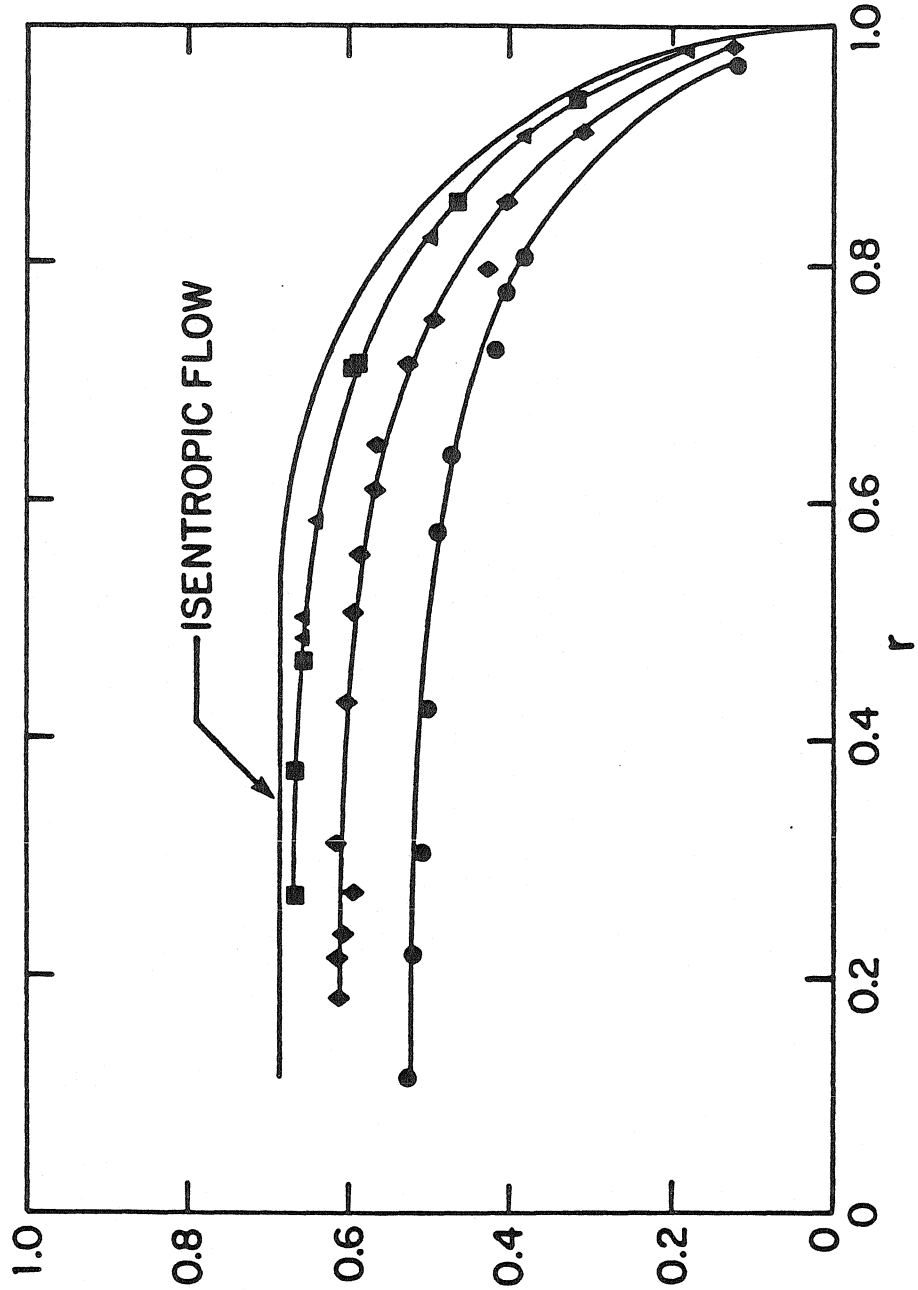

Figure 2.3 Variation of dimensionless mass flow rate through impactor stages with the overall pressure ratio for inlet at atmospheric pressure. ——— Isentropic flow. Impactor stages with S/D = 2.5: ● D=0.457 mm, L=12.95 mm; ◆ D=0.787 mm, L=12.12 mm; ■ D=1.00 mm, L=6.35mm; ▲ D=1.50 mm, L=9.65 mm.

is also shown. At pressure ratios greater than r^*, the flow rate decreases with increasing r. For r less than r^*, the flow is choked so the mass flow rate does not vary. The observed variation in flow rate is similar to that for isentropic flow, but the flow rates are less than the isentropic flow rate and vary from one stage to another.

The nonideal nature of the impactor nozzle flow rate may be taken into account by introducing the discharge coefficient, C_D, which is defined as the ratio of the actual flow rate to the isentropic flow rate through a nozzle of the same area, viz.

$$\tilde{m} = \begin{cases} C_D\, r^{1/\gamma} \sqrt{\frac{2\gamma}{\gamma-1}\left(1 - r^{\frac{\gamma-1}{\gamma}}\right)} & : \quad r > r^* \\ C_D \left(\frac{2}{\gamma+1}\right)^{\frac{1}{\gamma-1}} \sqrt{\frac{2\gamma}{\gamma+1}} & : \quad r \leq r^* \end{cases} \qquad (2.8)$$

The discharge coefficient depends on the inlet and outlet geometries of the nozzles and on the pressure drop in the nozzle throat. For a given impactor design with fixed S/D, the geometries of the inlets and outlets of the various stages are similar, but the jet Reynolds number, $Re = \rho_1 U_1 D/\mu_1$, and aspect ratio, L/D, vary. The major source of the variation of the discharge coefficient is, therefore, expected to be viscous dissipation in the nozzle throat. For a developing laminar flow in a tube, the pressure drop

depends on the parameter ReD/L. The discharge coefficients for pressure ratios ranging from 0.2 to 0.97 are plotted as a function of ReD/L in Figure 2.4. The Reynolds number was evaluated in terms of the fluid properties at the jet outlet (point 1 in Figure 2.1). These data are well correlated by the relationship

$$C_D = \begin{cases} 0.310(ReD/L)^{0.159} & : \quad 35 < ReD/L < 1000 \\ 0.930 & : \quad ReD/L > 1000 \end{cases} \tag{2.9}$$

which is indicated by the solid line. Data for S/D = 2.5 are indicated by solid points. Also shown as open points are results for S/D = 0.5. It is apparent that the discharge coefficient is not strongly influenced by the jet-to-plate spacing over this range.

A number of impactor calibration tests were conducted with a spacing ratio of S/D = 2.5, the inlet air at atmospheric pressure, and pressure ratios ranging from r = 0.95 to r = 0.2. The impaction parameter for these tests was evaluated in terms of P_2 (measured in the aforementioned experiments) and $T_2 = T_0$, i.e.,

$$St \text{ or } \quad \psi = \frac{\rho_p U_1 d^2}{18 \mu_2 D} C\left(\frac{2\lambda_2}{d}\right) . \tag{2.10}$$

The measured collection efficiencies are plotted vs. $(St)^{1/2}$ in Figure 2.5. These results indicate that the value of the Stokes number corresponding to 50 % collection efficiency, St_{50}, does not vary significantly with the pressure ratio,

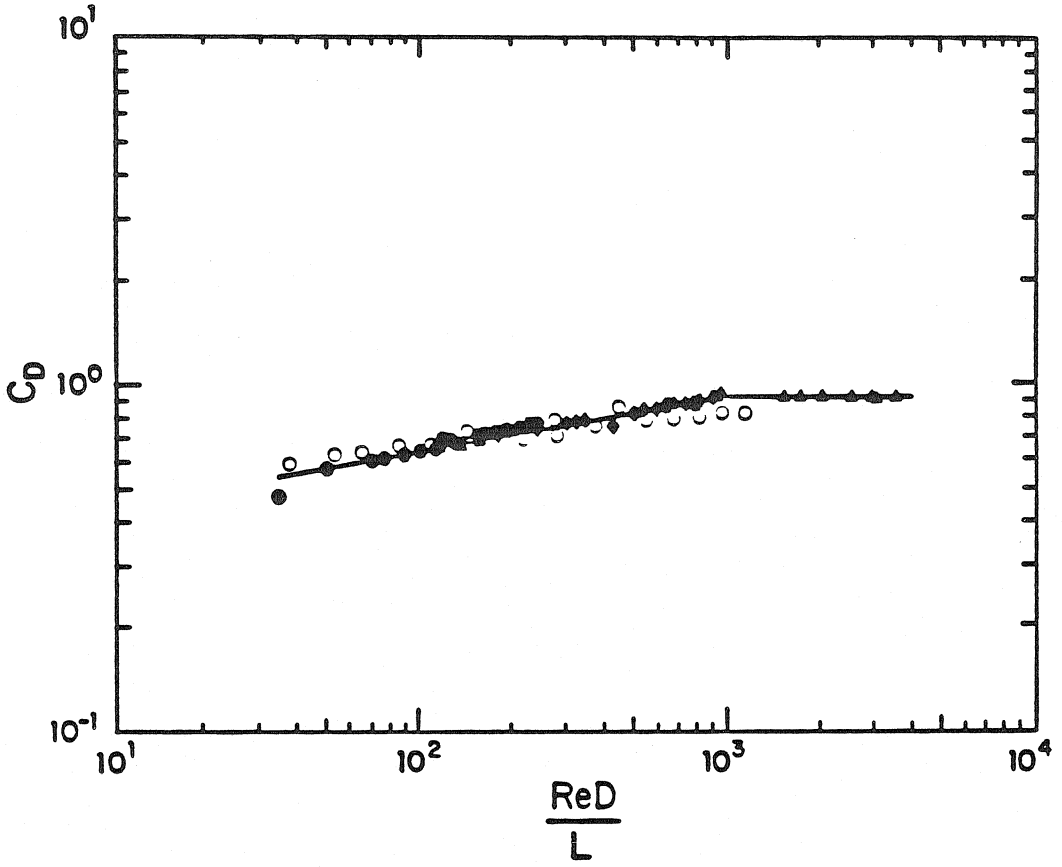

Figure 2.4 Discharge coefficients for impactor stages with impaction plates installed at S/D = 2.5 and S/D = 0.5 Impactor stages with S/D = 2.5: ● D = 0.457 mm, L= 12.95 mm; ◆ D = 0.787 mm, L = 12.12 mm; ■ D = 1.0 mm, L = 6.35 mm; ▲ D = 1.50 mm, L = 9.65 mm.

——— Correlation (Eq. 9)

o Impactor stages with S/D = 0.5

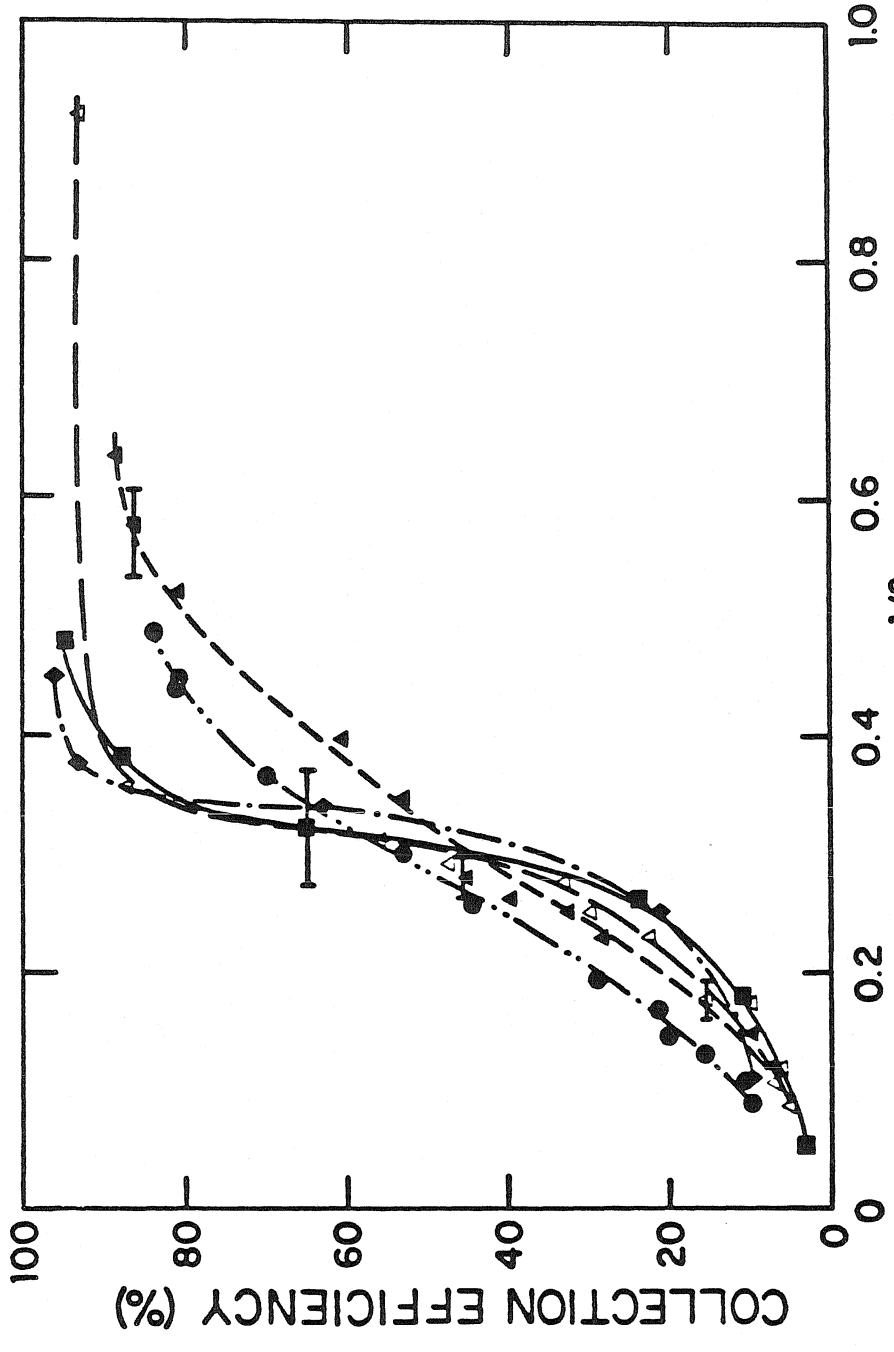

Figure 2.5 Impactor calibration data at inlet atmospheric pressure for various pressure ratios: Δ r = 0.95; ◆ r = 0.70; ■ r = 0.50; ● r = 0.34; ▲ r = 0.19. Curves are approximate fits to data to aid in visualizing the collection efficiency curves. The impaction parameter is evaluated in terms of fluid properties at T_0 and P_2.

r. The shape of the collection efficiency curve is also invariant for pressure ratios larger than 0.5. As the pressure ratio is reduced below the sonic limit, the size cuts become somewhat less sharp than observed for subsonic flows. The increased uncertainty (indicated as one standard deviation by error bars) at large Stokes numbers is due primarily to the limited ability of the electrostatic classifier to classify particles larger than about 0.1 micron.

At high jet velocities, the pressure and temperature variation in the jet impingement region influences the particle drag coefficient through the gas viscosity and the slip correction factor, C (which is a function of the mean free path). A series of experiments were conducted to determine whether, at a fixed pressure ratio of 0.5, the shape of the collection efficiency curve is influenced by the particle Knudsen number. The results presented in Figure 2.6 indicate that the shape of the collection efficiency curve does not change with particle Knudsen number (evaluated for the particle size which is collected with 50 % efficiency). The reduction of St_{50} at Kn_{50} = 0.62 may be due to the large jet Reynolds number of that experiment.

The impaction parameter for 50 % collection efficiency is plotted as a function of the overall pressure ratio, r, in Figure 2.7. The value of St_{50} obtained by Rao and Whitby (3) is also shown. The solid points correspond

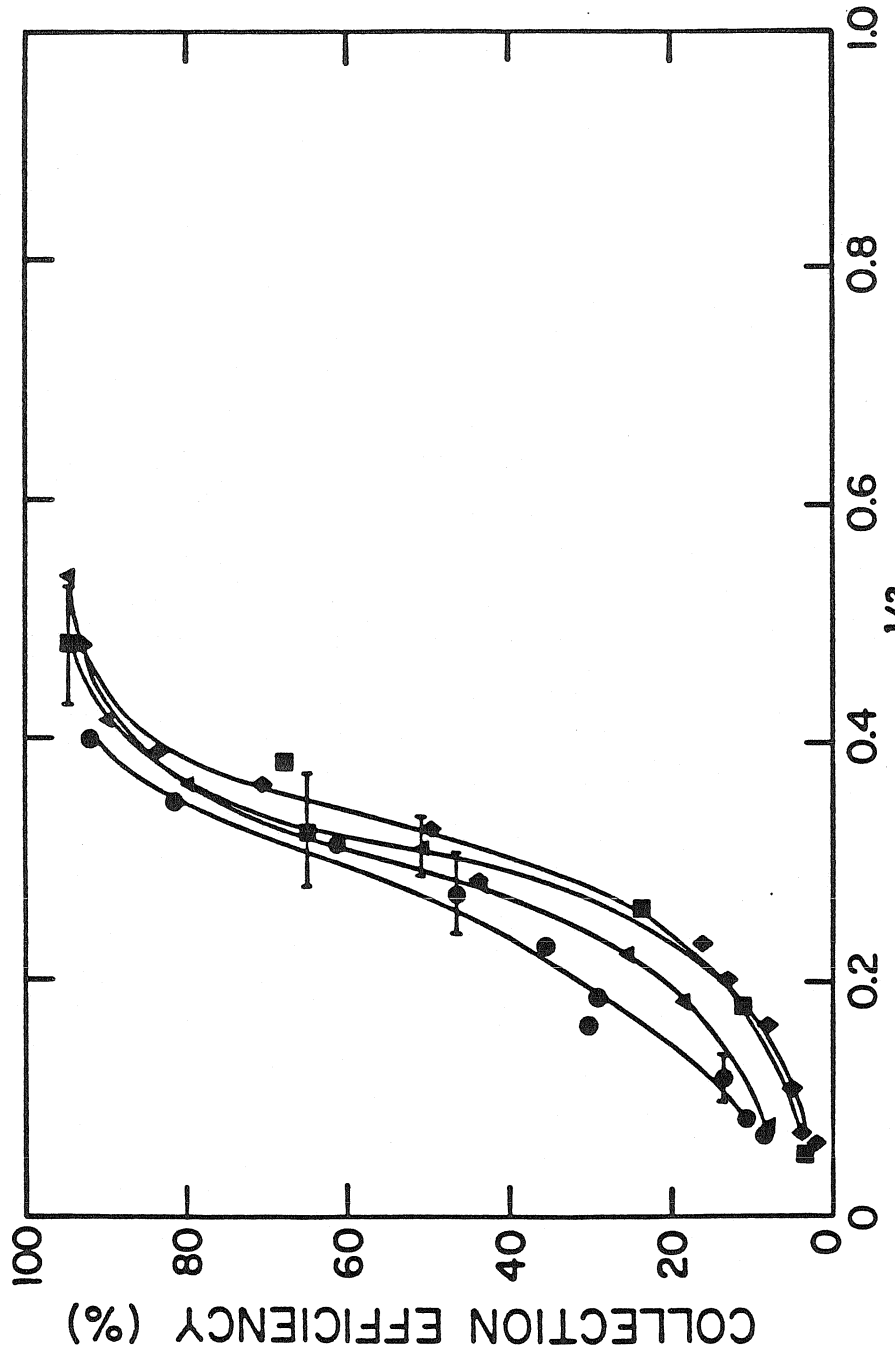

Figure 2.6 Impactor collection efficiency curves for r = 0.5, and of:
● Kn_{50} = 0.62, Re_1 = 20500; ■ Kn_{50} = 1.33, Re_1 = 5050;
◆ Kn_{50} = 1.36, Re_1 = 3930; ▲ Kn_{50} = 2.43, Re_1 = 5050.

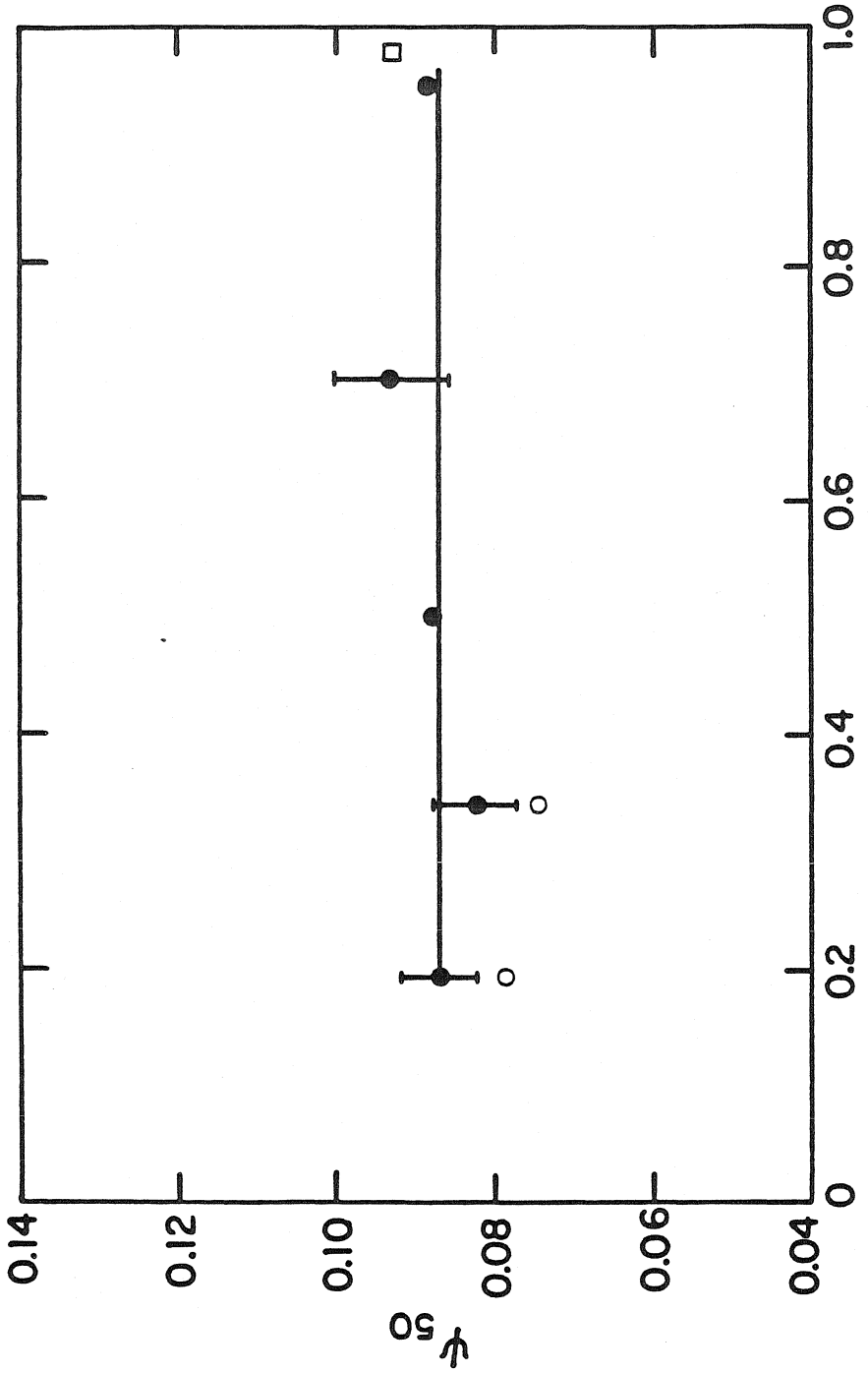

Figure 2.7 Variation of the 50 % cutoff impaction parameter with overall pressure ratio, r.

- ● Fluid properties at T_0 and P_2;
- ○ Fluid properties at T_0 and P_0;
- □ Measurement of Rao and Whitby (3)

to the Stokes number evaluated in terms of the measured stagnation point pressure, P_2, while the open points correspond to evaluation in terms of the upstream stagnation pressure, P_0. It is apparent that St_{50} evaluated in terms of P_2 is, within experimental uncertainty, independent of the pressure ratio. The use of the upstream stagnation pressure as previously suggested by Flagan (12), on the other hand, results in a dependence on r for the present jet-to-plate spacing of S/D = 2.5.

2.4 Cascade Impactor Performance

A multistage impactor sampling a gas stream at temperature T and pressure P may be operated entirely in the subsonic flow regime. Alternatively, choked flow through a critical orifice or through one or more impaction stages may be used to faciltate classification of very small particles. In the former case, the flow rate through the impactor may be varied to control impactor performance. In the latter case, the flow rate through the impactor is fixed by the first choked stage or orifice. Control of performance of stages downstream of the last stage which is choked may still be possible through control of the pressure downstream of the impactor. In either case, iterative calculations are required to compute the pressures and size cuts of an impactor which incorporates high velocity stages. The preceding sections have presented the scaling criteria

necessary to predict, on the basis of limited calibration data, the flow rate or pressure drop and the size cut of an impactor stage. In this section we shall briefly consider applications of these results to predict the size cuts for two cases of high velocity impactor operation:

(i) an instrument designed for low velocity use which is operated at flow rates high enough to introduce the effects of compressibility, and

(ii) a low pressure impactor with sonic stages which is operated at pressures or temperatures other than those for which calibration data are available.

Consider first a subsonic impactor in which the flow rate is known. The pressure ratio across each stage and the absolute stagnation pressure, P_2, must be known to compute the jet velocity and the size cut. The dimensionless mass flow rate is related to the pressure ratio through equation 2.8. The discharge coefficient may be evaluated by using a correlation such as equation 2.9. In order to calculate the jet Reynolds number, we need the velocity and viscosity at point 1. The jet velocity is calculated by using equation 2.5. The viscosity is a function of the temperature but is independent of pressure (14). Assuming the nozzle flow is adiabatic, the temperature at the jet outlet, point 1 in Figure 2.1, is related to the upstream stagnation temperature, T_0, by

$$T_1 = T_0 - \frac{U_1^2}{2C_p} \quad . \tag{2.11}$$

The discharge coefficient, pressure ratio, and jet velocity for the subsonic stage may be evaluated iteratively. The pressure downstream of an impaction stage, P_3, becomes the inlet pressure, P_0, for the following stage. Assuming the impactor flows to be adiabatic, the stagnation temperatures for all of the stages will be equal to the inlet temperature. The cutoff diameter, d_{50}, for each stage may be evaluated by an iterative solution of equation 2.10 by using a measured value for St_{50}. Impactor performance is predicted by marching through the successive stages. A computer program, CASCAD.FOR, to carry out the above, is listed in Appendix B.1.

The predicted variation with flow rate of the size cuts of the circular jets of the Sierra Instruments Model 266 impactor, an instrument with a single jet per stage, based on Marple's design, is shown in Figure 2.8. The solid lines indicate the size cuts predicted when compressibility effects are taken into account. The jet Mach numbers for the fifth and sixth stages are also shown. As the flow rate is increased above about 5 lpm (liters per minute), the sixth stage enters the compressible flow regime and its size cut begins to deviate from that estimated for incompressible flow. At the sonic limit for this impactor, the d_{50} is about two-thirds of the value estimated on the basis of incompressible flow.

If $r < r^*$ for any stage, the flow through that

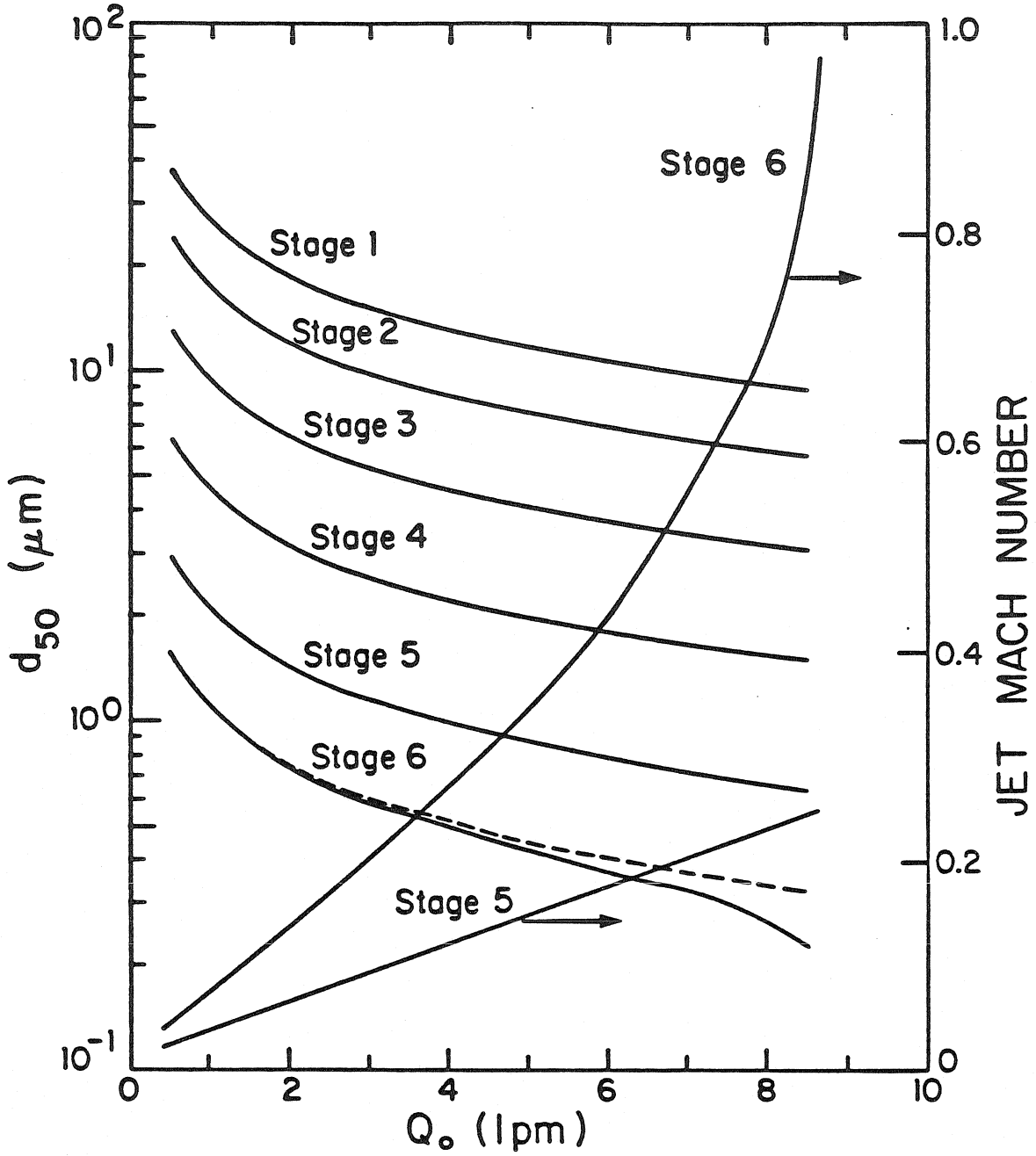

Figure 2.8 Variation of aerodynamic cutoff size with flow rate for stages 1 to 6 of the Sierra Impactor Model 266.

——— compressible flow prediction

-------- incompressible flow prediction

Also shown are jet Mach numbers for stages 5 and 6.

stage is choked. The mass flow rate is then determined by the first stage (or orifice) which is choked according to equation 2.8. The pressure upstream of the choked stage is determined by the pressure drops across the preceding subsonic stages, so an iterative solution is required to calculate the flow rate. A flow rate is first assumed. Following the procedure outlined above for the incompressible flow impactor, the inlet pressure for the choked stage is calculated. If the calculated flow through the choked stage differs from that used for the subsonic stage calculations, a new flow rate must be estimated and the subsonic flow calculations repeated. The pressure downstream of the choked stage then becomes the iteration parameter for any low pressure stages downstream of the choked stage. Under some circumstances two or more stages in series may be choked. The flow rate through each choked stage must be matched to the flow rate through the impactor by iteration. If none of the downstream stages is choked, the impactor outlet pressure becomes a control variable which must be matched by iteration.

This procedure has been used to predict the performance of the low pressure impactor of Hering, et al. (6,7) as a function of inlet air temperature and pressure. This eight stage impactor uses a critical flow orifice with no impaction plate to reduce the pressure for the last four stages. In addition to the orifice, the seventh and eighth

stages are choked at the calibration conditions ($P_{0,1}$ = 745 mm Hg., T_0 = 295 K). The predicted variation of the size cuts with inlet pressure and temperature is shown in Figures 2.9 and 2.10. The size cuts may be expected to vary dramatically if the inlet pressure or temperature differs significantly from the calibration conditions.

2.5 Conclusions

Inertial impactors can be successfully operated with jet Mach numbers substantially greater than the limit for incompressible flow. The cutoff Stokes number, St_{50}, is to a reasonable approximation independent of the impactor stage pressure ratio, provided the impaction parameter is calculated in terms of the fluid properties corresponding to the stagnation point on the impaction plate. The flow through an impactor stage may be modeled as the flow through a nonideal nozzle with a discharge coefficient which is a function of ReD/L.

These results provide a basis for estimating impactor performance at conditions other than those for which calibration data are available and for designing high velocity impactors. The errors on size cuts introduced by operating a conventional impactor in the compressible flow regime were found to approach 30 % as the Mach number approaches unity. The cutoff diameter of a low pressure

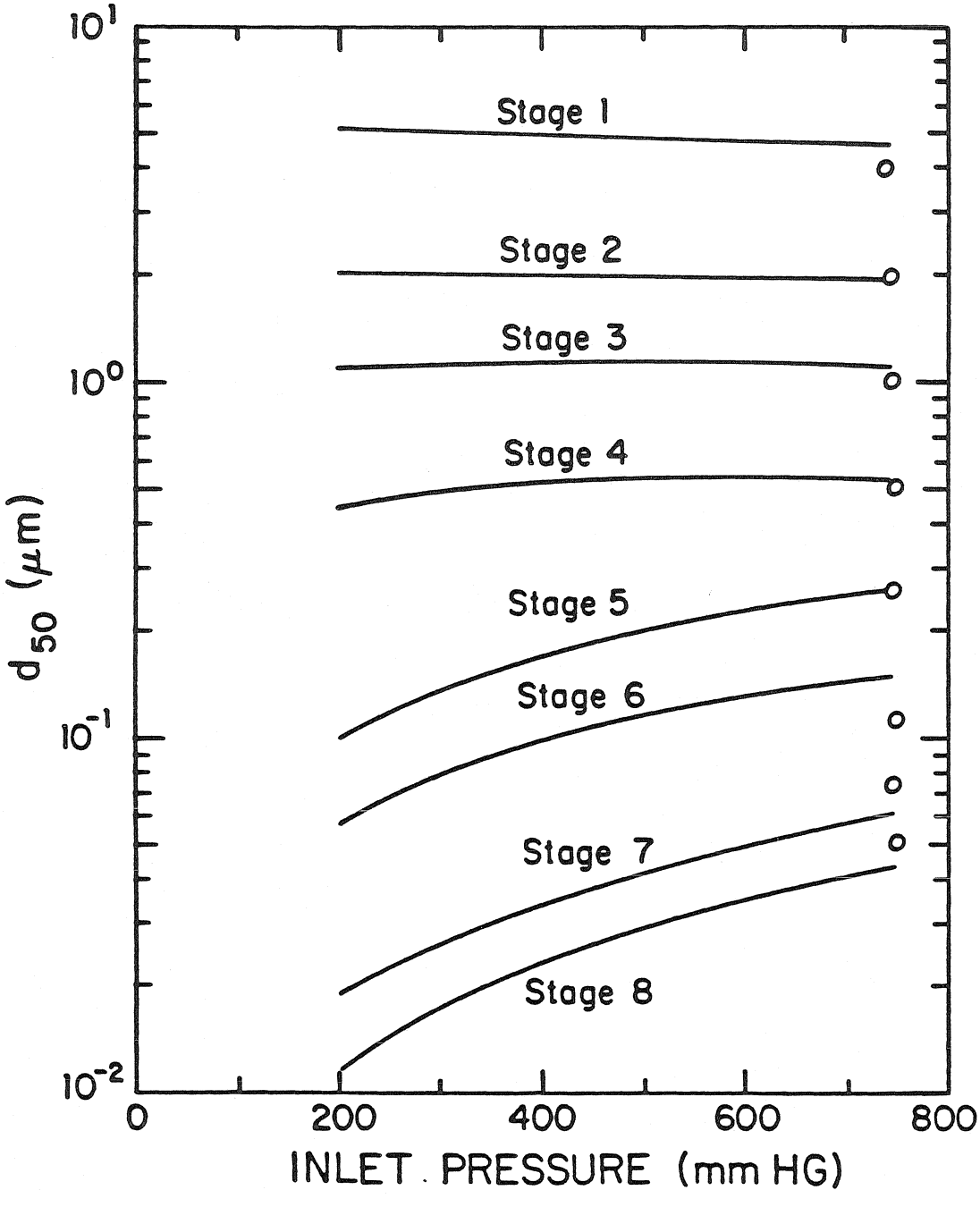

Figure 2.9 Variation of aerodynamic cutoff size with inlet pressure for stage 1 to stage 8 of the low pressure impactor (6,7). O calibration data obtained by Hering, et al. (6,7).

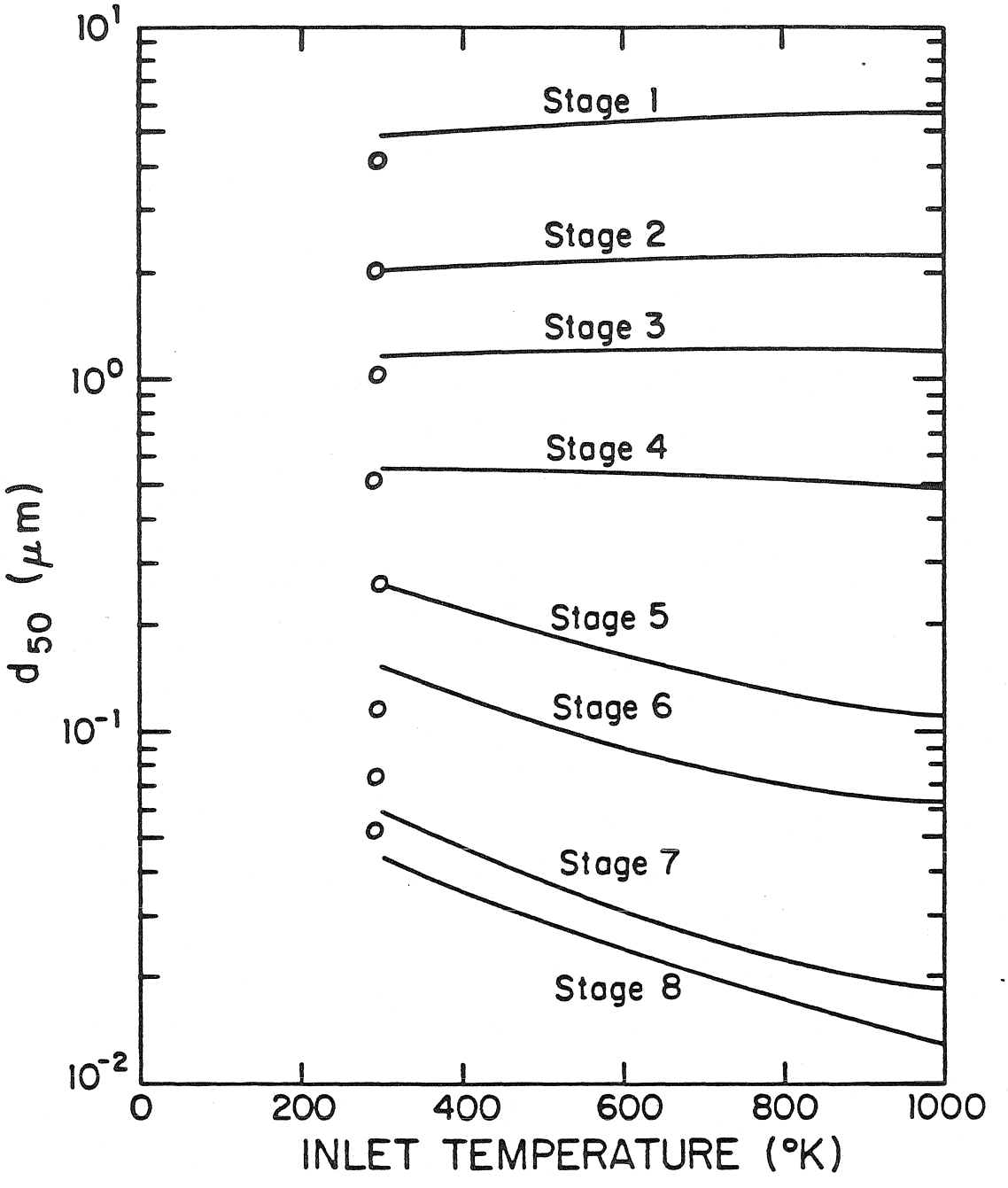

Figure 2.10 Variation of aerodynamic cutoff size with inlet temperature for stage 1 to 8 of the low pressure impactor (6,7).

O calibration data obtained by Hering (6,7).

impactor with sonic stages was found to vary substantially with inlet pressure and temperature. Operation at a 3000 m elevation reduces d_{50} for the low pressure stages by about 50 %. Increasing the impactor operating temperature also reduces the cutoff diameters of the low pressure stages. Gas composition can also be expected to influence the size cuts through changes in the ratio of specific heats, γ, and the viscosity μ.

Although methods for estimating the pressure drops across the impactor stage and the pressure in the jet impingement region have been presented, these pressures should be measured for the particular impactor geometry under consideration, preferably at conditions close to those of ultimate impactor use. These simple and inexpensive measurements can minimize error accumulation in the calculation of pressure drops through successive stages.

High collection efficiencies were achieved for the collection of solid particles when greased substrates were used on impactor stages with sonic jets; i.e., particle bounce is not necessarily a more severe problem at high velocities than at lower velocities.

Nomenclature

a : Speed of sound

A : Area of nozzle throat

C : Cunningham slip correction factor

C_D : Discharge coefficient

C_p : Specific heat at constant pressure

C_v : Specific heat at constant volume

d : Particle diameter

D : Diameter of nozzle (or jet)

L : Length of nozzle throat

$\dot{m}$: Mass flow rate

$\bar{m}$: Dimensionless mass flow rate

M : Mach Number of jet (= U/a)

P : Pressure

Q_0 : Volume flow rate at 1 atmosphere

r : Pressure ratio (downstream of impaction stage to that upstream)

R : Gas constant

Re : Reynolds number

S : Jet-to-plate spacing

St : Stokes number

T : Temperature

U : Velocity of jet

Greek Characters

γ : Ratio of specific heats (= C_p/C_v)

η : Efficiency of particle collection

Nomenclature (Continued)

ρ : Density of particles

μ : Dynamic viscosity

ψ : Stokes number (= St)

Subscripts

0, 1, 2, 3 : Locations in the impactor (see Figure 2.1)

p : Particle

s : Isentropic

Superscript

* : Critical

References

(1) Marple, V.A.; Liu, B.Y.H.: Environ. Sci. Technol., 8, 648-654 (1974).

(2) Marple, V.A.; Liu,B.Y.H.: J. Colloid Interface Sci., 53, 31-34 (1975).

(3) Rao, A.K.; Whitby, K.T.J.: J. Aerosol Sci., 9, 87-100 (1978).

(4) Buchholz, H.: Staub-Reinhalt. Luft, 30, 15 (1970).

(5) McFarland, A.R.; Nye, H.S.; Erickson, C.H.: EPA Report EPA-650/2-74-014 (1973).

(6) Hering, S.V.; Flagan, R.C.; Friedlander, S.K.: Environ. Sci. Technol., 12, 667-673 (1978).

(7) Hering, S.V.; Friedlander, S.K.; Collins, J.J; Richards,L.W.: Environ. Sci. Technol., 13, 184-188 (1979).

(8) Pilat, M.J.; Raemhild, G.A.; Powell, E.P.; Fibretti, G.M.;Meyer, D.F.: Electric Power Research Institute Report EPRI FP-844 (1978).

(9) Macias, E.S.; Zwickey, J.O; Ouimette, J.R.; Hering, S.V.; Friedlander, S.K: Atmos. Environ., 15, 1971-1986 (1981).

(10) Hering, S.V.; Bowen, J.L.; Wengert, J.G.; Richards, L.W.: Atmos. Environ., 15, 1999-2009 (1981).

(11) Israel, R.; Rosner, D.E.: Aerosol Sci. Technol., 2, 45-51 (1983).

(12) Flagan, R.C.: J. Colloid Interface Sci., 87, 291-299 (1982).

(13) Liu, B.Y.H.; Lee, K.W.: Am. Ind. Hyg. Assoc. J., 36, 861-865 (1975).

(14) Bird, R.B.; Stewart, W.E.; Lightfoot, E.N.: Transport Phenomena, Wiley: New York (1960).

CHAPTER 3

DISTORTION OF SIZE DISTRIBUTION BY AEROSOL SAMPLING INSTRUMENTS

3.1 Introduction

Aerosols containing volatile species or condensable vapors may be altered by changes in pressure, temperature, and vapor concentration. When such changes occur within aerosol sampling instruments, the measured size distribution may be distorted significantly. Pressure drops are associated with most flows. In low pressure impactors, the pressure is reduced intentionally to facilitate collection of small particles. The air flows in the instrument may be heated by pumps and electrical dissipation. On the other hand, if the flow is accelerated to high velocity, aerodynamic cooling may result.

Most aerosol instruments are calibrated with dry, non-volatile particles in the absence of any condensable vapors. However, they are routinely used to sample aerosols at non-zero humidity (atmospheric conditions), and in the presence of condensable vapors (combustion exhausts). Extreme conditions approaching or exceeding 100% relative humidity are occasionally encountered, e.g., in sampling fog. Pressure and temperature changes within these instruments may disturb the vapor equilibrium and bias size distribution measurements. Roeber (1) reported that particle adhesion in impactors improved at high jet velocities due to a thin layer of water forming around the particles. Hochrainer and Zebel (2) looked at this problem for the impactor built by Mercer, et al (3). With non-hygroscopic

aerosols, no condensation was observed, unless the inlet aerosol was highly supersaturated. Hygroscopic aerosols showed condensation only if the inlet humidity was above the deliquescent point. The occurrence of condensation was determined qualitatively, by observing whether the particle deposit was wet or dry. The use of polydisperse hygroscopic aerosols made it difficult to determine whether size changes occurred within the impactor. Their calculation (2) for 2 micron particles at saturation conditions in the last stage of the Mercer impactor (3) (corresponding to an inlet humidity of 12.7 %) indicated no significant size increase. However, with impactors sampling at higher inlet relative humidities and/or classifying smaller particles, size changes may be more severe.

This work explores both theoretically and experimentally the distortion of particle size distributions in a number of commonly used instruments:

(i) a low pressure impactor (4)

(ii) a six stage impactor, operated in the incompressible flow regime (5)

(iii) a laser optical particle counter (6)

(iv) a large particle counter (7).

Ammonium sulfate aerosols under humid conditions are taken as a test case for this study. Ammonium sulfate was chosen because activity data are readily available (10,11,12), and it forms a droplet which is chemically

stable, thus making data interpretation easier. Droplet growth within the instrument was predicted for different inlet conditions. Experiments performed corroborate the predictions and uncovered some additional problems in the use of these instruments. Some modifications were also made to eliminate sampling biases.

3.2 Theory

The amount of vapor in a gas is expressed in terms of its partial pressure. If the vapor is water, the more commonly used term is humidity. The relative humidity, RH, is defined as the ratio of the water vapor pressure present to the saturation vapor pressure at the local temperature. A similar definition could be used for vapors other than water. In this paper, relative humidity is used in this broader sense.

If the amount of vapor condensed is negligible relative to the total amount present, the relative humidity, $(RH)_1$, at a temperature, T_1, and pressure, P_1, can be expressed as:

$$(RH)_1 = (RH)_0 \cdot \frac{p_{sat}(T_0)}{p_{sat}(T_1)} \cdot \frac{P_1}{P_0}$$

where, p_{sat} is the saturation vapor pressure, and P the total pressure. Temperature and pressure variation are the two factors that lead to changes in the relative humidity (in the absence of vapor absorbing or desorbing surfaces).

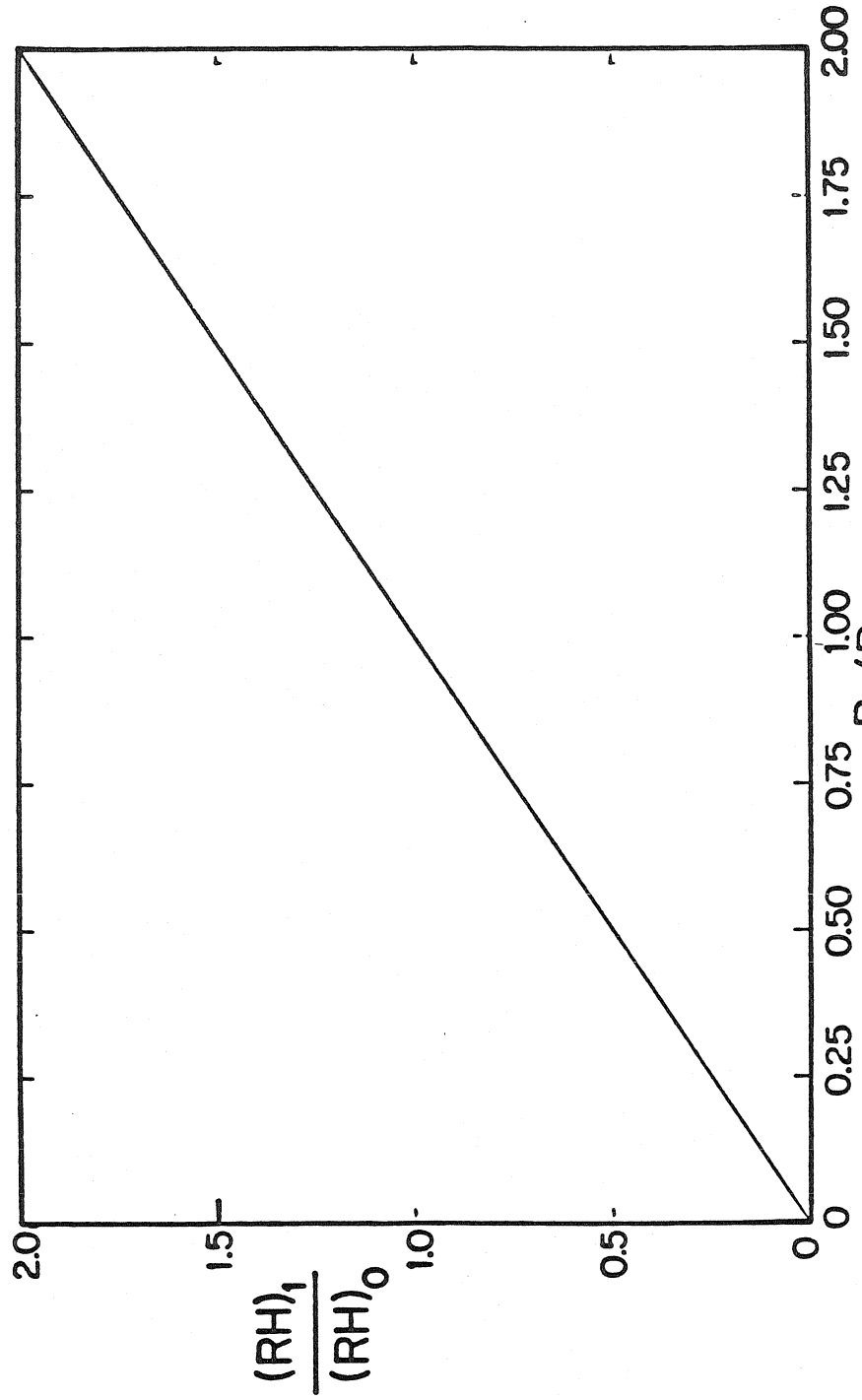

Figure 3.1 (a) Variation of $(RH)_1/(RH)_0$ with pressure ratio (Temperature constant).

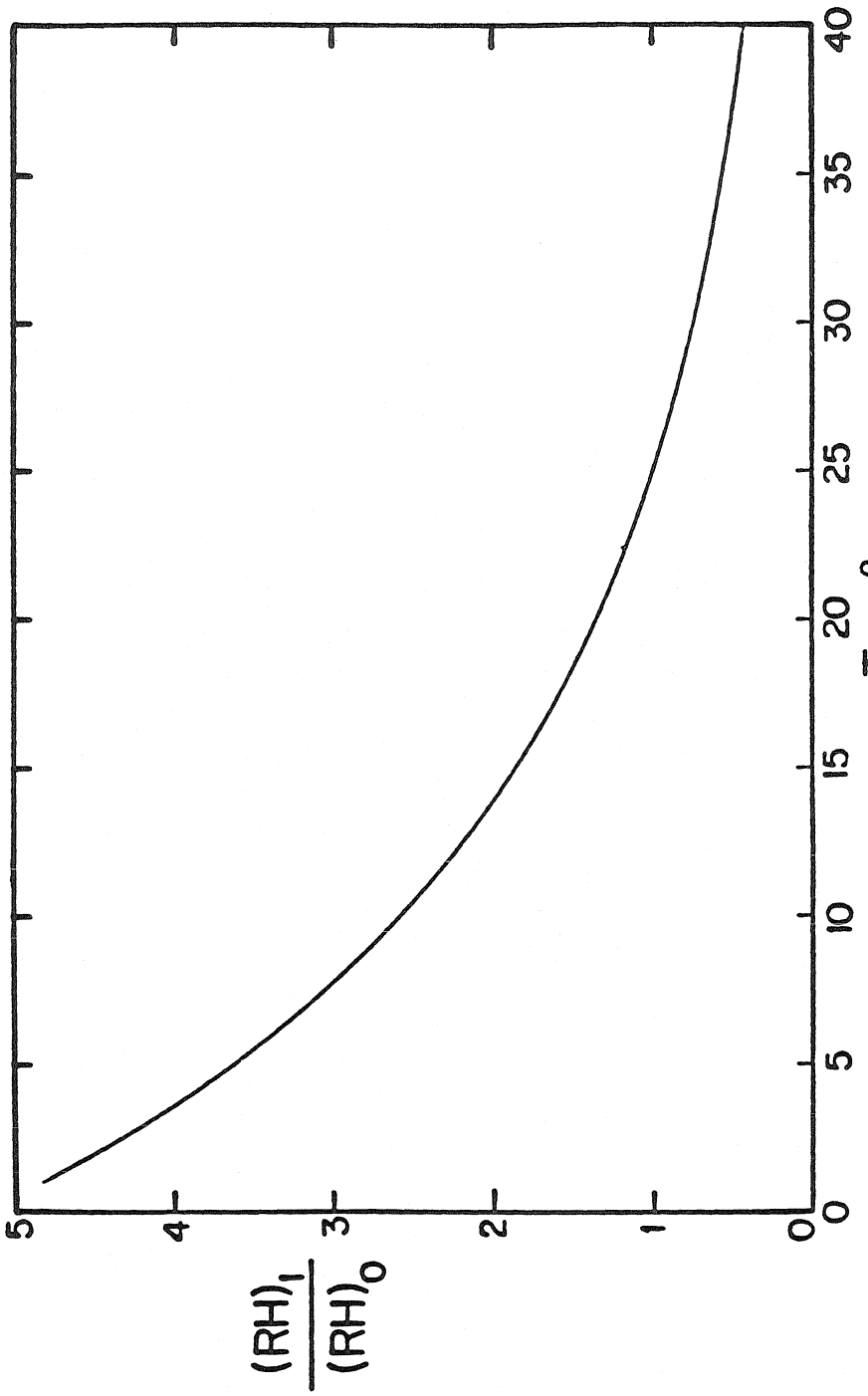

Figure 3.1 (b) Variation of $(RH)_1/(RH)_0$ with temperature for an air-water vapor mixture (at constant pressure).

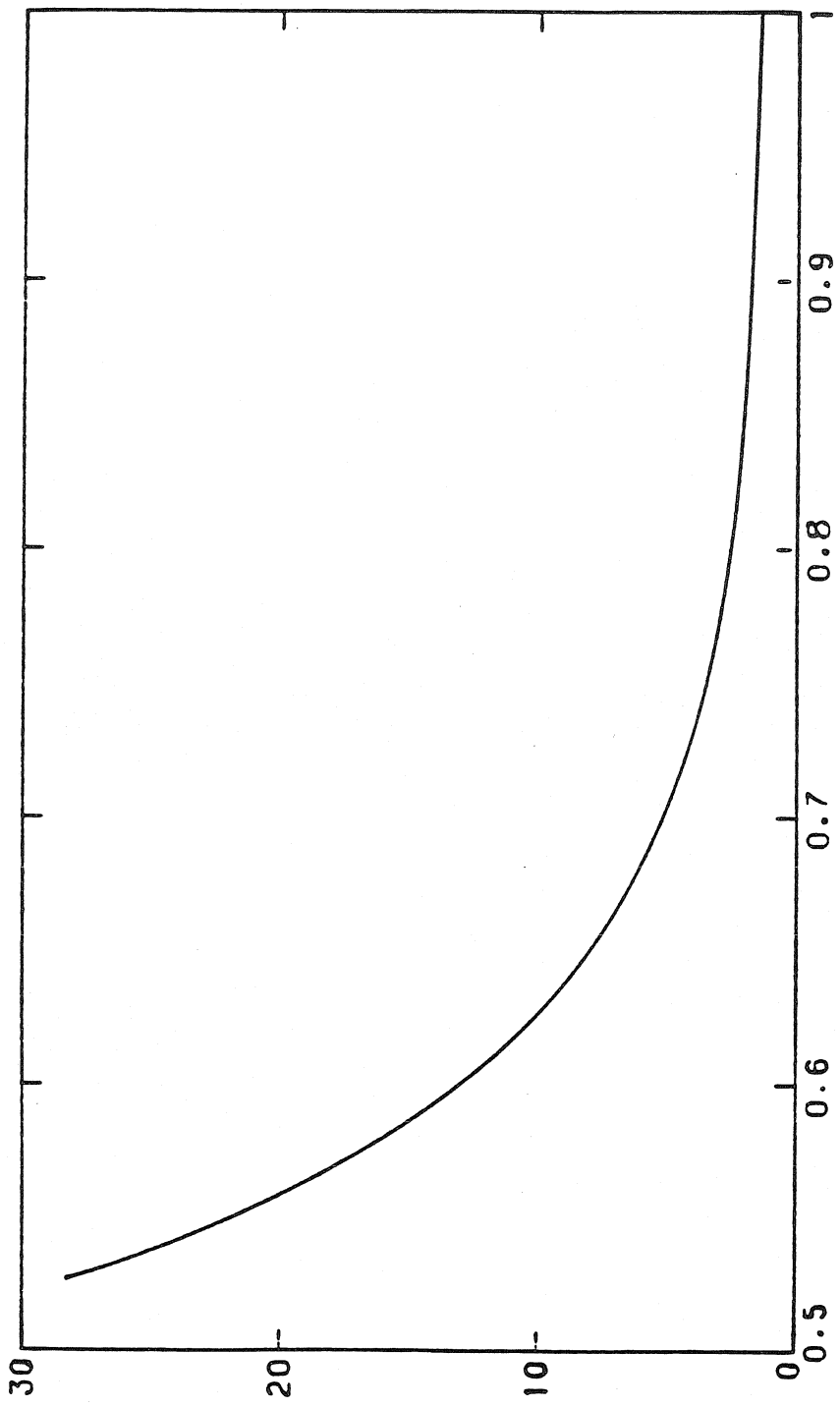

Figure 3.1 (c) Variation of $(KH)_1/(KH)_0$ with adiabatic pressure ratio, r_{ad}, ($r_{ad} = P/P_0$, P_o = 1 atm., T_0 = 298 K) for flow in a converging nozzle.

A drop in total pressure tends to decrease the relative humidity, whereas a drop in temperature leads to an increase in relative humidity since p_{sat} decreases with a decrease in temperature. These two effects are shown in Figures 3.1a and 3.1b for water vapor in air. The value of $(RH)_1/(RH)_0$, when both temperature and pressure vary can be obtained by multiplying the individual ratios obtained from Figures 3.1a and 3.1b. In the case of an adiabatic, isentropic flow, $T \propto P^{\gamma-1/\gamma}$ ($\gamma = C_p/C_v$), leading to an increase in relative humidity with decreasing pressure as shown in Figure 3.1(c).

3.2.2 Particle Growth

Consider a droplet as shown in Figure 3.2. The vapor pressure is p_d at the droplet surface, and p_{vap} far from the droplet. When p_d equals p_{vap}, there is a vapor equilibrium and no net transport of vapor. However, a change in ambient conditions (such as pressure or temperature) would lead to vapor transport until a new vapor equilibrium state is attained. The equation for vapor transport can be written as (8)

$$\frac{dv}{dt} = \frac{2\pi D\, d\, v_m}{kT} \cdot (p_{vap} - p_d) \cdot F(Kn) \qquad (3.1)$$

where,

v : volume of droplet at time t ($= \pi/6\ d^3$)

D : Diffusion coefficient for the vapor

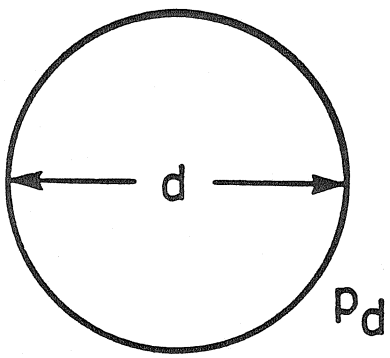

- P
- T
- $p_{vap} = RH\, p_{sat}(T)$

$p_{vap} > p_d$: Droplet growth

$p_{vap} < p_d$: Droplet shrinkage

Figure 3.2 Droplet in a humid environment.

d : droplet diameter at time t

v_m : molecular volume of the vapor

k : Boltzmann constant

T : Temperature

F(Kn) : correction factor to account for vapor transport in the transition and non-continuum regime, a function of the Knudsen number. A number of different expressions for F have been suggested; a detailed description can be found in Appendix A.1. The modified Fuchs-Sutugin expression is reasonably accurate over the entire range of Knudsen numbers and was used for the present calculations. The vapor pressure in the region surrounding the droplet, p_{vap}, can be expressed as

$$p_{vap} = (RH)\ p_{sat}. \tag{3.2}$$

The vapor pressure at the droplet surface, p_d, is given by:

$$p_d = a_w(m) \cdot \exp\left(\frac{4\sigma v_m}{dkT}\right) \cdot p_{sat}(T)$$

$$= RH_d \cdot p_{sat}(T) \tag{3.3}$$

where, a_w, the water activity of the droplet solution, is a function of the molality, m, of the droplet solution. The exponential term is the Kelvin expression which accounts for the increased vapor pressure at the surface due to curvature. For simplicity, the product of this term and the activity is called RH_d.

Substituting equations (3.2) and (3.3) into (3.1), and rewriting in terms of the particle diameter:

$$\frac{d(d)}{dt} = \frac{4 D v_m p_{sat}(T)}{dkT} \cdot [RH - RH_d] \cdot F(Kn) \quad . \qquad (3.4)$$

Given the ambient conditions, initial size and composition of the droplet, activity data, (3.4), can be integrated to describe particle growth or evaporation. We may define a time scale which is a characteristic of the time required to reach equilibrium

$$\tau = \frac{d^2 kT}{4D v_m p_{sat} \cdot (\Delta RH) \cdot F(Kn)} \quad . \qquad (3.5)$$

This is of the order of about a few microseconds for an ammonium sulfate droplet 0.1 micron in diameter, and a relative humidity difference of about 20 %. The variation of the characteristic time with particle size is shown in Figure 3.3. Most hygroscopic aerosols are deliquescent; that is, they do not become wet until a certain relative humidity called the deliquescent point, RHD. For example, ammonium sulfate particles which are initially dry at 20°C will remain dry as RH is increased below a humidity of 81 %, above which they deliquesce to form liquid droplets. When the relative humidity is reduced from above the deliquescent point, the transition to a dry state does not occur at RHD, but at a lower value due to the 'hysteresis' effect. The relative humidity at which the droplet solution crystallizes is called the 'Crystallization Humidity', RHC. This value is determined experimentally, and is between 36% and 40% for ammonium sulfate droplets (16,17).

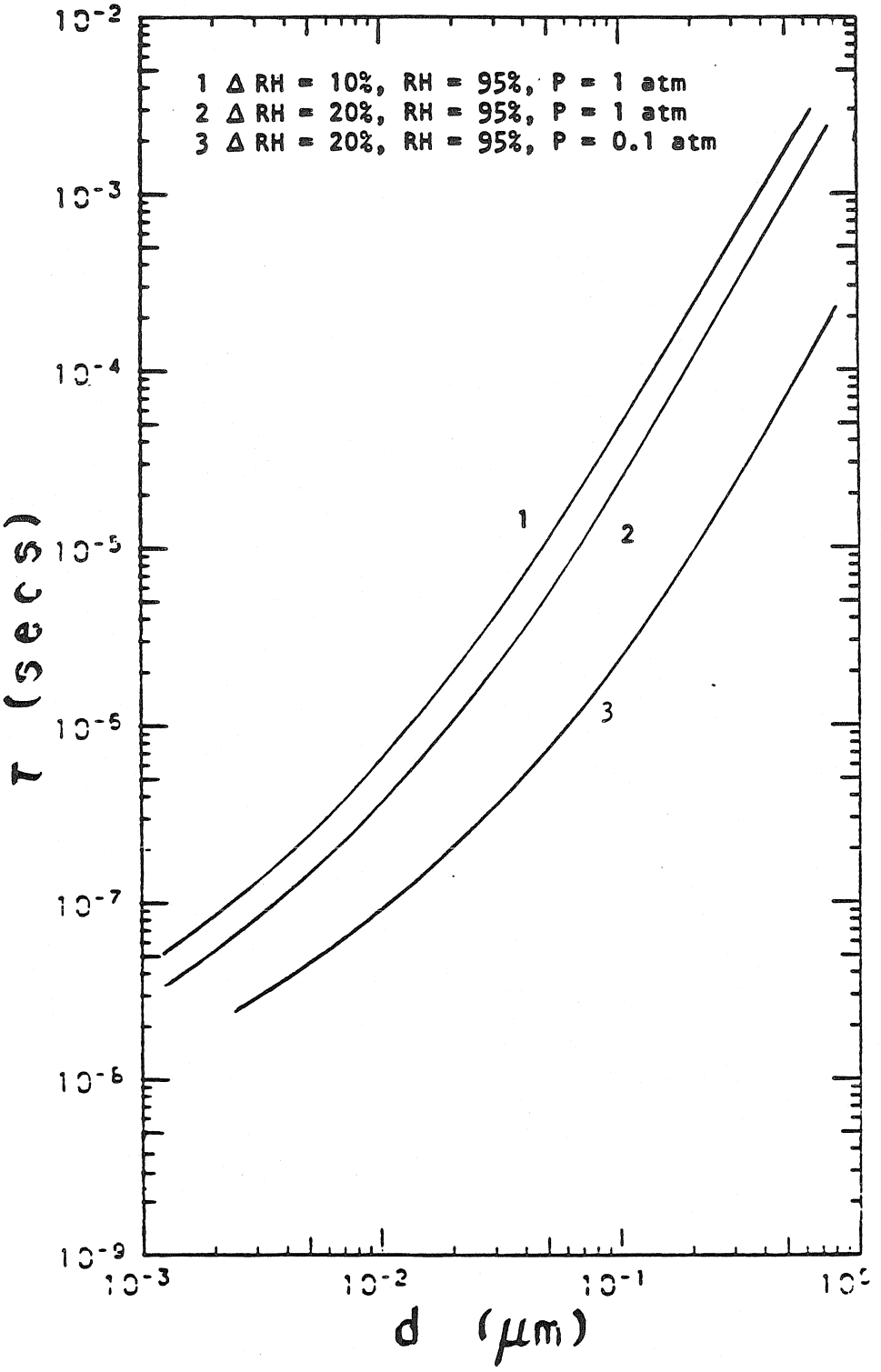

Figure 3.3 Characteristic time for droplets of different diameters.

3.3 The low pressure impactor

3.3.1 Description

The instrument developed by Hering, et al. (4) is an eight stage cascade impactor with a critical orifice between the fourth and fifth stages. The last four stages operate at a reduced pressure, thus allowing the classification of smaller particles. The last two stages are operated at high jet velocities (Mach number = 1), leading to considerable aerodynamic cooling. The pressure at each stage is measured, and listed in Table 3.1. The temperatures calculated by the expressions given in (9) are also listed.

Each stage has four regions as indicated in Figure 3.4. The region of interest is in between the jet and the impaction plate. This can be divided into two zones: a zone close to the exit of the jet, where the gas velocity equals the jet velocity, and the other closer to the plate. The first zone extends to about half the distance between the jet and the plate (3). This is also observed in the streamlines plotted for the high velocity stages by Flagan (18). Plane stagnation flow, or Heimenz flow conditions were used to obtain the flow field in the other region (19). In reality, viscous boundary layer effects complicate the flow field (20). The relations in Chapter 2 were used to obtain the temperature variation. The variation of relative humidity, RH, was calculated knowing the variation in

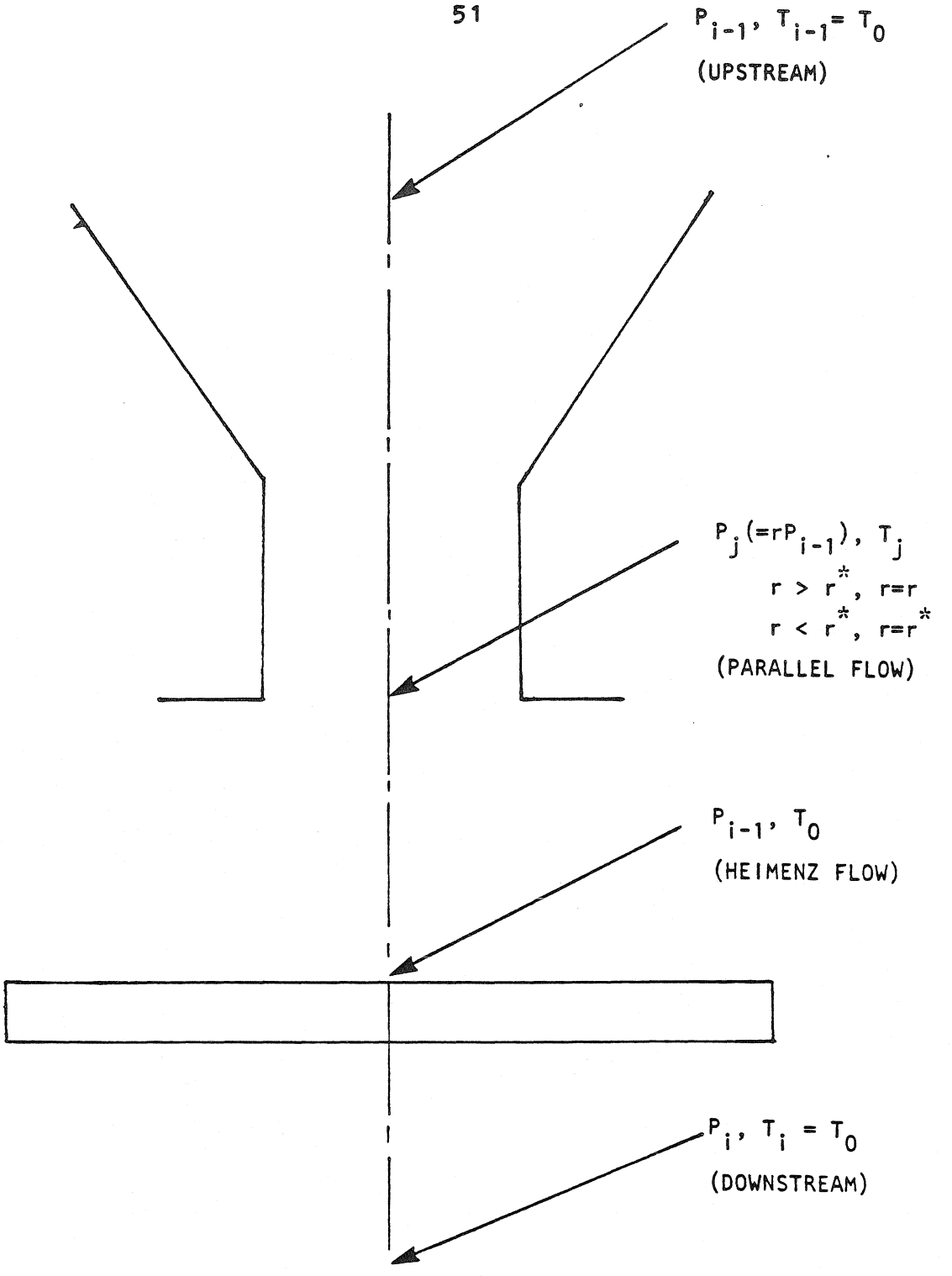

Figure 3.4 Stage of an impactor showing the four different regions.

pressure and temperature.

There is not much change in relative humidity in the first two stages. The reduction in temperature is more significant than the pressure drop in stages 3 and 4, resulting in an increase in relative humidity of 1.5% and 11%, respectively. The orifice operates at a Mach number of 1, and due to the aerodynamic cooling there is a large increase in relative humidity (see Table 3.1). Stage 5 operates at a lower pressure, which is the dominating effect, and a large reduction in RH results. On going down to stage 7, though the pressure has dropped considerably, the temperature drop is significant (high velocity jet), and there is a threefold increase in relative humidity. Though stage 8 is also a high velocity stage, the reduction in pressure is considerable, and it offsets the drop in temperature, and there is a net reduction in relative humidity.

The growth equation, (3.4), is then integrated to obtain the size history of the particle as it goes through the impactor.

Table 3.1: CONDITIONS FOR THE LOW PRESSURE IMPACTOR

Conditions at throat for a 1 lpm flow rate
Inlet Pressure = 745 mm Hg.
Inlet Temperature = 298 K

Stage	Velocity (m/s)	Pressure (mm Hg)	Temperature (K)	Residence Time (microsec)	$(RH)_{jet}$ / $(RH)_{inlet}$
I	3.5	744	297.9	1635	1.005
II	11.0	743	297.9	544	1.004
III	22.0	740	297.7	272	1.015
IV	54.0	720	295.7	111	1.111
Orifice	300.0	150	248.4	20	9.750
V	93.0	140	292.2	65	0.268
VI	150.0	106	275.3	40	0.627
VII	300.0	56	248.4	20	3.254
VIII	300.0	29	248.4	20	0.521

3.3.2 Growth calculations

A computer code was developed to integrate the growth equation (see Appendix B.2) and determine the particle size at each stage of the impactor. Two cases of inlet relative humidities are examined here: one slightly below the deliquescent point (= 81% for $(NH_4)_2SO_4$), and the other at high values (90 to 100%).

The results are shown in Figure 3.5. There is not much change in size in the first two stages of the impactor. For example, at an inlet humidity of 80%, the particle is entering the impactor in a dry state; increase in size may occur as soon as the surrounding humidity exceeds the deliquescent point of 81%. A dry particle, 3 micron in diameter, at an inlet humidity of 80%, grows to about 4 micron in stage 3, a 30% increase. A 0.04 micron diameter particle at the same inlet humidity of 80%, grows to about 0.07 micron, an 80% increase in size. Due to considerable reduction in humidity on stages 5 and 6, droplets tend to lose their water content and shrink in size. A 0.15 micron diameter ammonium sulfate droplet at an inlet humidity of 95%, shrinks to about 0.07 micron at stage 5, a 65% decrease in size. A large increase in the relative humidity on stage 7 leads to considerable growth of particles. A particle entering at a humidity as low as 25% grows in stage 7. A 0.03 micron droplet, at an inlet relative humidity of 95%,

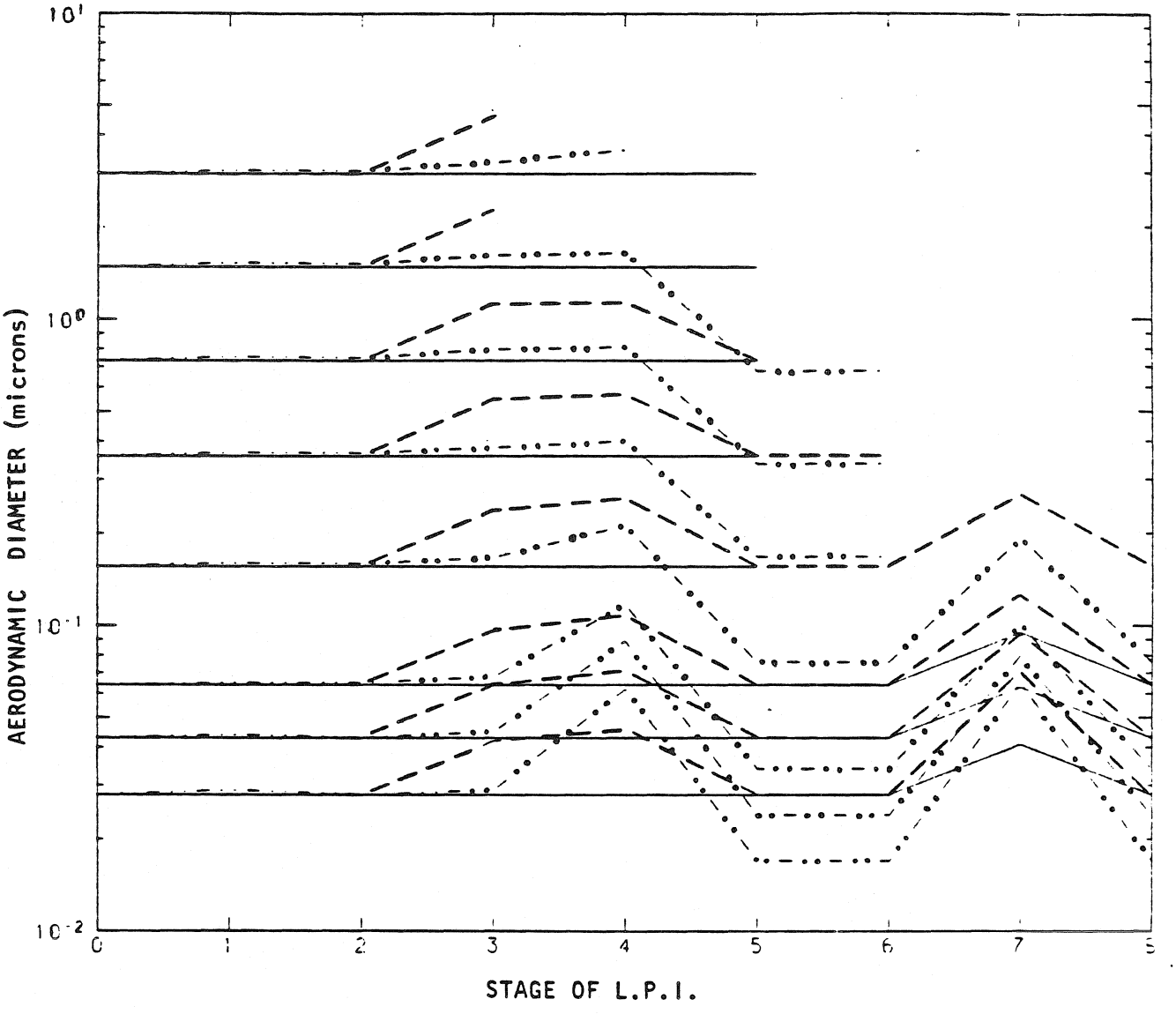

Figure 3.5 Size history of ammonium sulfate particles through the L.P.I. at three different inlet relative humidities: (——) 25 %; (- - - -) 80 %; and (--••••--••) 95 %. Inlet sizes correspond to the cutoff sizes of the stages.

grows to about 0.06 micron (100% increase in size) in stage 7, whereas the same size particle at a 25% inlet humidity grows to 0.04 micron (33% increase).

The cumulative effect of these size changes can be seen clearly when one plots the fraction of particles collected at each stage as a function of the aerodynamic diameter at the inlet. They are plotted for stages 3 to 8 in Figures 3.6 (a) through (f) for several inlet relative humidities from 0 to 95%. Density changes occurring with size changes as the droplets passed through the impactor were taken into account for these computations. The solid lines are obtained from the calibration data using dry particles in the absence of any condensable vapor, i.e., RH = 0% (4). Consider stage 3: about fifty percent of 2 micron-size particles entering the impactor are collected on this stage, the other 50% being collected on the upper stages; and about 50% of particles 1 micron in diameter are also collected on this stage, the other 50% proceeding to the lower stages to be collected there. At an inlet humidity of 80% (< RHD = 81%), particles grow, increasing the collection of small particles on stage 3. The increase in fraction collected is more than that for an inlet humidity of 95% (wet droplets at inlet), because at the 80% inlet humidity, particles are in a dry state (see Figure 3.6a). A similar effect is observed on stage 4 (Figure 3.6b). The fraction of larger particles collected on this stage

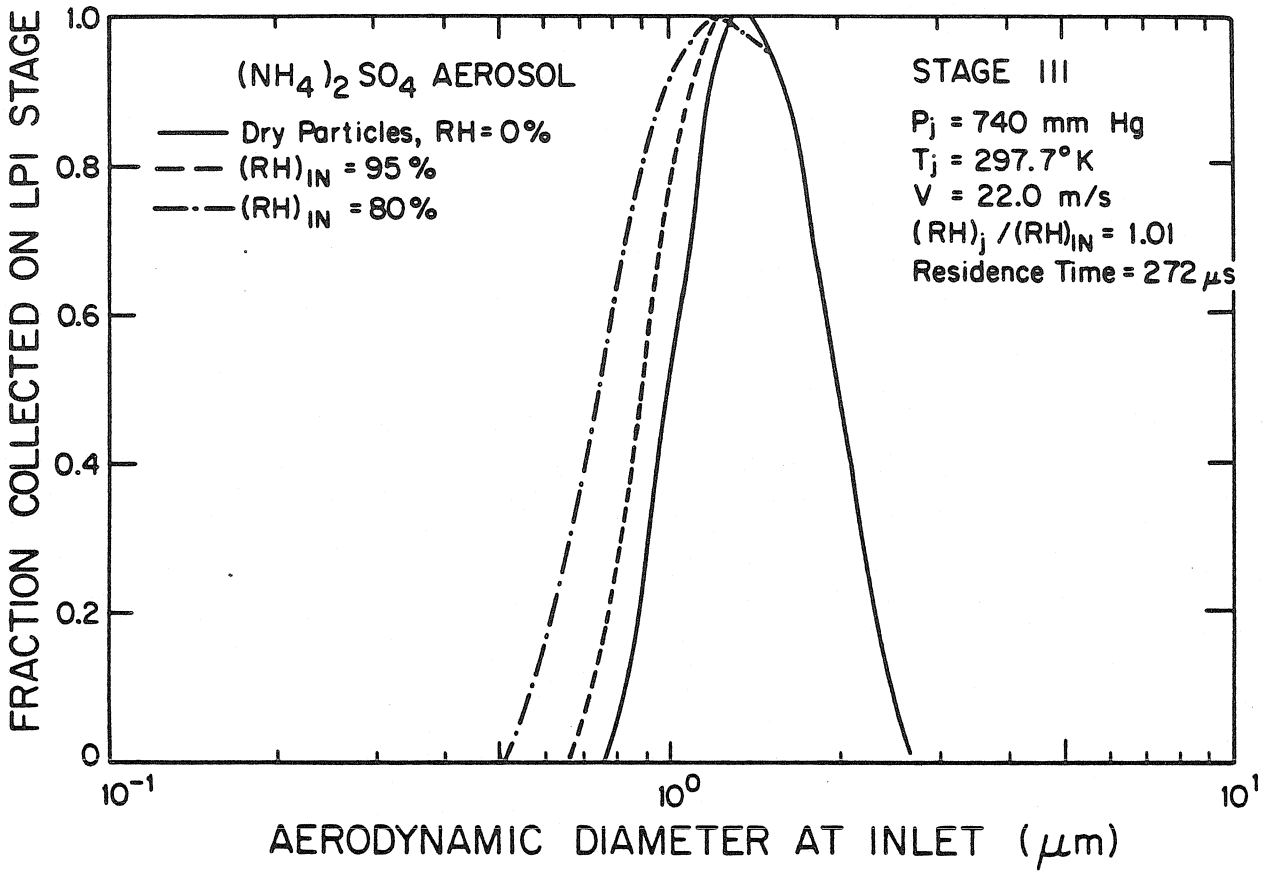

Figure 3.6 (a) Fraction of mass collected on stage III of the L.P.I. at different inlet relative humidities.

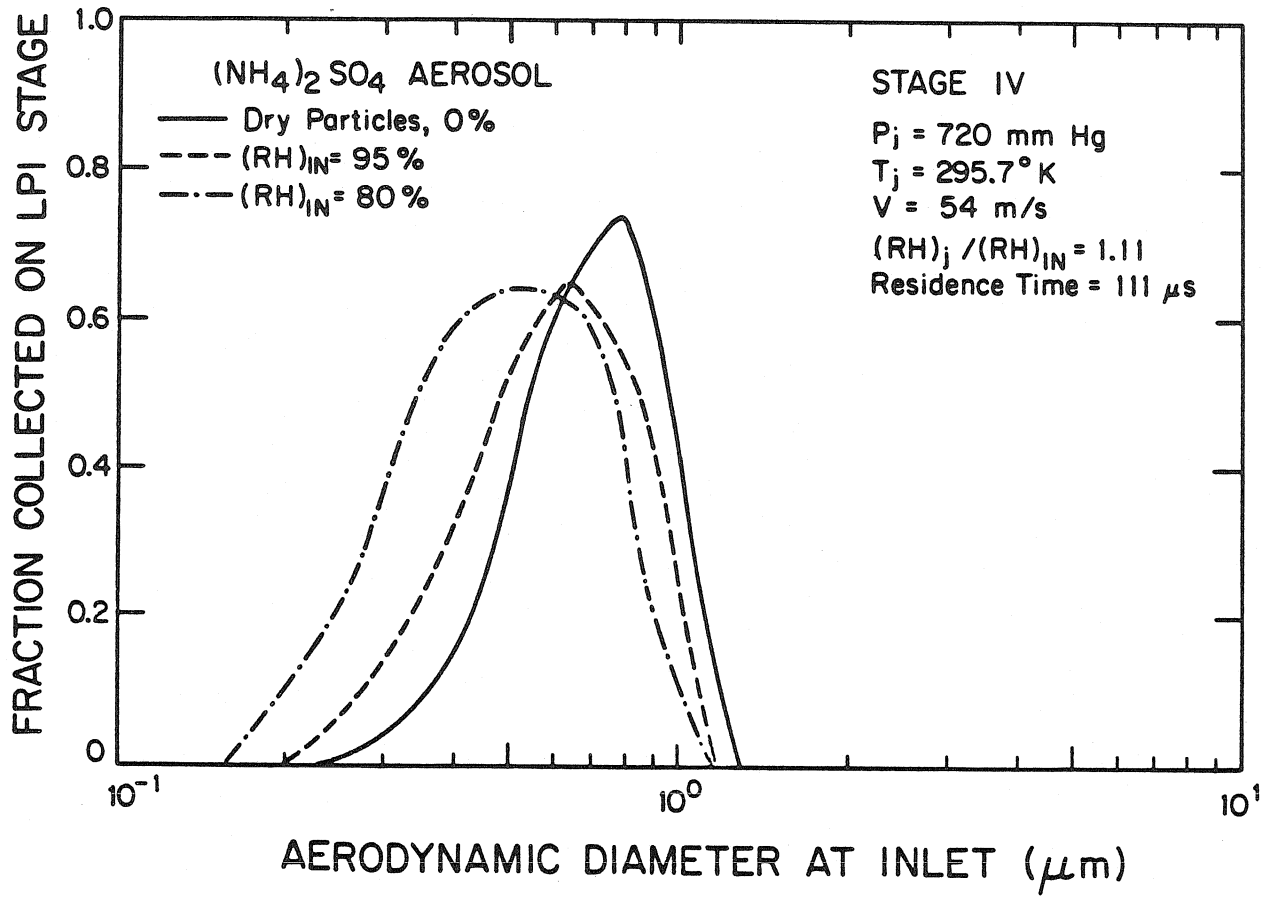

Figure 3.6 (b) Fraction of mass collected on stage IV of the L.P.I. at different inlet relative humidities.

decreases because of the increased collection on stage 3 (due to growth occurring there) reduces the number of particles entering stage 4.

As expected, the fraction collected on stage 5 decreases substantially due to the considerable drop in relative humidity (Figure 3.6c). It is more pronounced for the higher inlet relative humidity values. Similar shifts are observed on stage 6 as shown in Figure 3.6d. The fraction collected on stage 7 increases dramatically with relative humidity as shown in Figure 3.6e. Even inlet humidities as low as 25% lead to particle growth and size distribution distortion. The amounts collected on stage 8 (Figure 3.6f) are greatly reduced at elevated humidities because most of the particles have been collected on stage 7.

The results of Figure 3.6 clearly indicate the severity of measurement biases at high humidity in this instrument. The nature of the distortion is very much dependent on the kind of aerosol particle (thermodynamic properties) and the inlet conditions (pressure, temperature, relative humidity). For ammonium sulfate particles, at inlet relative humidities greater than about 25% but less than 70%, size changes occur only in stages 7 and 8. The size distribution curve tends to shift to the right. Particles entering at relative humidities between 70 and 81% (dry at the inlet) become wet in the upper stages,

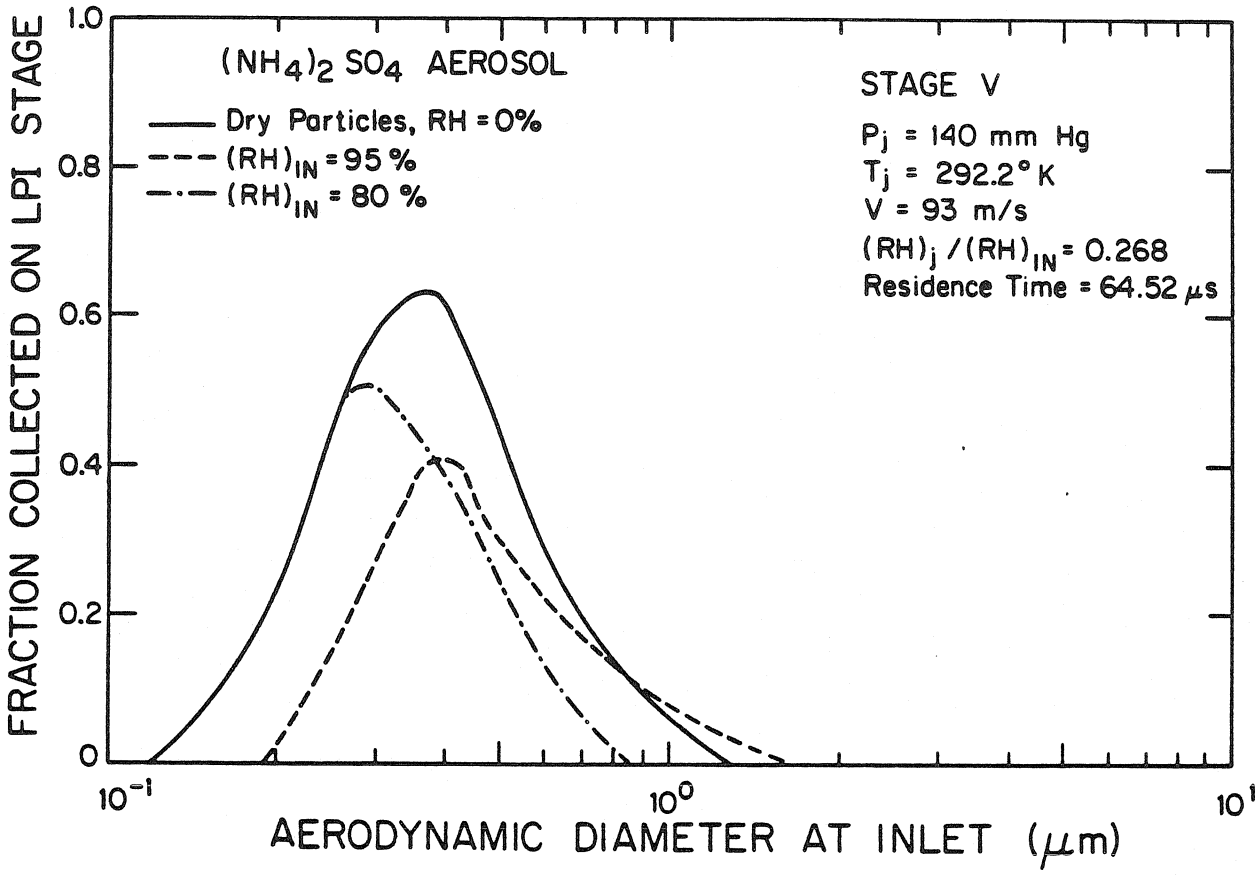

Figure 3.6 (c) Fraction of mass collected on stage V of the L.P.I. at different inlet relative humidities.

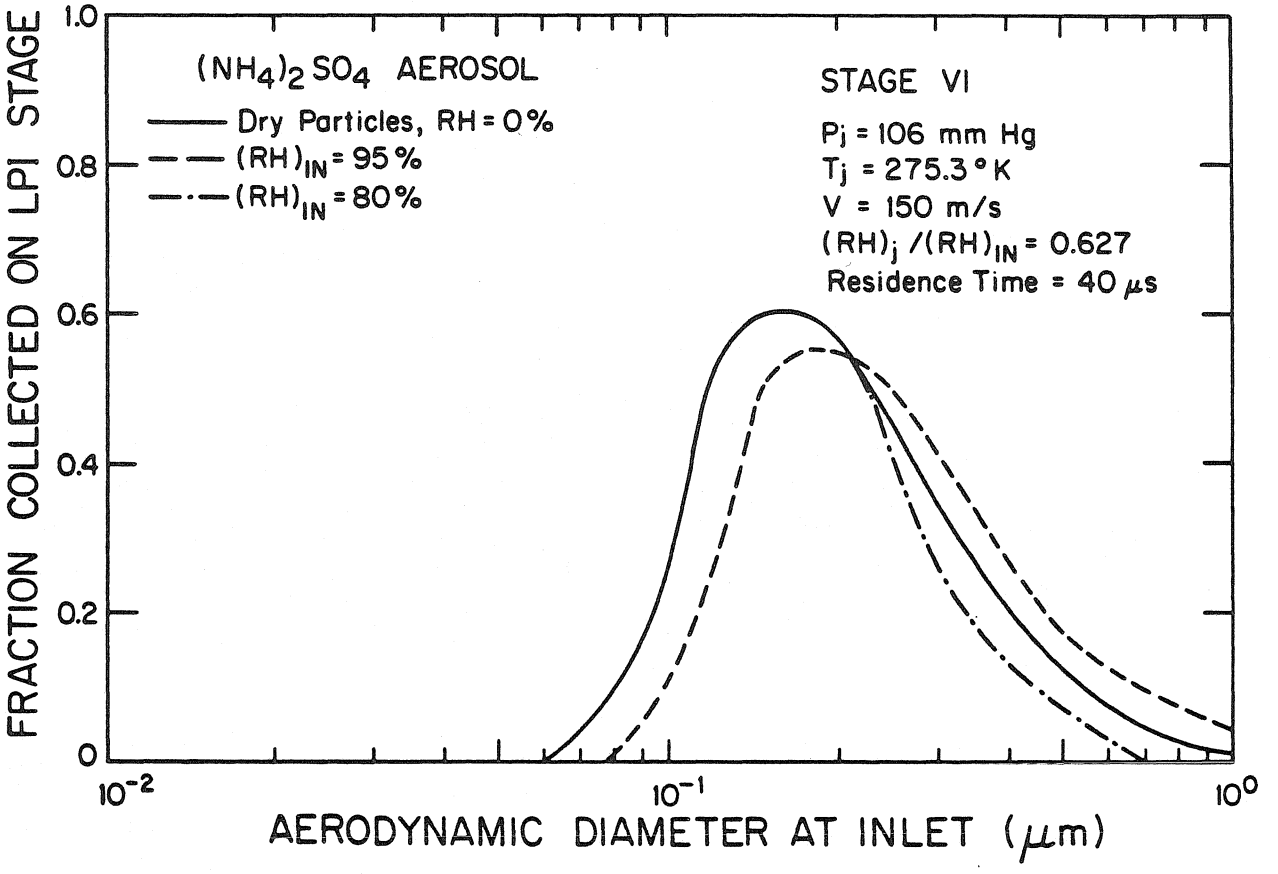

Figure 3.6 (d) Fraction of mass collected on stage VI of the L.P.I. at different inlet relative humidities.

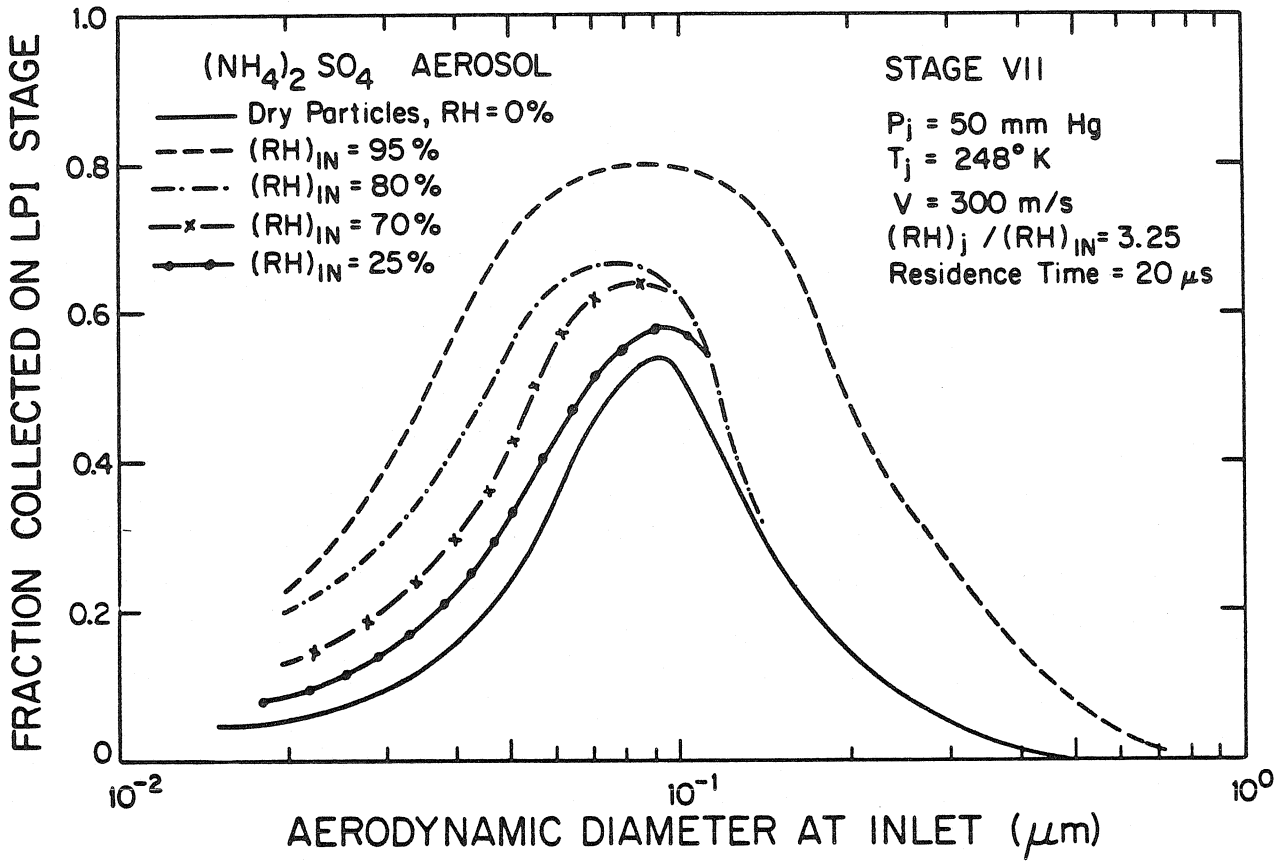

Figure 3.6 (e) Fraction of mass collected on stage VII of the L.P.I. at different inlet relative humidities.

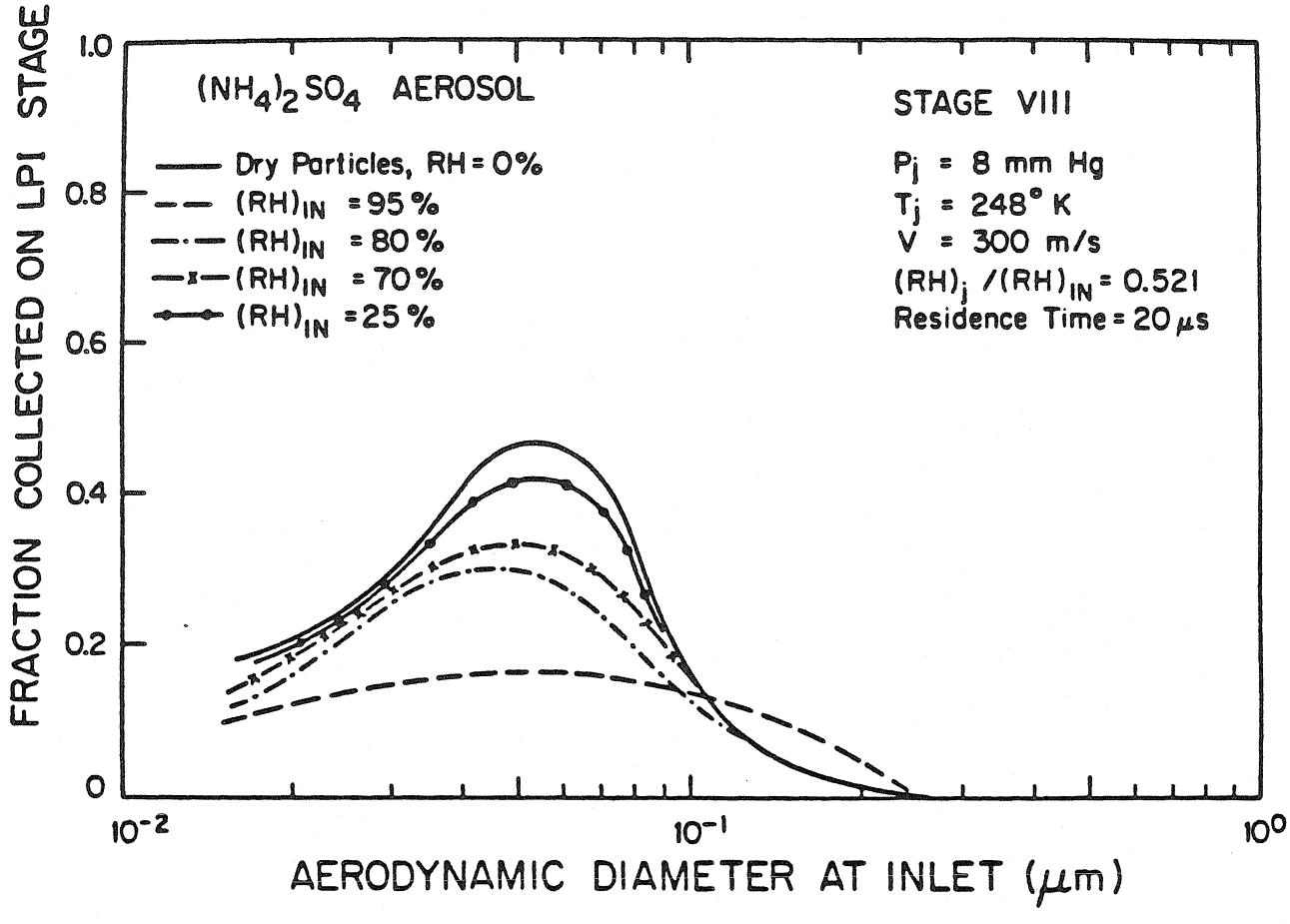

Figure 3.6 (f) Fraction of mass collected on stage VIII of the L.P.I. at different inlet relative humidities.

increasing the fraction collected there and decreasing collection on the next few stages. Large increases are observed in stage 7. This complicated shift sometimes causes unimodal size distributions to become multimodal. For inlet relative humidities greater than the deliquescent point, the general trend is for slight increase in fraction collected on the upper stages, a considerable decrease in stages 5 and 6, followed by a large increase in stage 7, and again a decrease in stage 8. Many of the data obtained with this instrument show a more pronounced minimum on stages 5 and 6 than has been observed with other instruments (21), quite possibly the result of evaporation.

3.3.3 Experimental Verification

Tests were carried out using monodisperse ammonium sulfate aerosol particles at different inlet conditions: below the deliquescent point (dry), and above the deliquescent point (wet). Because of the hysteresis effect (described in 3.2.2), two different aerosol generation systems were used (see Figure 3.7). Size classification was performed on dry particles, and the particle size at the inlet to the impactor was calculated, assuming it to be at equilibrium at the inlet relative humidity. The modified ROYCO optical particle counter (described in section 3.5) was used to confirm the inlet sizes of the particles. Temperature and relative humidity were monitored using the Model 911 Digital Humidity Analyzer, manufactured by EG&G.

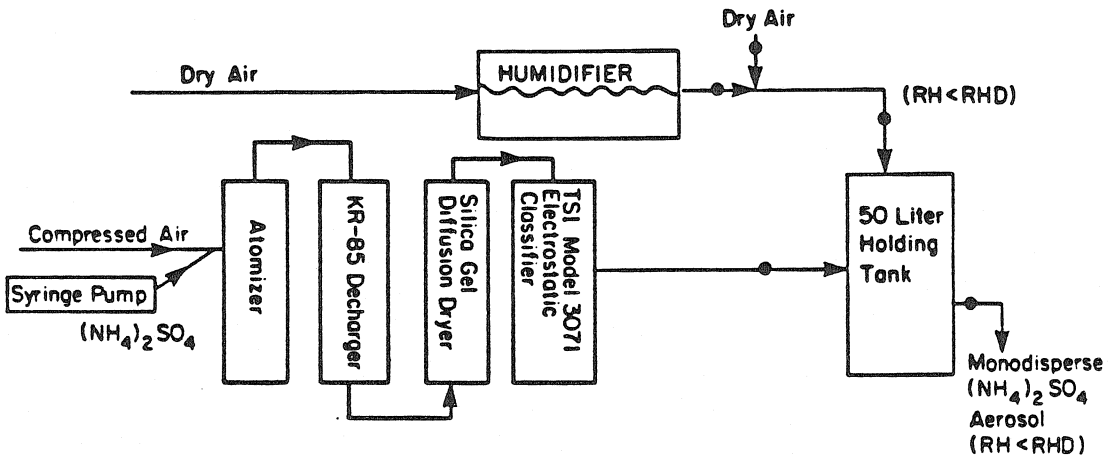

(a)

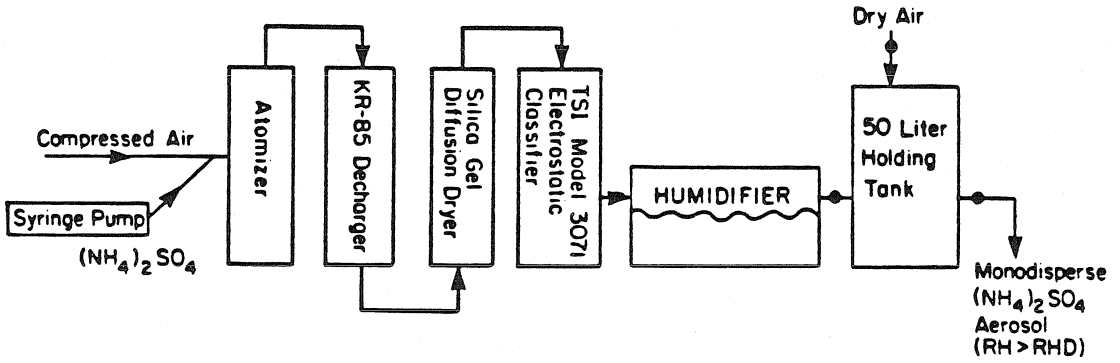

(b)

Figure 3.7 Schematic of test loop to generate monodisperse ammonium sulfate aerosols at different relative humidities. (a) RH < RHD, (b) RH > RHD

Thin stainless strips, pretreated in a furnace at 900 ^{o}C, coated with vaseline were used as impaction substrates. The quantity of ammonium sulfate collected on each stage was determined by the flash vaporization technique developed by Roberts, et al (13). The gaseous sulfur was detected by means of a Meloy 285 Sulfur analyser.

The results for inlet relative humidities from 96 to 97% are plotted in Figures 3.8, 3.9, and 3.10. Particles are wet when they enter the impactor, and are expected to lose water in stages 5 and 6, and grow in stage 7. The aerodynamic inlet diameter, for the experiment whose result is plotted in Figure 3.9, is 0.27 micron; and most of the particles should be collected on stages 5 and 6 as indicated by the dotted line. However, due to loss of water from the droplets leading to a reduction in size at those stages, they reach stage 7 where they grow in size and end up being collected there. A similar observation is made for the experiment whose result is plotted in Figure 3.10. When the aerodynamic inlet diameter is 0.024 micron, most of the particles are expected to be collected on the backup filter. However, they grow considerably in stage 7, and a large fraction is collected there (Figure 3.11).

The results for inlet humidities of 90% and 92% are plotted in Figures 3.12 and 3.13. Particles to be collected on stages 5 and 6 are again observed to lose water and shrink in size, bypass these stages and end up being

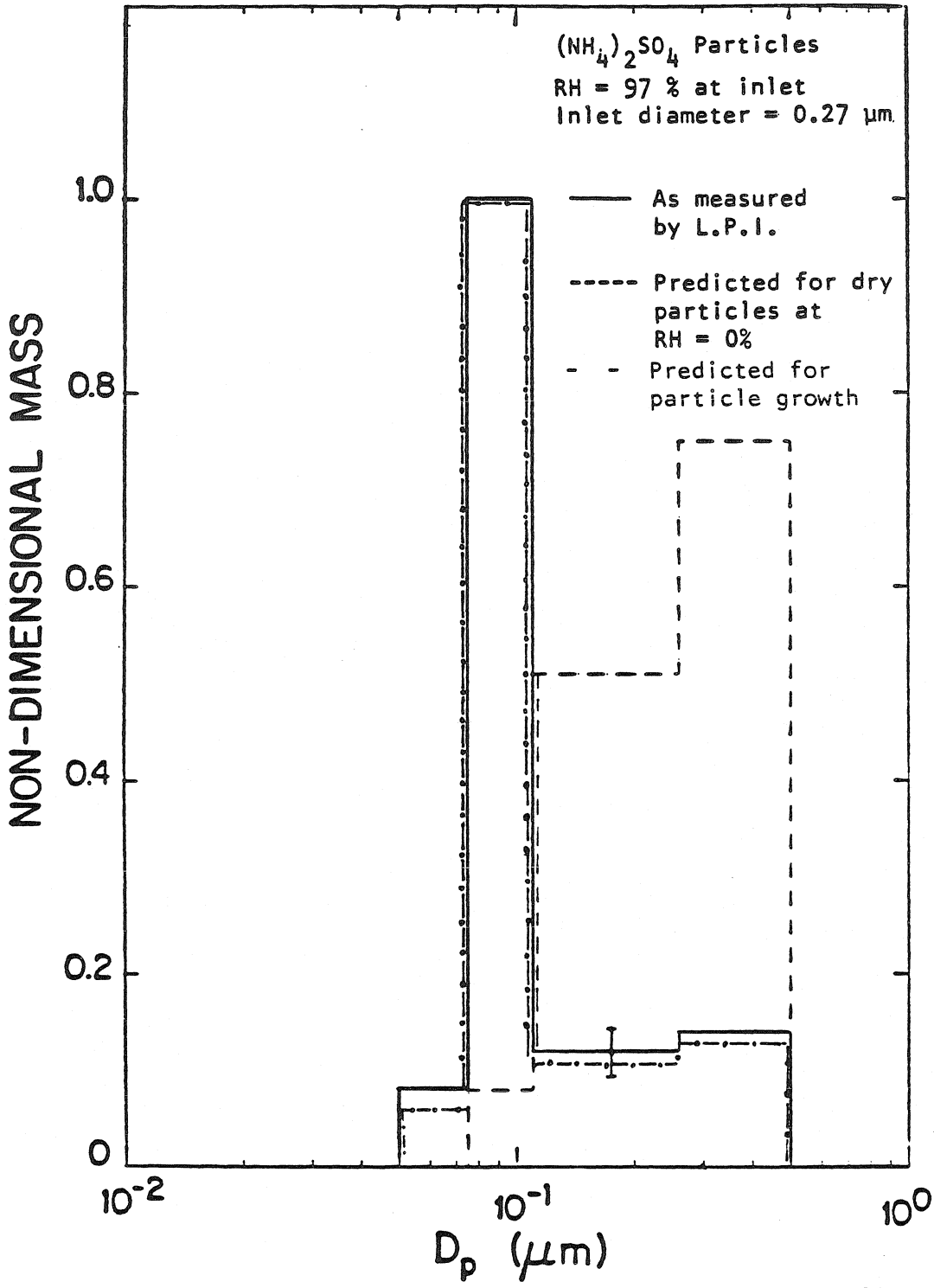

Figure 3.8 Variation of measured non-dimensional mass collected on the L.P.I. stages with aerodynamic diameter for a monodisperse ammonium sulfate aerosol.

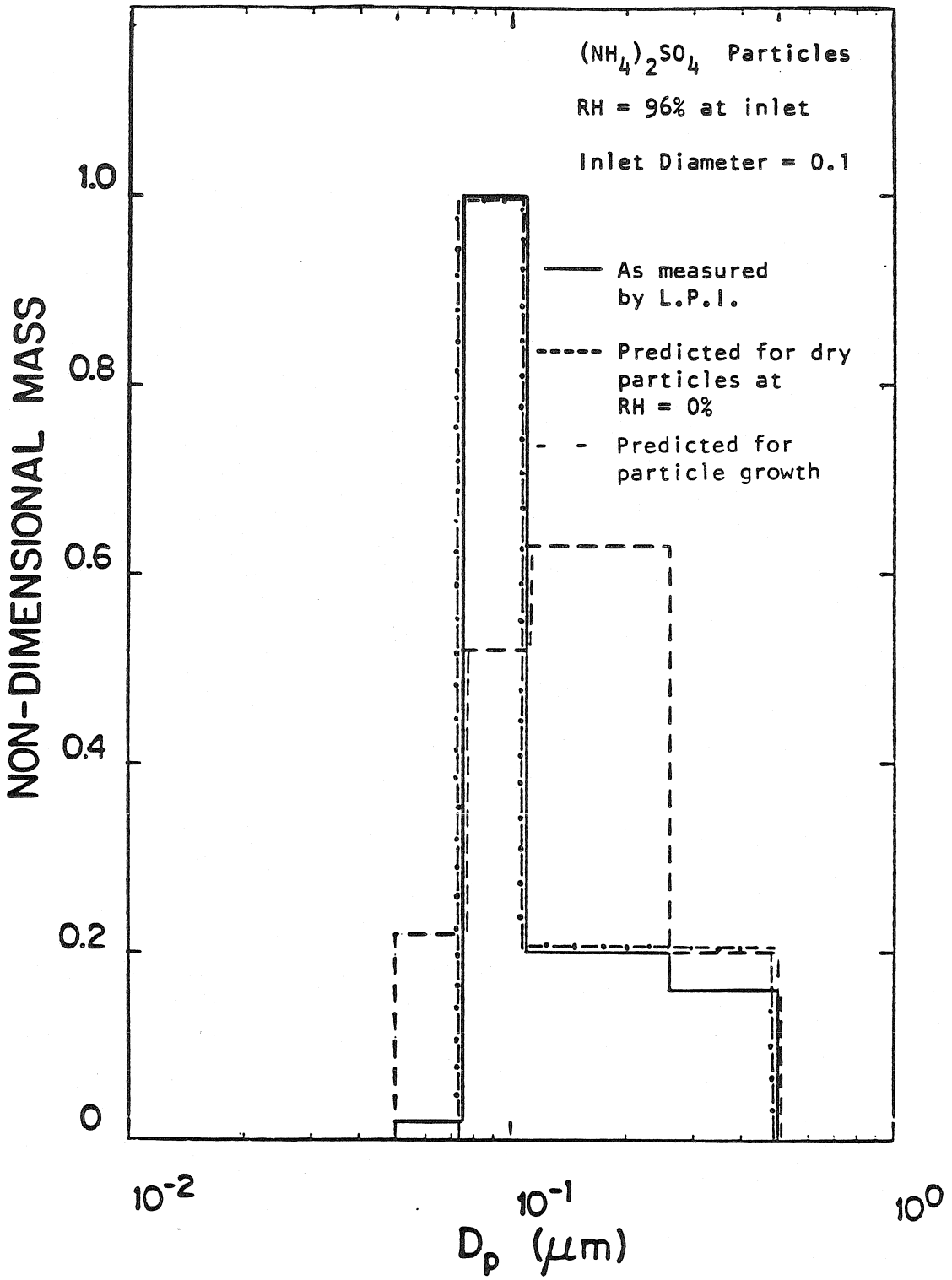

Figure 3.9 Variation of measured non-dimensional mass collected on the L.P.I. stages with aerodynamic diameter for a monodisperse ammonium sulfate aerosol.

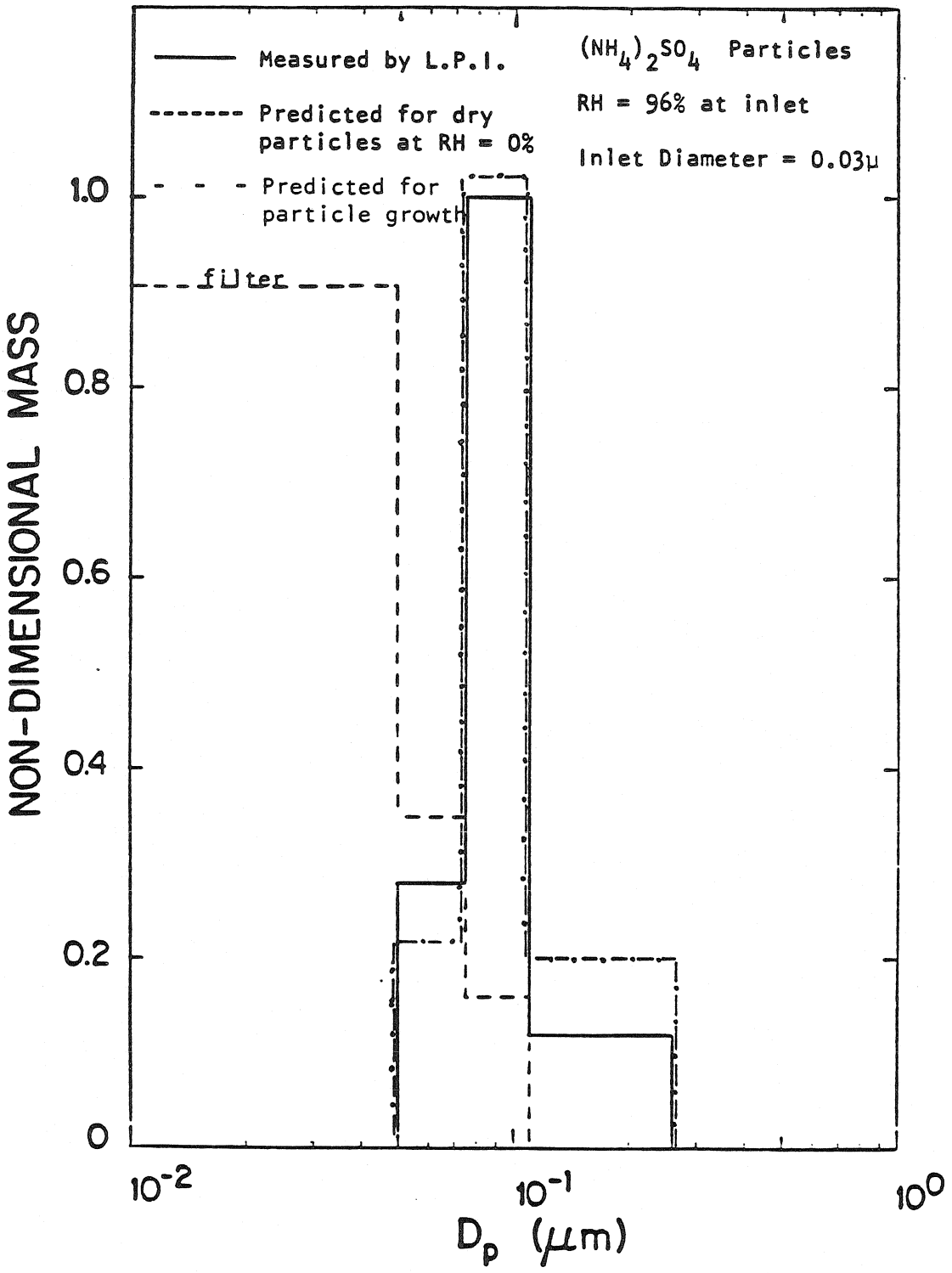

Figure 3.10 Variation of measured non-dimensional mass collected on L.P.I. stages with aerodynamic diameter for a monodisperse ammonium sulfate aerosol.

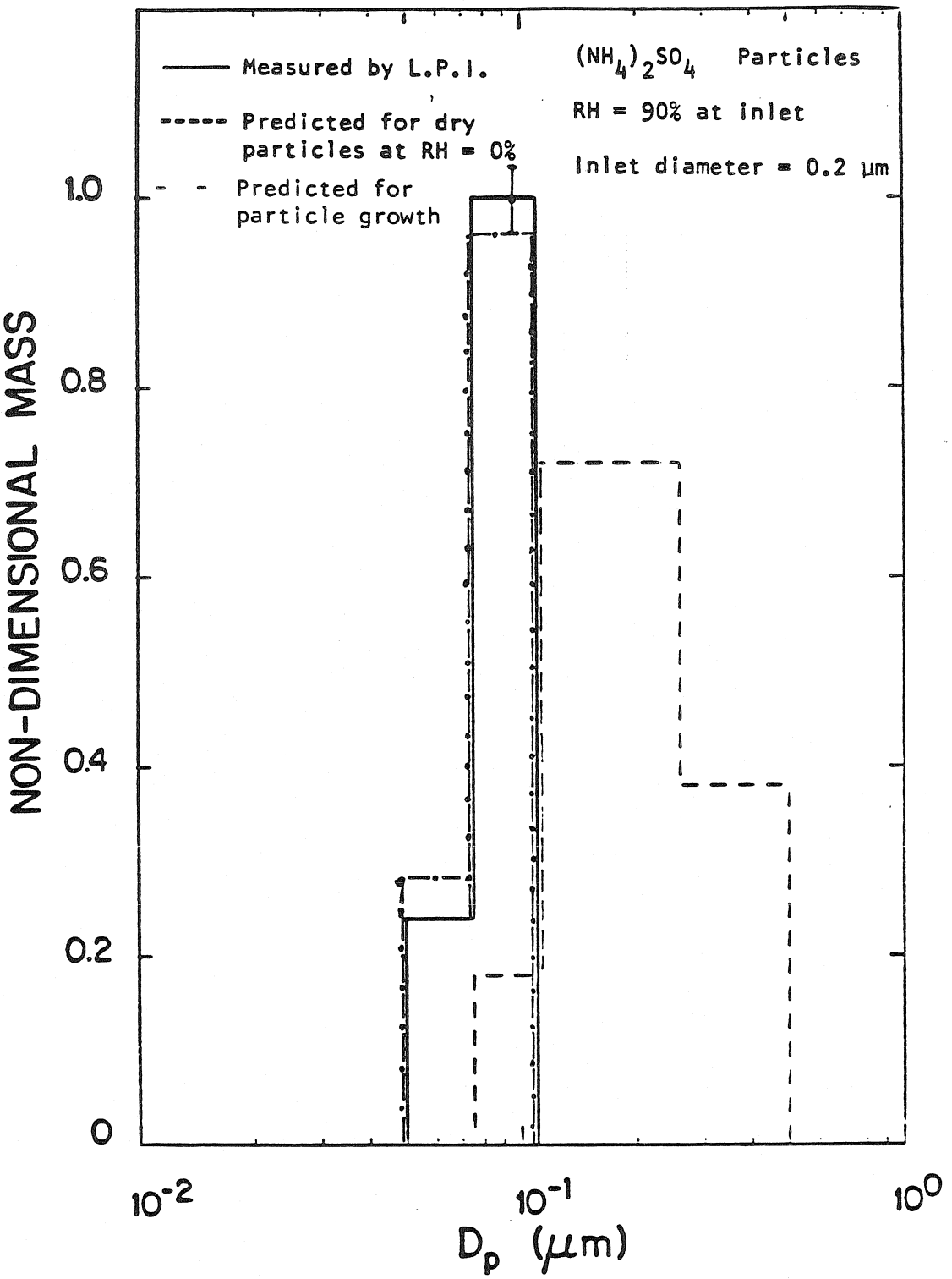

Figure 3.11 Variation of measured non-dimensional mass collected on L.P.I. stages with aerodynamic diameter for a monodisperse ammonium sulfate aerosol.

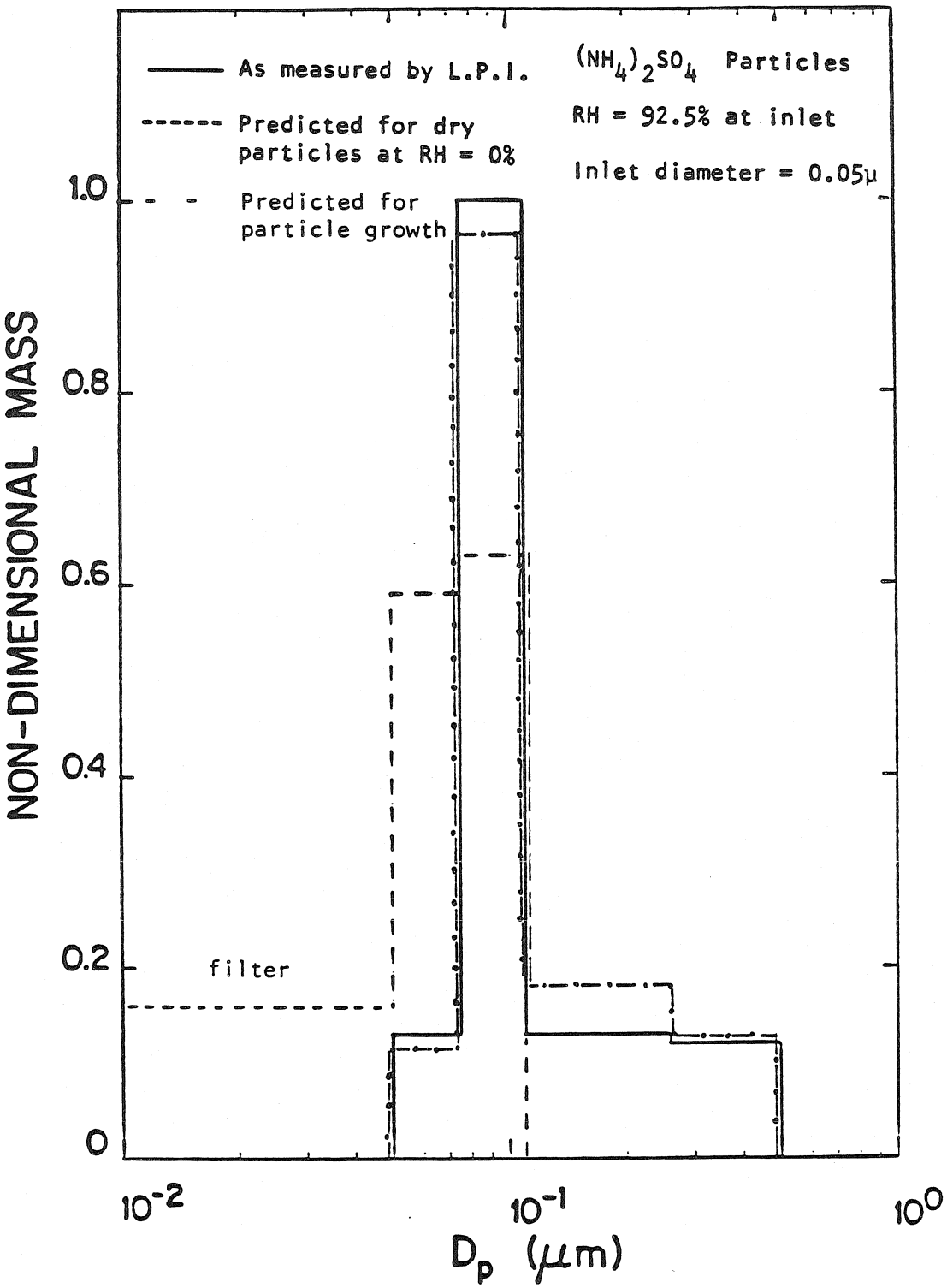

Figure 3.12 Variation of measured non-dimensional mass collected on L.P.I. stages with aerodynamic diameter for a monodisperse ammonium sulfate aerosol.

collected on stage 7 (Figure 3.12). Very small particles (0.052 micron) to be collected on stage 8 or the backup filter grow considerably in stage 7 and are collected there (Figure 3.13).

Small particles (0.024 micron) entering at lower humidities (RH_{inlet} = 63%) grow considerably in stage 7 and are collected there, as shown in Figure 3.14.

Wet ammonium sulfate particles at stages 5 and 6 lose water and shrink in size, and are not collected there. This is clear from Figures 3.9 and 3.12. Particles, wet or dry, grow considerably in stage 7 (above a certain inlet relative humidity, computed to be 25% for ammonium sulfate particles), and a large fraction is collected there (demonstrated for inlet relative humidities above 63% in Figures 3.10, 3.11, 3.12, and 3.13).

3.4 Sierra Impactor, Model 266

3.4.1 Description

We have seen that the distortion of particle size distributions by impactors operated at low pressures and high velocities can be severe. Some shifts were predicted for stages operated with Mach numbers well below 0.3, the nominal limit of incompressible flow. Thus, some size bias may occur in conventional impactors operated strictly within the accepted guidelines of Mach number.

Sierra's Model 266 multistage impactor is designed

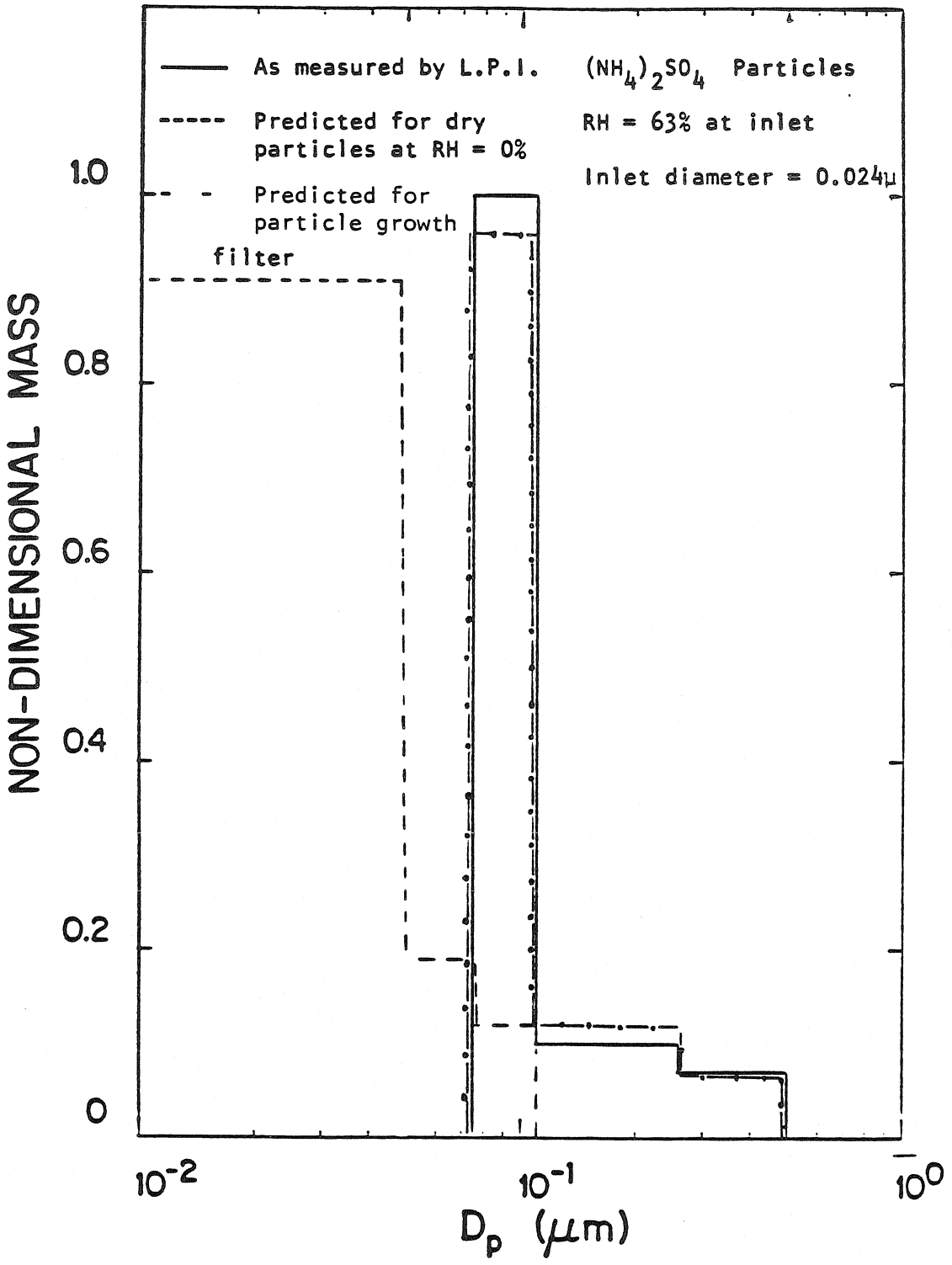

Figure 3.13 Variation of measured non-dimensional mass collected on L.P.I. stages with aerodynamic diameter for a monodisperse ammonium sulfate aerosol.

according to these guidelines and has been very well characterized in numerous studies. It has circular nozzles and was designed for operation in the incompressible flow regime. Thus, there is not a significant pressure drop across any stage. Table 3.2 lists the various conditions at the different stages of the impactor. The increase in relative humidity in the first four stages is minimal, that in stage 5 and 6 being about 4% and 19%, respectively.

3.4.2 Growth Calculations

Growth calculations, analogous to those described in section 3.2.2, were carried out for the Sierra Impactor. It was found that, for humidities above 67% at the inlet, particle growth was expected to occur in stage 6. Also, if the inlet humidity was greater than about 84%, the relative humidity at stage 6 exceeded 100%, and considerable growth could be expected. The results are shown in Figures 3.14(a) and 3.14(b).

TABLE 3.2 : SIERRA IMPACTOR, MODEL 266

Conditions at 4 lpm
Inlet Pressure = 760 mm Hg
Inlet Temperature = 298 K

STAGE	MACH NUMBER	T_J (^oK)	P_J (mm Hg)	RESIDENCE TIME (ms)	$(RH)_J / (RH)_{inlet}$
I	0.004	298.0	760.0	6.32	1.000
II	0.008	298.0	760.0	2.32	1.000
III	0.017	297.9	759.9	2.51	1.003
IV	0.044	297.9	759.2	0.836	1.004
V	0.122	297.3	753.7	0.259	1.035
VI	0.273	294.4	728.5	0.118	1.190

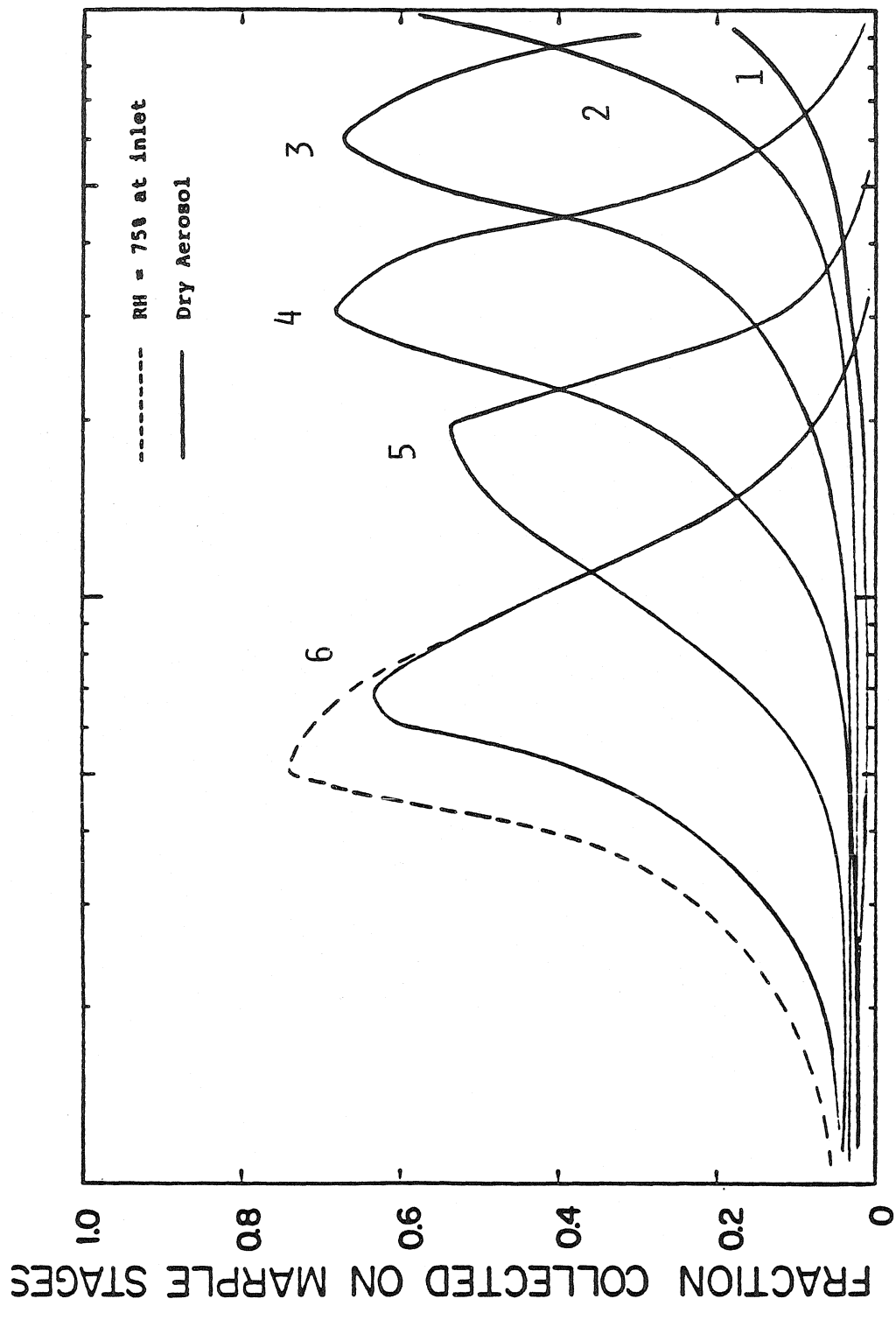

Figure 3.14(a) Fraction of ammonium sulfate particles collected on differnt stages of the Sierra Impactor at an inlet relative humidity = 75 %.

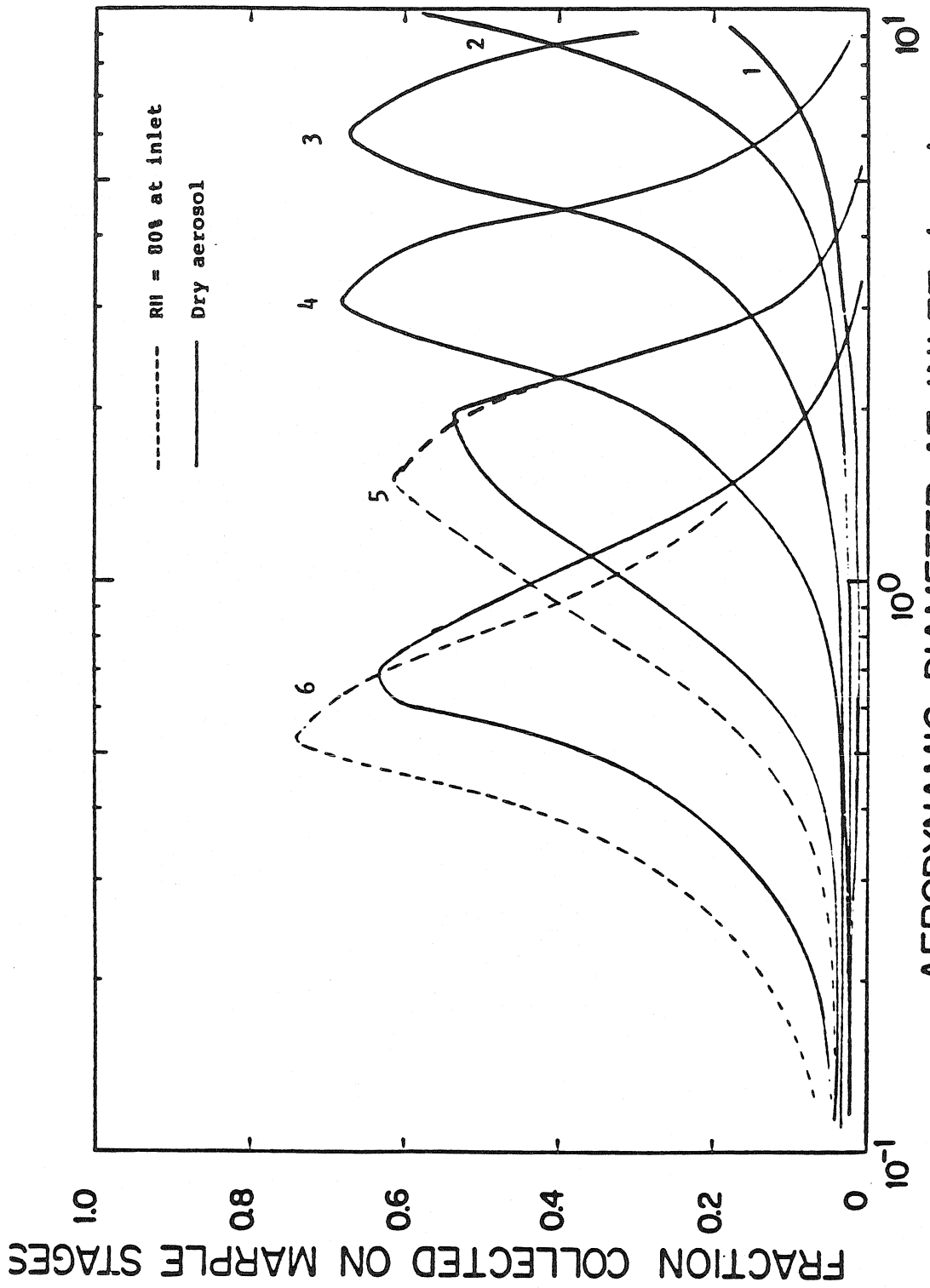

Figure 3.14 (b) Fraction of ammonium sulfate particles collected on different stages of the Sierra Impactor at an inlet relative humidity = 80%.

3.4.3 Experimental Results

The two systems described in section 3.3.3 were used to generate $(NH_4)_2SO_4$ aerosols for the study. The masses collected on each greased stage was determined by first extracting the ammonium sulfate from the slide, and then doing a quantitative analysis to determine the amount of NH_4^+ ion (14).

The results for a number of different combinations of inlet relative humidity and size are plotted in Figures 3.15 through 3.17. They indicate that significant distortions could occur on stage 6 of the device. Thus, operating impactors at Mach numbers less than 0.3 (incompressible flow limit) may be all right from the momentum point of view, but it may still lead to biased size distributions.

A recently developed impactor by Marple (15) using microorifice nozzles, would probably have the same problem. The Mach number of the last stage is 0.7, leading to a temperature drop of 25 ^{o}C. This results in a sixfold increase in humidity, and should lead to considerable growth of particles.

3.5 The ROYCO OPC

3.5.1 Instrument Characteristics

The Model 226 Laser Aerosol Counter (6) has a laser illuminated optical system and solid state photo

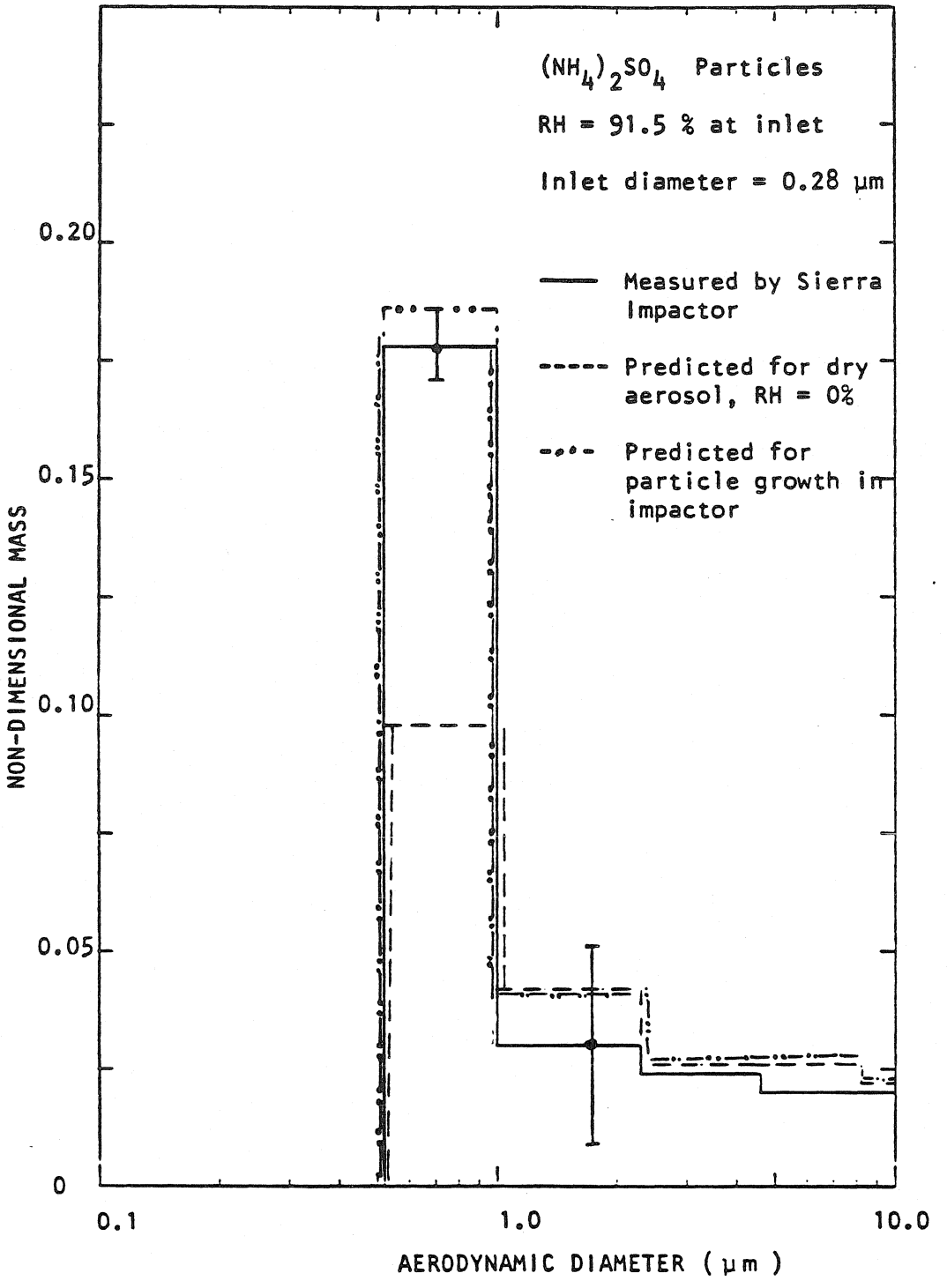

Figure 3.15 Variation of measured non-dimensional mass collected on the Sierra Impactor stages with aerodynamic diameter.

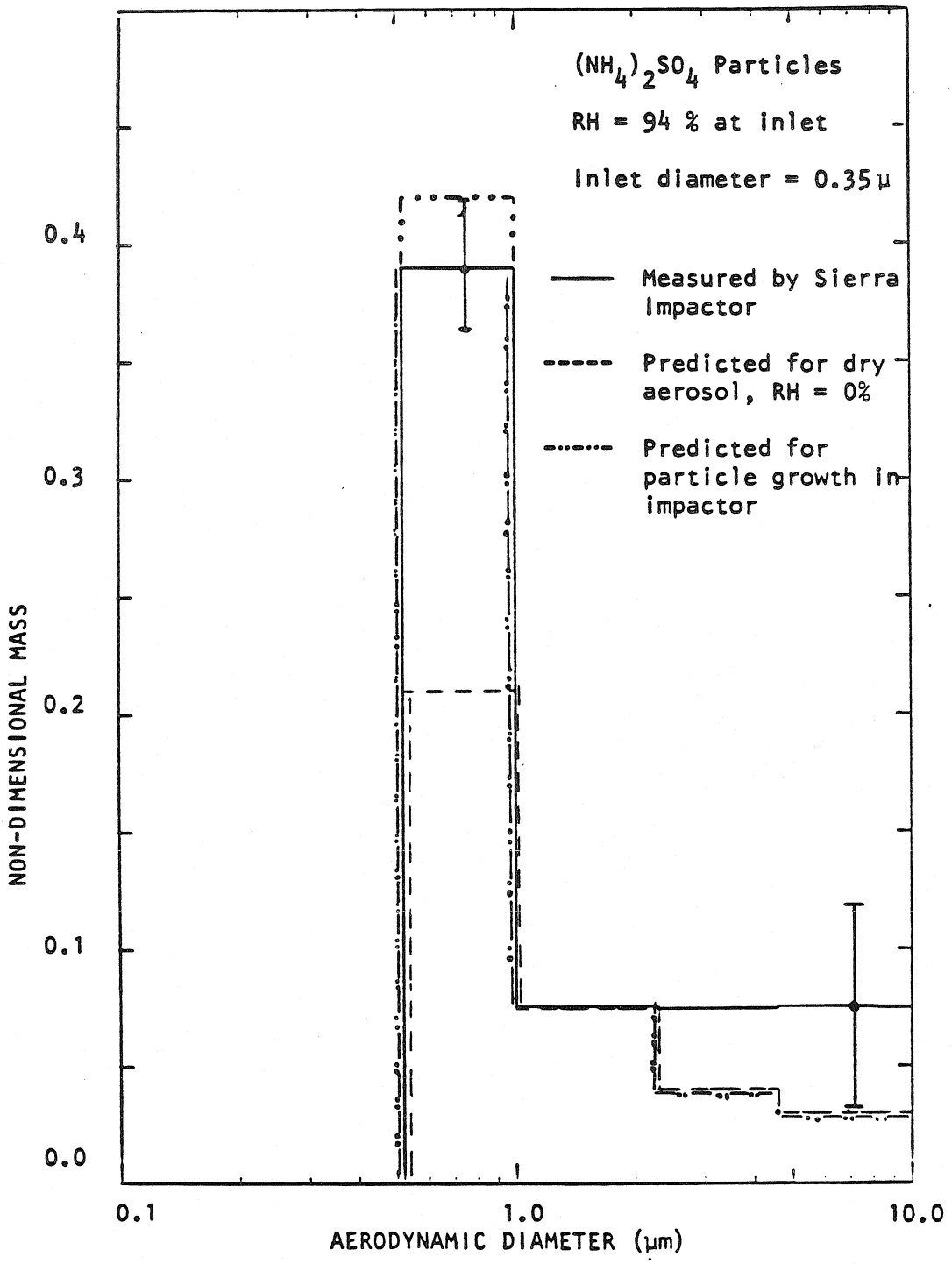

Figure 3.16 Variation of measured non-dimensional mass collected On the Sierra Impactor stages with aerodynamic diameter.

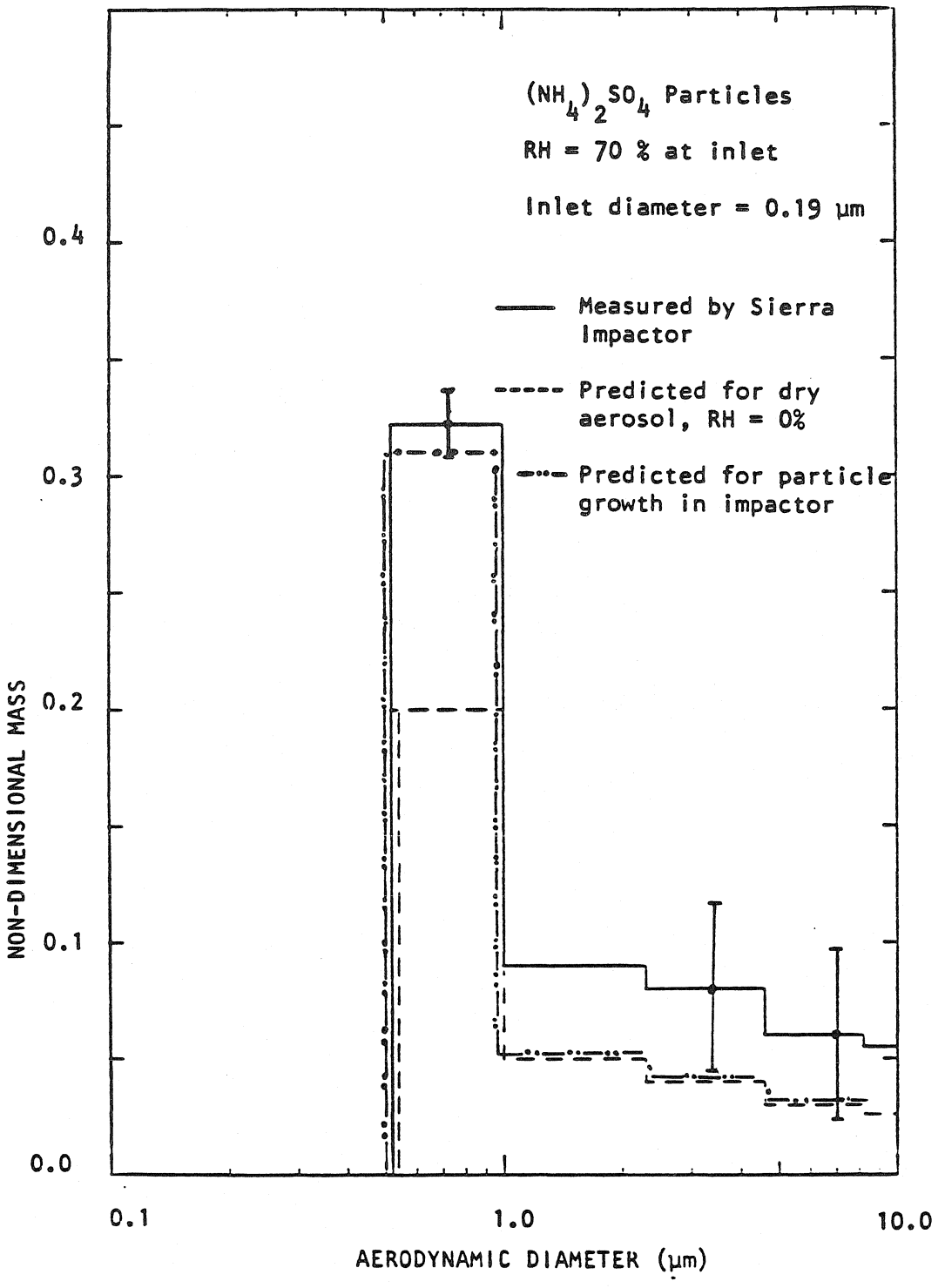

Figure 3.17 Variation of measured non-dimensional mass collected on the Sierra Impactor stages with aerodynamic diameter.

detector for single particle counting and sizing by collecting light scattered from each particle as it passes through the active cavity of the laser. The components in the airflow assembly are shown in Figure 3.18. The sheath air flow is derived from the sample flow, and is recirculated by means of a diaphragm pump. The exhaust flow is made up by the sample inlet flow.

Dissipation by the electronics and the pump lead to a heating up of the sheath air flow. Increases of 2 to 3 ^{o}C were observed, as shown in Figure 3.19 (a). This tends to reduce the relative humidity in the measuring region. The cartridge filters supplied by the manufacturer are made of a water absorbent material (6). Also, as hygroscopic salts are deposited onto these filters, they can act as a source or sink for water. The measured sheath air relative humidity is plotted as a function of time in Figure 3.19 (b), for a fixed inlet relative humidity of 95%. These factors, heating up of the sheath air and water absorption by filters, clearly indicate that wet particles would lose water and shrink in size in the OPC. This has also been observed experimentally.

3.5.2 Instrument Modifications

The problems, described in section 3.5.1, can be rectified easily. The temperature is maintained at the same value as the sample stream temperature by addition of a

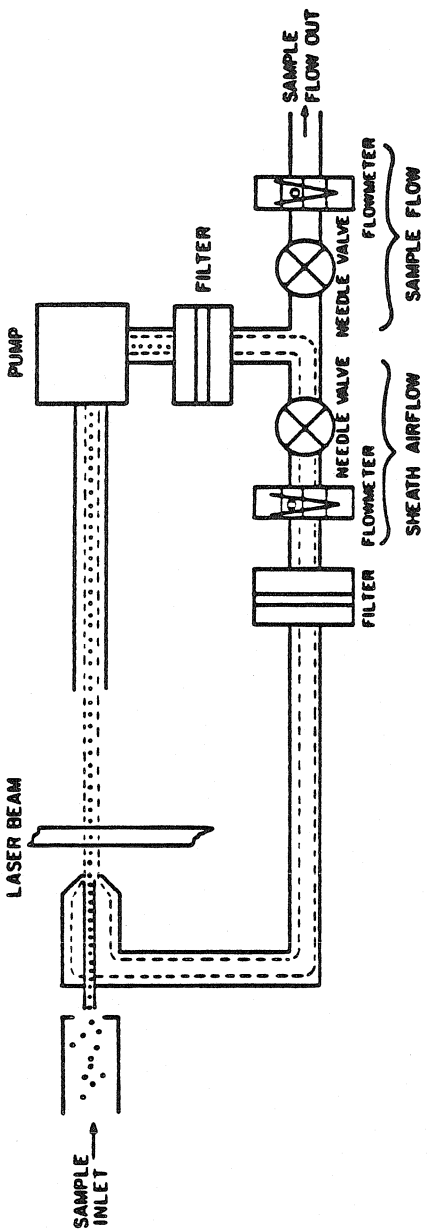

Figure 3.18 FLOW DIAGRAM FOR THE LASER PARTICLE COUNTER (ROYCO MODEL 226).

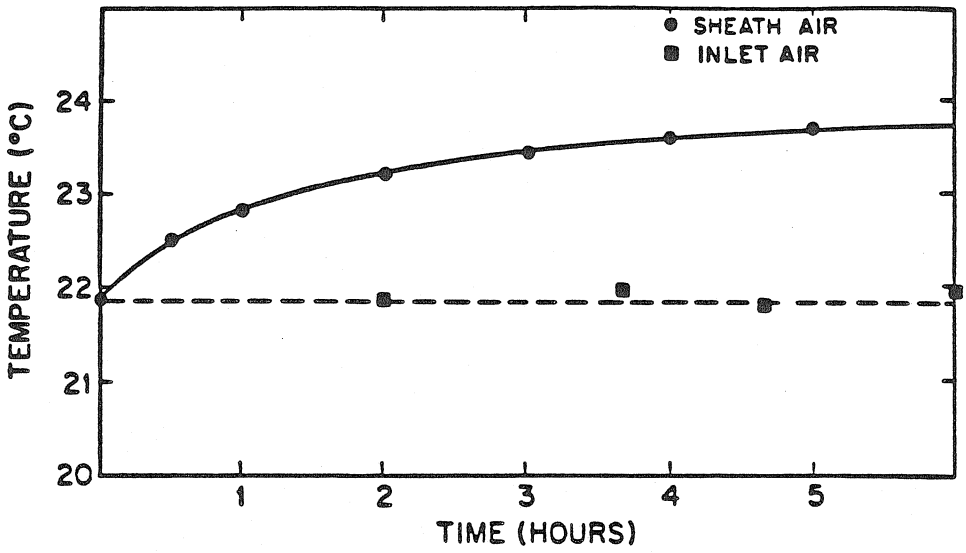

(a) Variation of sheath air temperature with time for the ROYCO OPC .

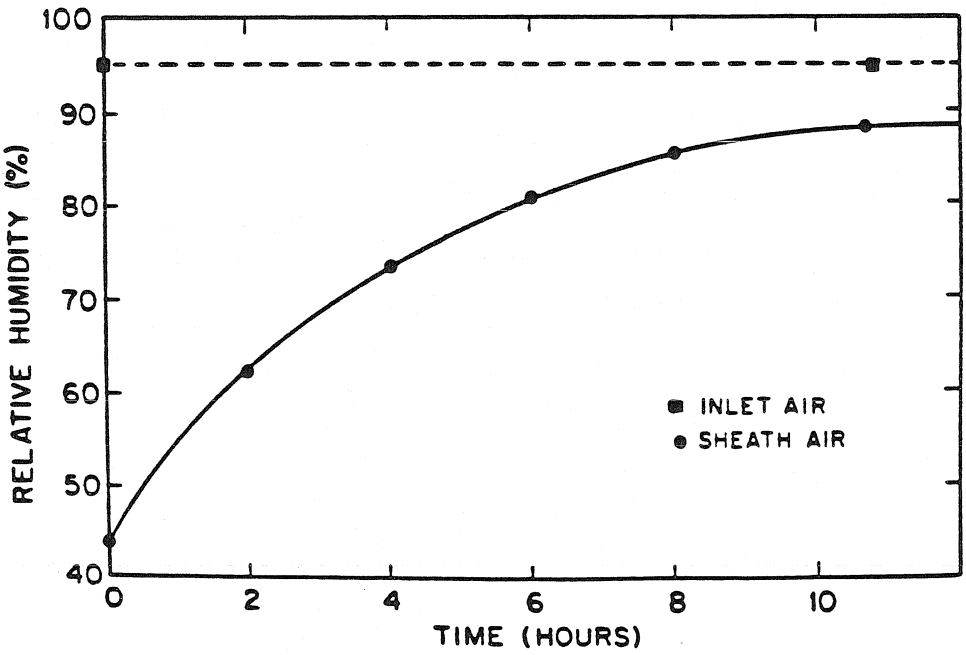

(b) Variation of sheath air relative humidity with time for a constant inlet relative humidity of 95% .

counterflow heat exchanger. The water temperature in the heat exchanger was controlled by a 'constant temperature' bath. The cartridge filters (both) in the flow path were replaced by a single Teflon membrane filter, 47 mm in diameter. The filter holder was placed outside the instrument for ease of replacement of the filter. The filter is replaced at the begining of each run to avoid the problem of loading by hygroscopic particles. These modifications are shown in Figure 3.20. The sheath air humidity was monitored and found to reach a steady value in a relatively short duration.

3.5.3 The Nozzle Problem

A schematic of the nozzle, used to focus the particles into the measuring region, is shown in Figure 3.21. The converging nozzle accelerates the flow, and leads to aerodynamic cooling. Table 3.3 lists some of the parameters. There is about a 30% increase in humidity. This calculation assumes the modifications to the OPC have been made (that is, temperatuure and relative humidity of the sheath air was the same as that of the inlet sample stream). Although growth of particles may be expected to occur under certain inlet conditions, the resolution of the instrument is not high enough to detect such changes.

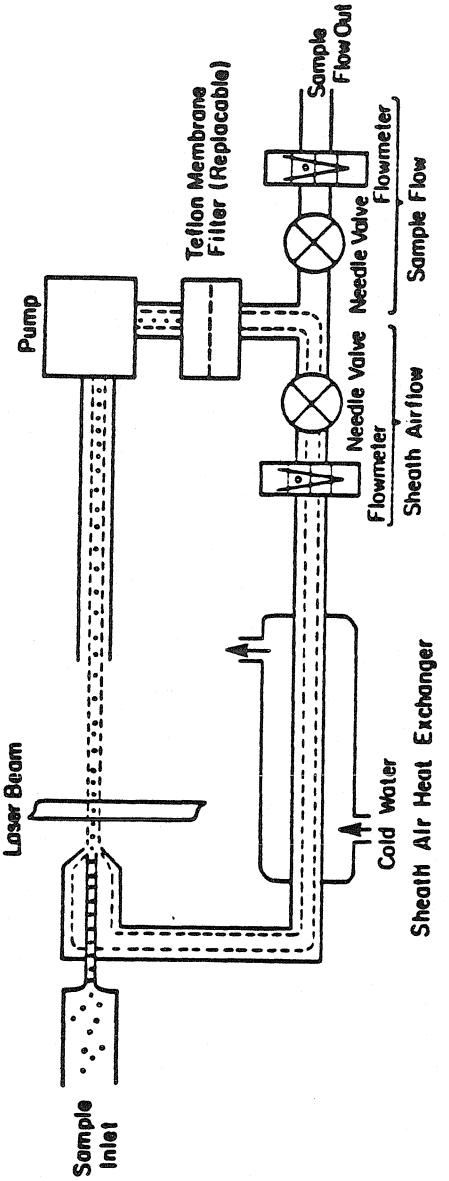

Figure 3.20 **MODIFIED FLOW DIAGRAM FOR THE ROYCO OPC.**

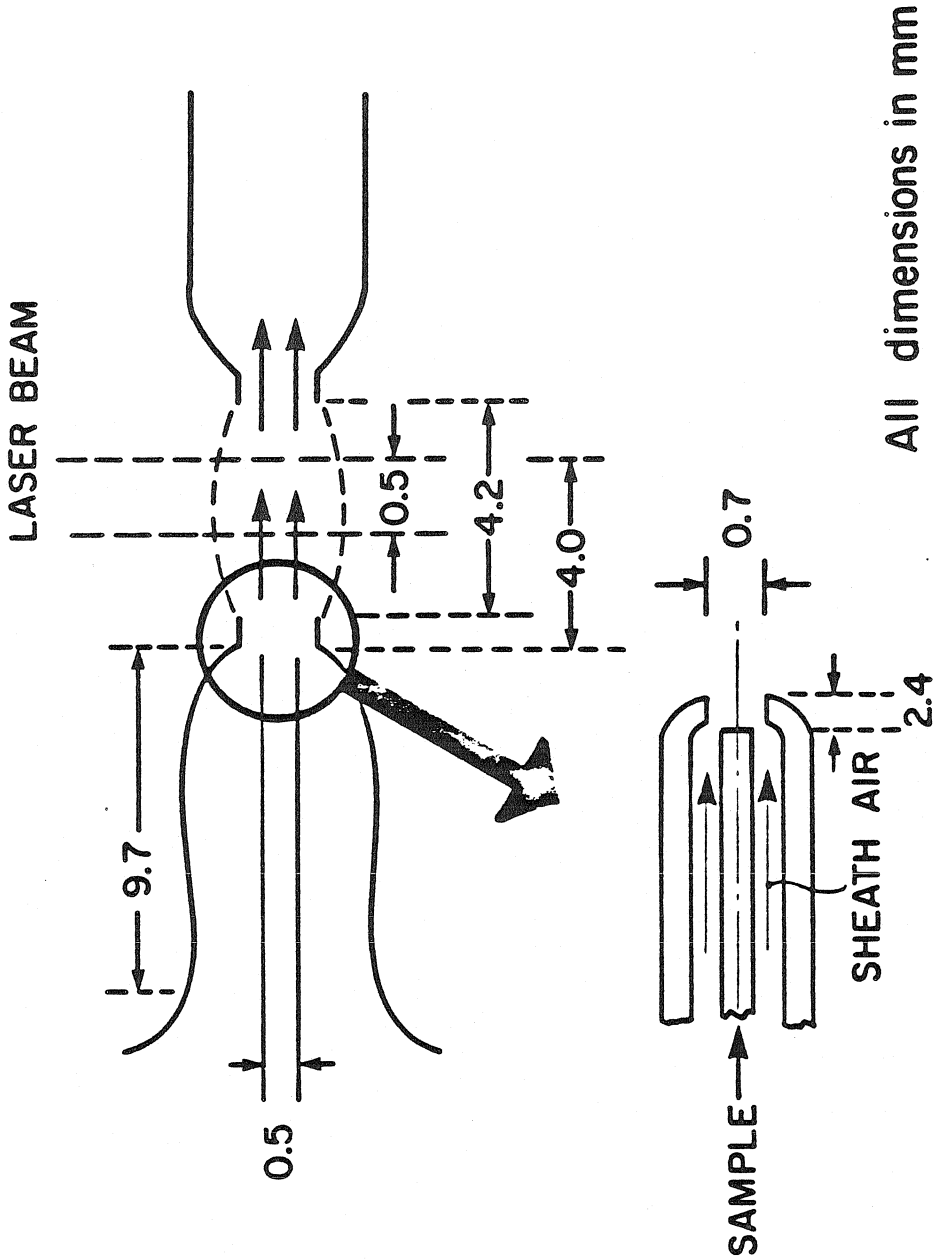

Figure 3.21 Schematic of the ROYCO OPC Model 226 nozzle.

TABLE 3.3: ROYCO OPTICAL PARTICLE COUNTER, MODEL 226

Sample Flow Rate	:	5 cc/s
Sheath Flow Rate	:	30 cc/s
U (Jet Velocity)	:	103 m/s
Mach Number	:	0.3
Pressure Ratio (Measuring Region to Inlet)	:	0.94
$(RH)_{measuring\ region}$ $(RH)_{inlet}$	:	1.3
Residence Time	:	39 microseconds

3.6 The Large Particle Counter

The CSASP-100-HV, built by Particle Measuring Systems (7), is an optical particle counter capable of sizing into fifteen classes. It has been designed to operate under a wide range of environmental conditions. One application where it has been used is the measurement of cloud and fog droplet sizes.

The instrument has a once-through flow system, with a converging section which accelerates the flow into the measuring region. A three percent increase in the relative humidity results in the measuring region due to this acceleration. The time available for growth is about 5.8 milliseconds. Fog droplets are assumed to be at 100% inlet relative humidity. The size of ammonium sulfate droplets in the measuring region is plotted against the size of particles at the inlet, as shown in Figure 3.22. A considerable increase in particle size in the 0.1 micron to 1 micron range is predicted; however, the bias is small for larger sizes.

3.7 Conclusions

The distortion of size distribution by some commonly used aerosol sampling instruments has been demonstrated both theoretically and experimentally. Pressure, temperature, and humidity changes in the instruments have been found to be the factors that lead to

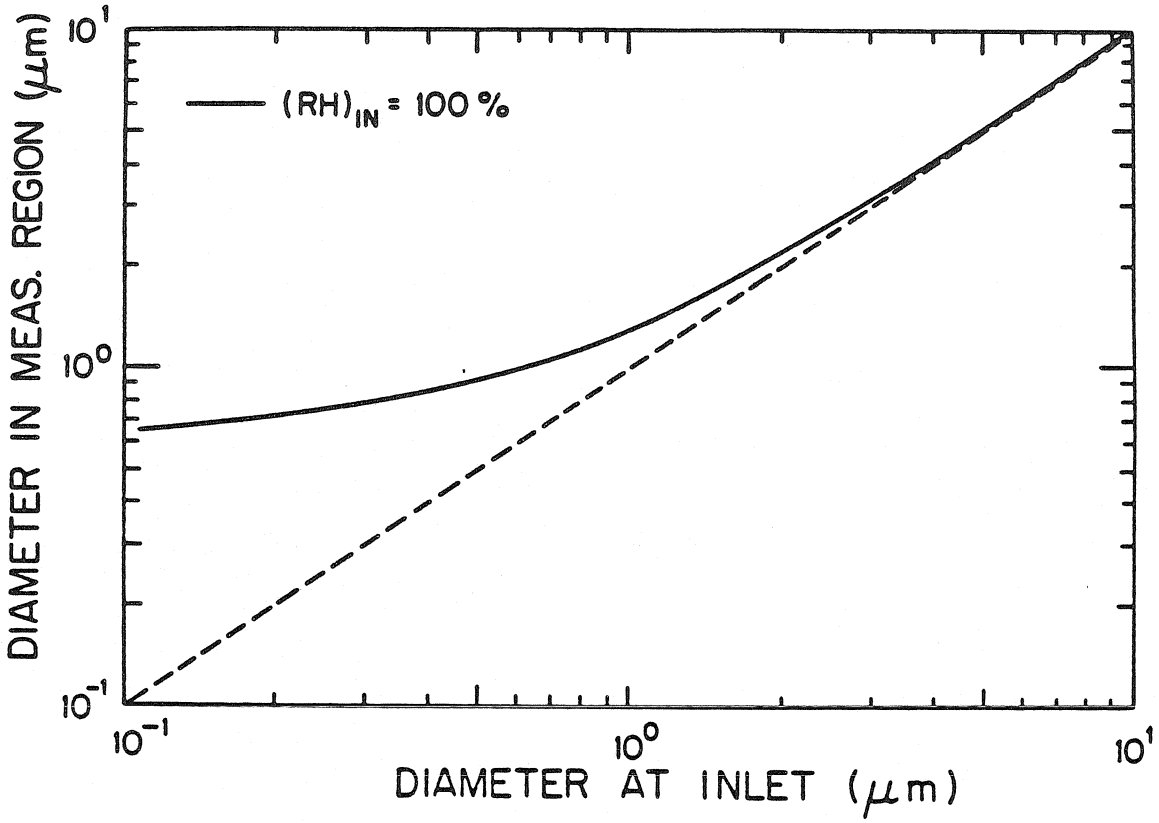

Figure 3.22 Variation of droplet diameter in measuring region with inlet diameter for the large particle optical counter

these distortions. The biases occur when aerosols with volatile species or in the presence of condensible vapors are sampled, and are most pronounced for small particles (less than 0.5 micron) at high humidities (close to 100%) or at humidities close to the deliquescent point of the particle.

Whenever aerosols, with volatile constituents or in the presence of a condensable phase are sampled, the possibility of size change within the instrument must be examined. The variation of pressure and temperature in the instrument must be first used to determine the change in relative humidity. The supplied code can then be used to determine the size changes occurring within the instrument. Restrictions in operating conditions can then be determined for obtaining unbiased aerosol-size distributions.

Footnote:

1) Transition from a solid particle to a droplet occurs suddenly when the relative humidity reaches a specific value corresponding to the water activity of the saturated solution (16). For the temperature range under consideration ($-25^{o}C$ to $30^{o}C$), the activity is a weak function of the temperature. The fit to experimental data (from 10, 11, 12) gives

$a(w) = 1.0011 - 0.0381\ m$ (Correlation coefficient = 0.998),

where, m is the molality of the droplet solution.

The solubility of ammonium sulfate is also a weak function of temperature (12),

$S(T) = 70.56 + 0.246\ T$ [gms $(NH_4)_2SO_4$/100 gms H_2O],

where, T is the temperature in ^{o}C. Using the above, the deliquescent humidity for ammonium sulfate varies from 81% at 20 ^{o}C to 83% at $-25^{o}C$. This is a minor variation, when compared to the saturation presuure, p_{sat}, which is a strong function of temperature.

2) The possibility of droplets freezing on stages 7 and 8 has been neglected.

3) A value of unity has been assumed for the accomodation coefficients (evaporation and condensation) in deriving the expression for the Fuchs-Sutugin factor. This has been shown to be the case (close to unity) for most liquids by Paul, B. (Am. Rocket Soc. J., 32, 1321, 1962); Nabavian, K. (Ph.D. Thesis, Univ. of Illinois, 1962); for water and

alcohols by Maa, J.R. (Ind. Eng. Chem. Fundam., 9, 283, 1970); and, Davies, E.J., et al. (Ind. Eng. Chem. Fundam., 14, 27, 1975).

Nomenclature

a_w : Water activity

d : Droplet diameter

D : Diffusion coefficient

k : Boltzmann's constant

Kn : Knudsen number

p : Partial pressure of the vapor

P : Total pressure

RH : Relative humidity

RH_d : Product of Kelvin correction term and activity

RHC : Crystallization Humidity

RHD : Deliquescent point

t : Time

T : Temperature (K)

v : Volume of droplet

v_m : Molecular volume

Greek

σ : Surface tension

Subscripts

d : Surface of droplet

sat : Saturated

vap : vapor

References

(1) Roeber, R.: Staub., 50, 418-420 (1957).

(2) Hochrainer, D.;Zebel, G.: J. Aerosol Sci., 12, 49-53 (1981).

(3) Mercer, T.T.; Tillery, M.I.; Newton, G.J.: J. Aerosol Sci., 1, 9-15 (1970).

(4) Hering, S.V.; Flagan, R.C.; Friedlander, S.K.: Environ. Sci. Technol., 12, 667-673 (1978).

(5) Bulletin No. 779-260, Model 266; Sierra Instruments, Inc. (1980).

(6) Operation Manual, Model 226, HIAC/ROYCO, Menlo Park, California.

(7) Operational Manual, CSASP-100-HV, Particle Measuring Systems, Denver, Colorado.

(8) Friedlander, S.K.: Smoke, Dust, and Haze, Wiley:New York (1977).

(9) Biswas, P.; Flagan, R.C.: Environ. Sci. Technol., 18, 611-616 (1984).

(10) Robinson, R.A.; Stokes, R.H.: Electrolyte Solutions, 2nd ed., Butterworths, London (1959).

(11) Wishaw, B.F.; Stokes, R.H.: Trasns. Faraday Soc., 50, 952-954 (1954).

(12) International Critical Tables, ed. Washburn, E.W., pp. 363, McGraw Hill Book Company: New York (1928).

(13) Roberts, P.S.; Friedlander, S.K.: Atmos. Environ., 10, 403-408 (1976).

(14) Stainton, M.P.; Capel, M.J.; Armstrong, F.A.J.: The Chemical Analysis of Fresh Water, pp 69-71, Freshwater Institute, Winnipeg (1977).

(15) Marple, V.A.: in Aerosols, ed. Liu, B.Y.H.; Pui, D.Y.H.; Fissan, H.J.; 112-114 (1984).

(16) Tang, I.N. : in Generation of Aerosols and Facilities for Exposure Experiments, ed. K. Willeke, 153-167, Ann Arbor Science: Ann Arbor (1980).

(17) Orr, C. Jr.; Hurd, F.K.; Corbett, W.J.: J. Colloid Sci., 13, 472-482 (1958).

(18) Flagan, R.C.: J. Colloid and Interface Sci., 87, 291-299 (1982).

(19) Schlichting, H.: in Boundary Layer Theory, 78-83, McGraw Hill: New York (1962).

(20) Marple, V.A.: Fundamental Study of Inertial Impactors, Ph.D. thesis, University of Minnesota (1970).

(21) Ouimette, J.R.: Aerosol Chemical Species Contributions to the Extinction Coefficient, Ph.D. thesis, California Institute of Technology (1980).

CHAPTER 4

THE PARTICLE TRAP IMPACTOR

4.1 Introduction

Inertial Impactors are widely used instruments for measuring aerosol size distributions. Design procedures have been developed by Marple, et al. (1,2) that result in sharp cut-off characteristics. Recently, Biswas and Flagan (3) have shown that their operation can be extended to the compressible flow limit; the characteristics remaining steep provided the Stokes number is computed at the stagnation point condition. Some limitations of impactor use were described in the previous chapter. However, they can be used for sampling dry aerosol particles or particles in the absence of condensible vapors. Hence, when impactors are designed, operated correctly and the data are interpreted carefully, reliable and accurate size distribution information can be obtained.

There are important operational restrictions in the use of these instruments. A detailed study of these has been carried out by Rao and Whitby (4,5). These problems are: particle bounce off the collection surface, blow off or reentrainment, deagglomeration or break up, and wall losses. Proper design and operation can minimize these losses. Particle bounce is generally minimized by coating the impaction surface by a sticky substrate such as grease or vaseline. Studies on particle bounce have been done by Cheng and Yeh (6) and a good description of impaction collection surfaces is given by Wesolowski (7).

Reentrainment refers to the dislodging of previously collected particles from the impaction surface. This is not such a severe problem provided the impaction surface is coated with a sticky substrate and the mass loading is not too high. Re-entrainment is also minimized by keeping the sampling times short enough to prevent collection of excessive material on any single stage, and consequent blow off. Wall losses, also known as interstage losses, can be reduced to small values by proper design and operation (8).

The problems of blow off, limited sampling time, and cumbersome extraction procedures led to the development of virtual impactors: instruments in which the collected particles are removed along with a portion of the flow to some quiescent region (9,10). Calculations have also been done for such impactors to decide on optimal geometries (11). Schott and Ranz (12) designed and tested out a jet-cone impactor, where they introduced a conical surface in the cavity to enhance trapping of particles. Marple and Chien (13) determined the characteristics of virtual impactors by numerical solution of the Navier-Stokes equations. They also determined the effect of various parameters on the efficiency-Stokes number characteristics. The important parameters are the jet Reynolds number, and Q_1/Q_0, the ratio of the secondary flow to the main flow. They showed that the penetration of streamlines into the collection probe is larger at lower Reynolds numbers.

Streamline penetration into the cavity also occurs because of the minor flow. These lead to less steep collection efficiency characteristics because a fraction (typically 10%) of the small particles which would bypass the stage of a conventional impactor are drawn into the collection system along with the sample. The use of bleed flow complicates the operation of the virtual impactor. In a multistage device, each stage would require a flow control device to obtain the desired minor flow. Also, many adjustments have to be made for different conditions of impactor operation.

These difficulties in virtual impactor operation led us to consider the concept of 'Particle Trap Impactors'. The secondary (or minor) flow is eliminated, and the collection surface is replaced by a quiescent cavity. A particle which would normally impinge on the collection surface now enters the cavity where it is ultimately captured. This is analogous to the case of $Q_1/Q_0 \dashrightarrow 0$; and results in the steepest efficiency-Stokes number curve (13). Because streamlines that do penetrate undergo sharp directional changes, it is likely that some particles that should bypass the stage may also end up being collected. Marple's (13) calculations indicate that this is not a very serious problem.

The parameters that are expected to have an effect on the collection characteristics are:

D_0/D, D_c/D_0, S_c/D_0, Re.

Ranz and Schott (12) suggested that particle retention could be enhanced by inserting a cone at the inlet to the cavity to bounce particles deeper into the cavity. This would then intoduce the additional design parameters:

H/D_0, Angle of cone (see Figure 4.2).

The paper presents an experimental evaluation of particle trap impactors.

4.2 Experimental

The impactor used for the particle trap studies is based on the design of Marple (1) and has been used for previous high jet velocity impaction studies (3). It is illustrated in Figure 4.1. It has the capability of easily varying the jet-to-plate spacing, jet diameter, and interchanging the impaction surface. Cavities of different shapes and sizes could be used (Figure 4.2). After assembly, a long needle was used to check the concentricity of the jet nozzle with the collection cavity opening.

Calibration aerosols were generated by the T.S.I. model 3050 vibrating orifice aerosol generator using sodium fluorescein solutions. The aerosol was neutralized using a Kr-85 decharger and then dried in a silica gel diffusion column. The T.S.I. model 3071 Electrostatic Classifier was used to classify the aerosol in some of the high velocity runs.

Extraction procedures described by Hering, et al.

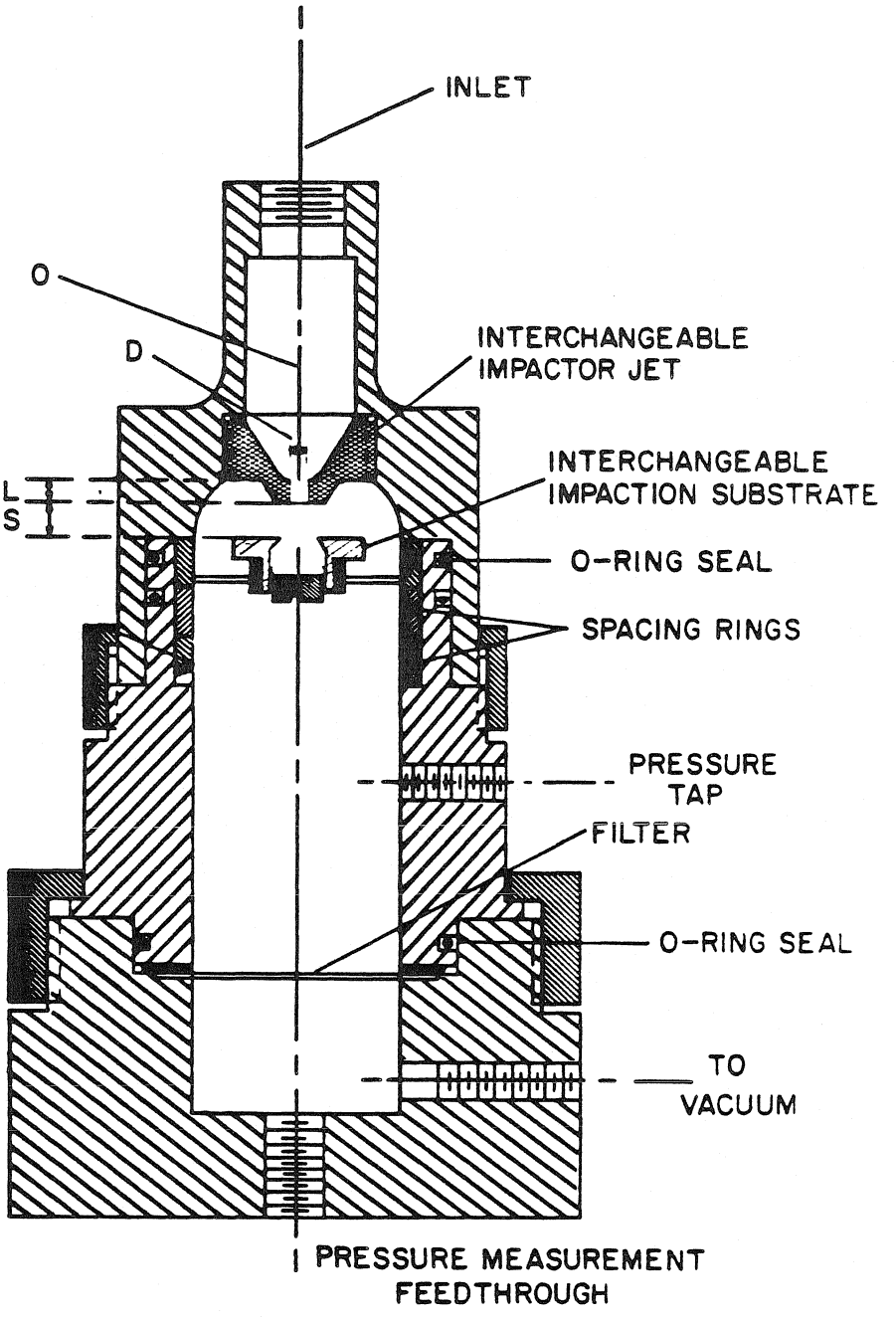

Figure 4.1 Schematic of the particle trap impactor.

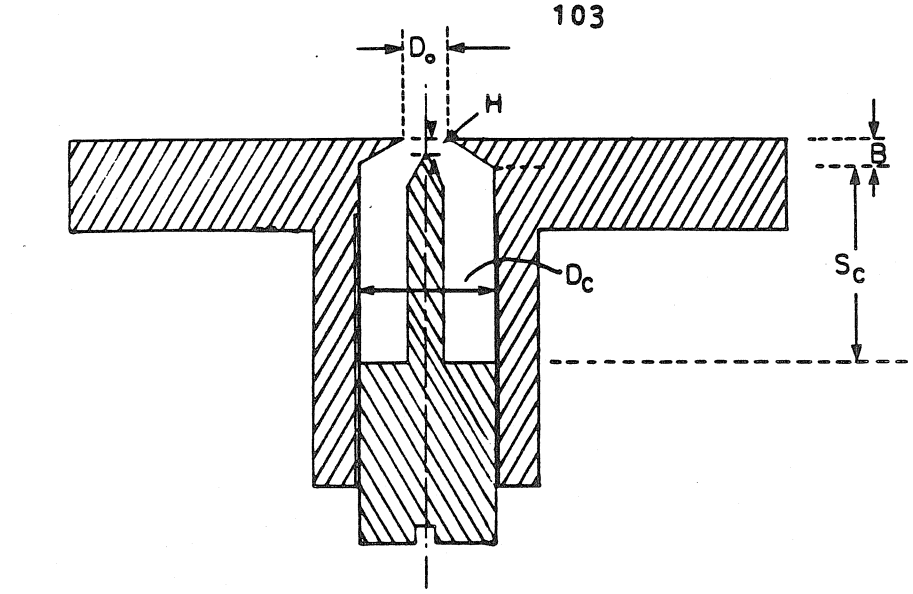

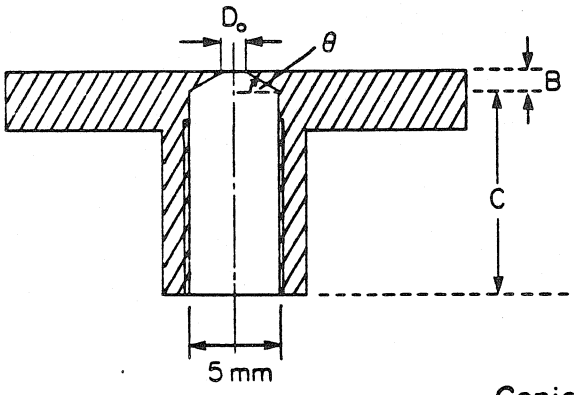

D_o (mm)	θ (°)	B (mm)	C (mm)
0.9	33	1.3	11.9
1.4	33	1.1	12.0
1.9	33	1.0	12.2

Conical Stainless Steel Plugs

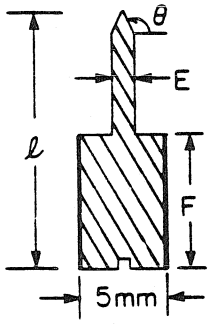

θ (°)	E (mm)	F (mm)	ℓ (mm)
45	0.9	6.7	13.2
60	0.9	6.6	13.2
45	1.4	6.7	13.2
60	1.4	6.7	13.2
45	1.9	6.7	13.2
60	1.9	6.7	13.2

Flat Stainless Steel Plugs

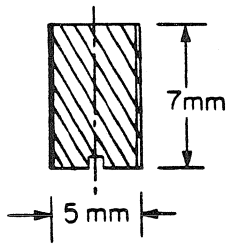

Figure 4.2 Shapes and sizes of ditferent cavities.

(14) were used to determine the collection efficiencies. The number concentrations of the particles upstream and downstream of the stage were measured using the ROYCO OPC to verify the result obtained by the extractive analysis. The downstream measurement was done far enough downstream to ensure a representative number concentration. The upstream and downstream measurements were compared without the impaction plate in place to ensure that the error in efficiency computation was within acceptable limits.

4.3 Results

Experiments were performed to determine the optimal combination of D_0/D, S_c/D_0, and the cavity type (empty or with conical needle). S/D, the ratio of the jet-to-plate spacing to jet diameter, was held constant (= 2) for all experiments. After a combination that gave a sharp efficiency-Stokes number characteristic was obtained, it was tested extensively under different conditions, e.g. high jet Mach number, large sampling durations.

4.3.1 Effect of cavity opening: Variation of D_0/D

This was done for two values of D_0/D = 1.4 and 1.9. The lower value of D_0/D gave an efficiency-$St^{1/2}$ characteristic with lot of spread (Figure 4.3). There is a spread in the particle stream impinging on the plate, and hence, if the cavity opening is smaller than this spread,

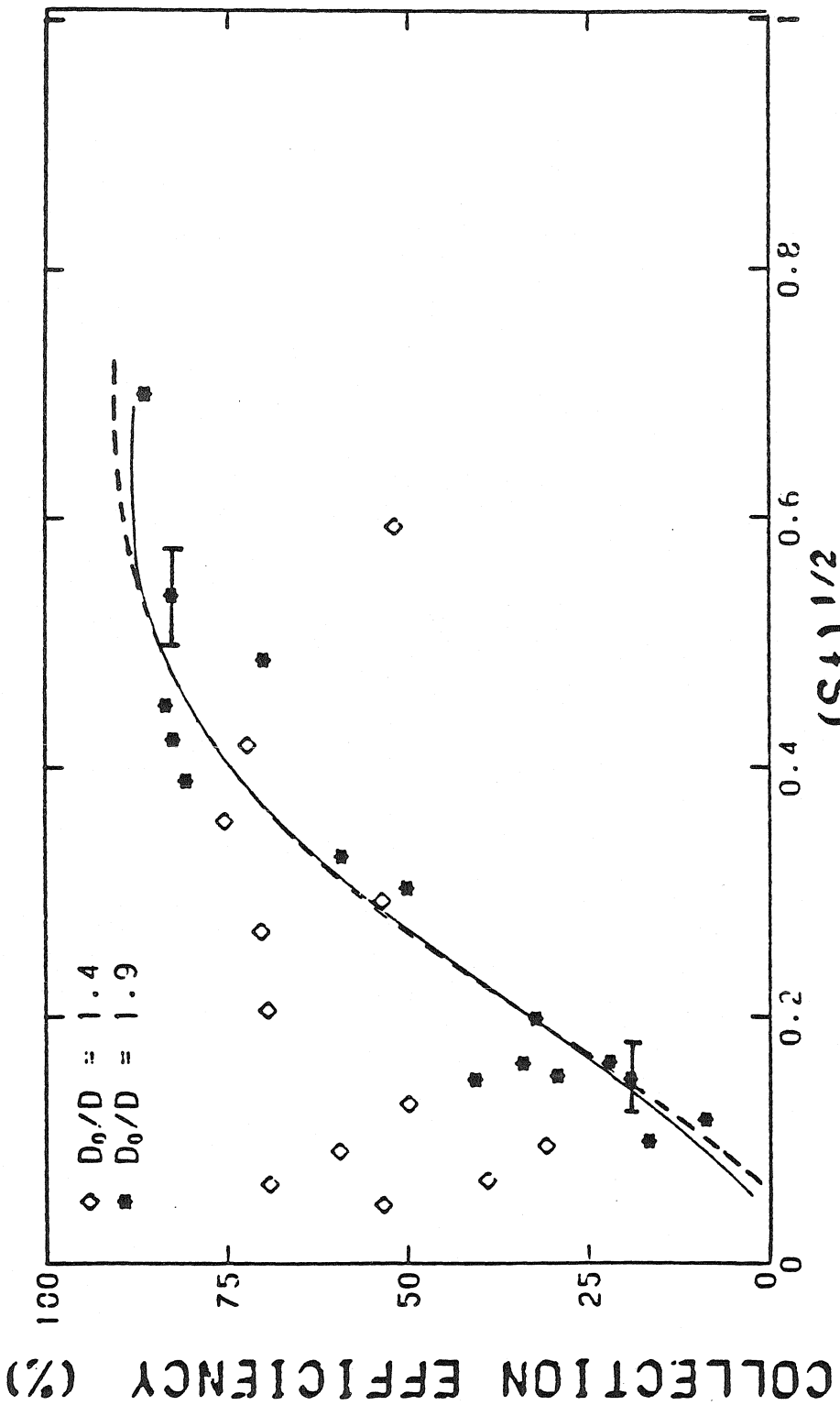

Figure 4.3 Effect of ratio of cavity opening to jet diameter on impactor performance (◇) $D_0/D = 1.4$; (★) $D_0/D = 1.9$ Solid line is fit to data for $D_0/D = 1.9$

Dotted curve is fit to calibration data for the impactor with a greased plate.

particles would impinge on the solid surface and would have a higher chance of bouncing off. A sharp efficiency-Stokes number characteristic is obtained for $D_0/D = 1.9$.

4.3.2 Effect of cavity depth, S_c (fixed $D_0/D = 1.9$)

The efficiency - $St^{1/2}$ characteristics for three different values of $S_c/D_0 = 3.0$, 3.9, and 4.9 are plotted in Figure 4.4. A slight upward (or leftward) shift can be noted for higher values of S_c/D_0. This may be due to the deeper penetration of the streamlines at larger cavity depths. The reduction in St_{50} is marginal and within the error bounds.

4.3.3 Effect of cavity shape: Empty cavity vs. cavity with cone

Although empty cavities give reasonably sharp efficiency - Stokes number characteristics (Figures 4.3 and 4.4), a cavity with a conical needle was examined to see if the collection characteristic could be improved. There are a number of parameters that could be varied: depth of cavity ratio (S_c/D_0), ratio of diameter of the conical needle to the diameter of the cavity opening, aspect ratio of the cavity (S_c/D_c), H/D_0, and the angle of the cone (see Figure 4.2). Figure 4.5 is a plot of the efficiency versus square root of Stokes number where H/D_0 is varied as a parameter. Comparing an empty cavity characterisitic with that of one with a conical needle, there is not any significant

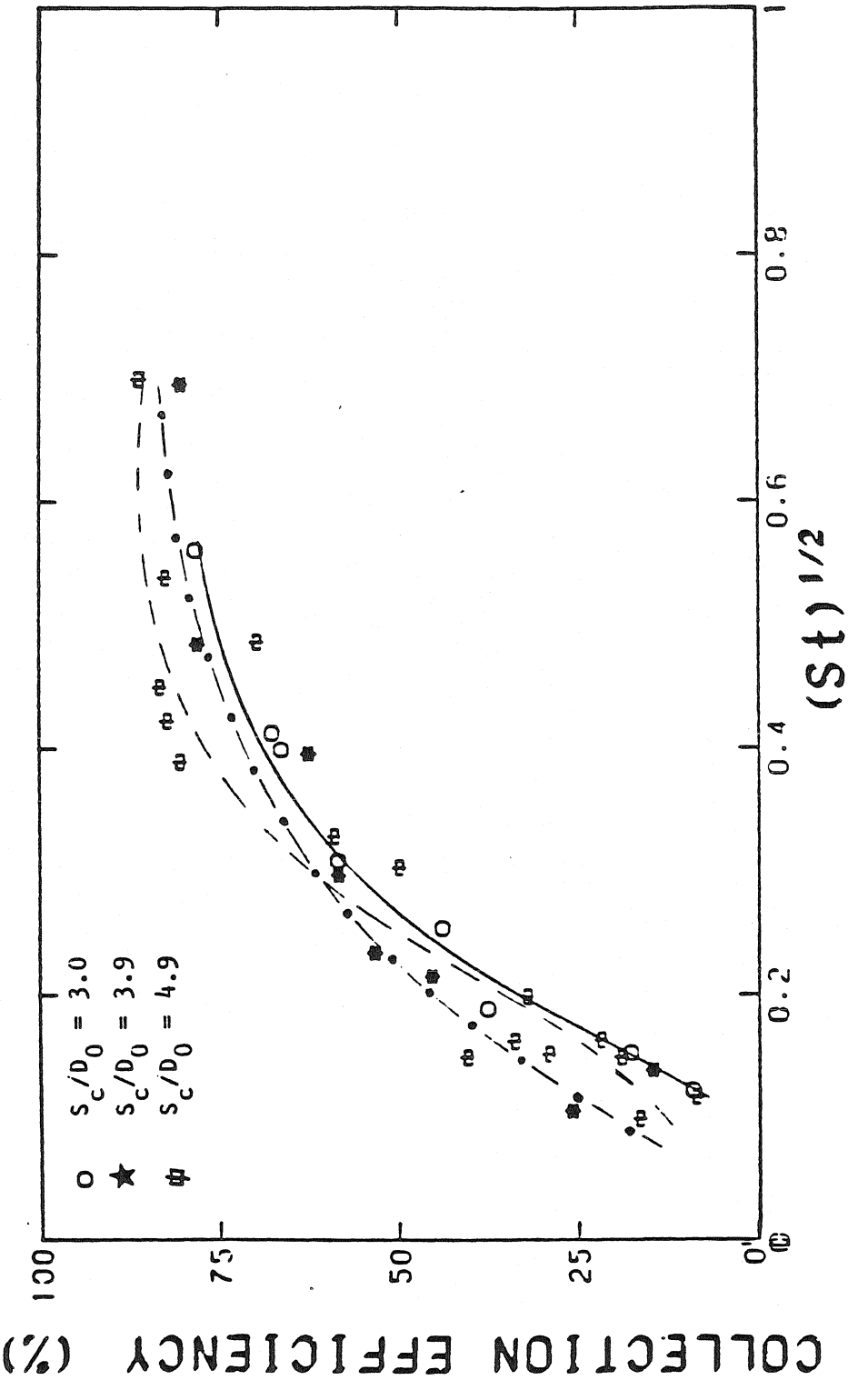

Figure 4.4 Effect of ratio of cavity depth (S_c) to diameter of cavity opening (D_0) on impactor performance for a fixed $D_0/D = 1.9$. Curves are approximate fit to data.

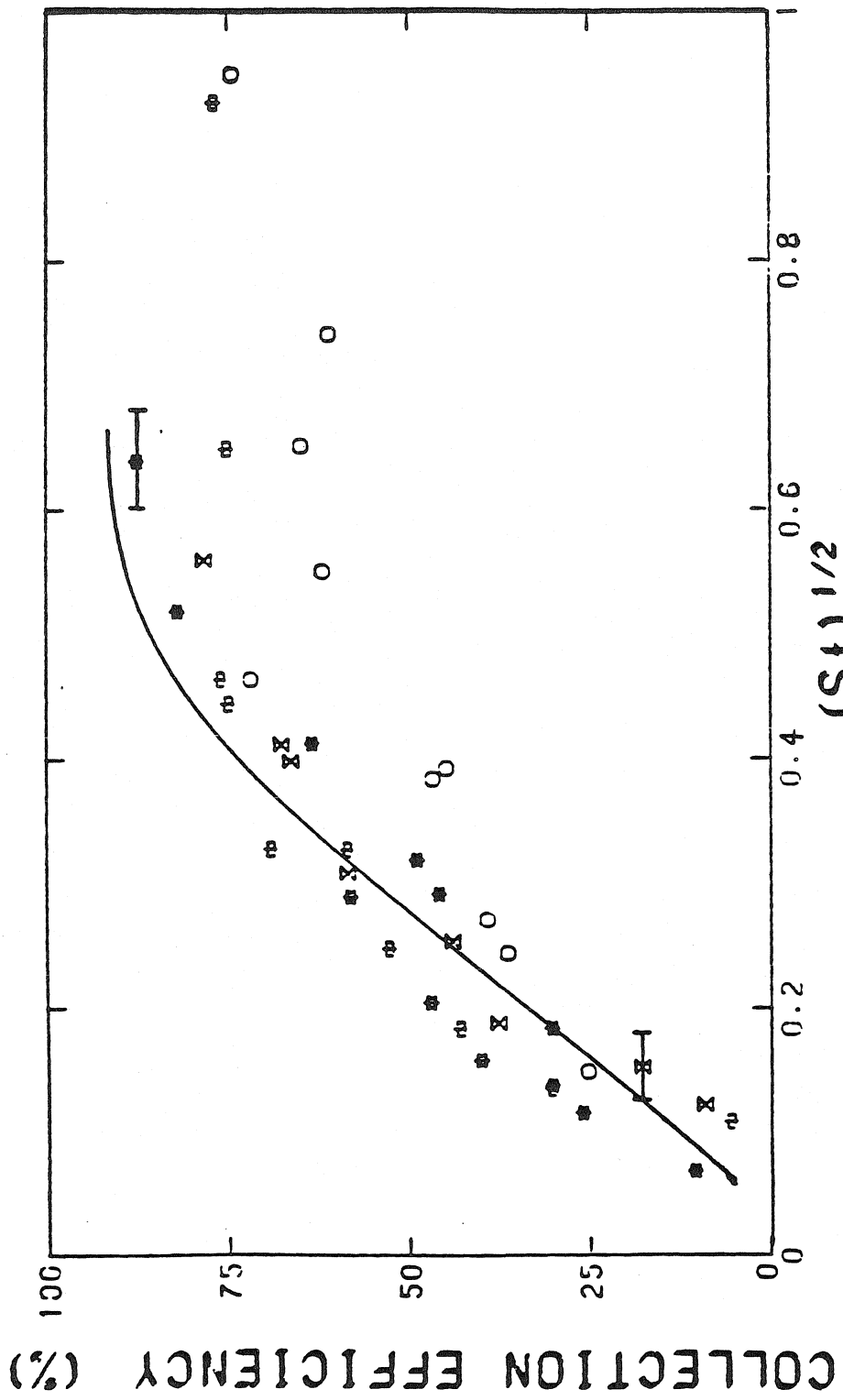

Figure 4.5 Comparison of performance of the particle trap impactor with and without a cone in the cavity for different values of H/D_0. (O) $H/D_0 = 1.94$; (✱) $H/D_0 = 0.94$; (⊕) $H/D_0 = 0.04$; (⊠) Cavity with no cone.

improvement in the collection characteristic.

Hence, for the ease of particle trap production and sample extraction for subsequent analysis, a cavity with no conical needle was used for further study.

4.3.4 Performance at pressure ratios ranging from 0.5 to 1.0

The performance of the particle trap impactor at high jet velocities was determined. The characteristics are plotted for five values of the pressure ratio, r = 0.98, 0.9, 0.83, 0.76 and 0.5; in Figure 4.6. Mach numbers ranged from 0.2 (incompressible flow) to 1.0 (sonic).

Apart from a slight leftward shift, which may be due to the Reynolds number effect, the results indicate that the characteristic is fairly independent of the pressure ratio as in the case of conventional impactors described in Chapter 2. The Stokes number was computed based on the property values determined at the stagnation condition (3). It was very important for the impactor jet and the opening of the collection cavity to be well aligned for obtaining a sharp efficiency - Stokes number characteristic.

4.3.5 Long sampling time performance

One of the limitations to the use of conventional impactors is that the sampling time is restricted to prevent reentrainment of collected particles. This is expected to be a less severe problem in the case of the particle trap impactor, as the particles are removed into a quiescent

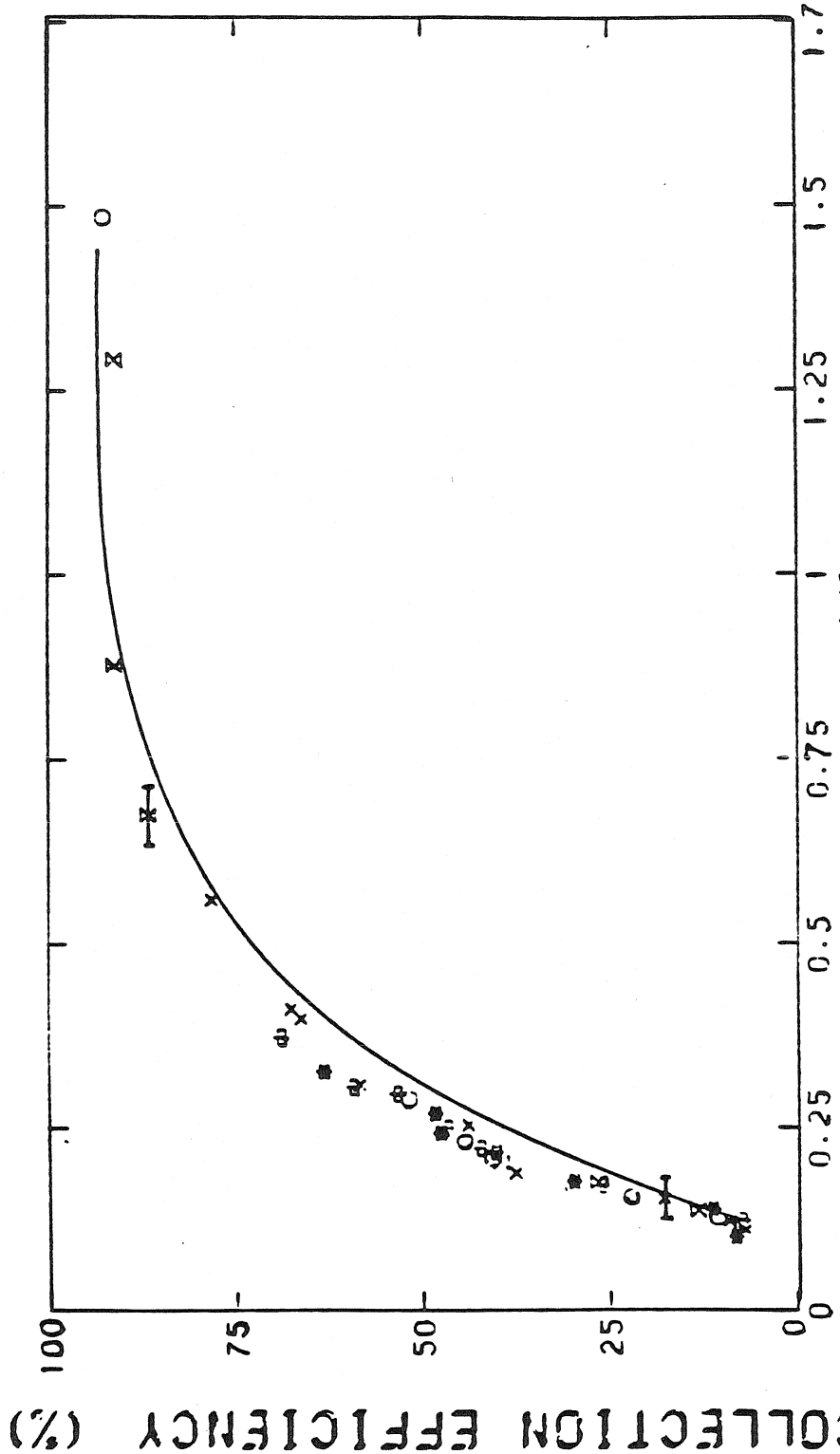

Figure 4.6 Particle Trap Impactor performance at inlet atmospheric pressure for different pressure ratios: (✱) r = 0.5, Jet Mach Number = 1, Re = 11355; (✱) r = 0.76, Jet Mach number = 0.7, Re = 9987; (O) r = 0.83, Jet Mach Number = 0.6, Re = 8618; (⧖) r = 0.9, Jet Mach Number = 0.4, Re = 7251; (X) r = 0.98, Jet Mach Number = 0.2. Curve is a fit to incompressible flow regime calibration data.

region, away from the main flow. Theoretically, the sampling time could be long enough until the cavity is nearly full of particles.

Three different experiments were carried out with sampling times of about 4, 8, and 25 hours. As a constant source of aerosol particles was required, the syringes in the vibrating orifice aerosol generator had to be refilled every four hours. After refilling, a check was made to ensure that the inlet monodisperse aerosol was stable and of the same size as the previous case (before refilling). At the end of the run, the collection cavity and backup filter were carefully weighed; the amounts of fluorescein collected were also determined by extraction and subsequent fluorometric analysis.

The results are shown in Figures 4.7, 4.8, and 4.9. Collection efficiency (as measured by the ROYCO OPC) was found to stay relatively constant over long periods of time. In the experiment, whose results are plotted in Figure 4.9, there is a drop in efficiency after about 24 hours of operation. On inspection, the cavity was found to be completely filled. The collected mass of fluorescein weighed as much as 8 mg.

4.4 Conclusion

The particle trap impactor is a very promising modification of the conventional cascade impactor. The

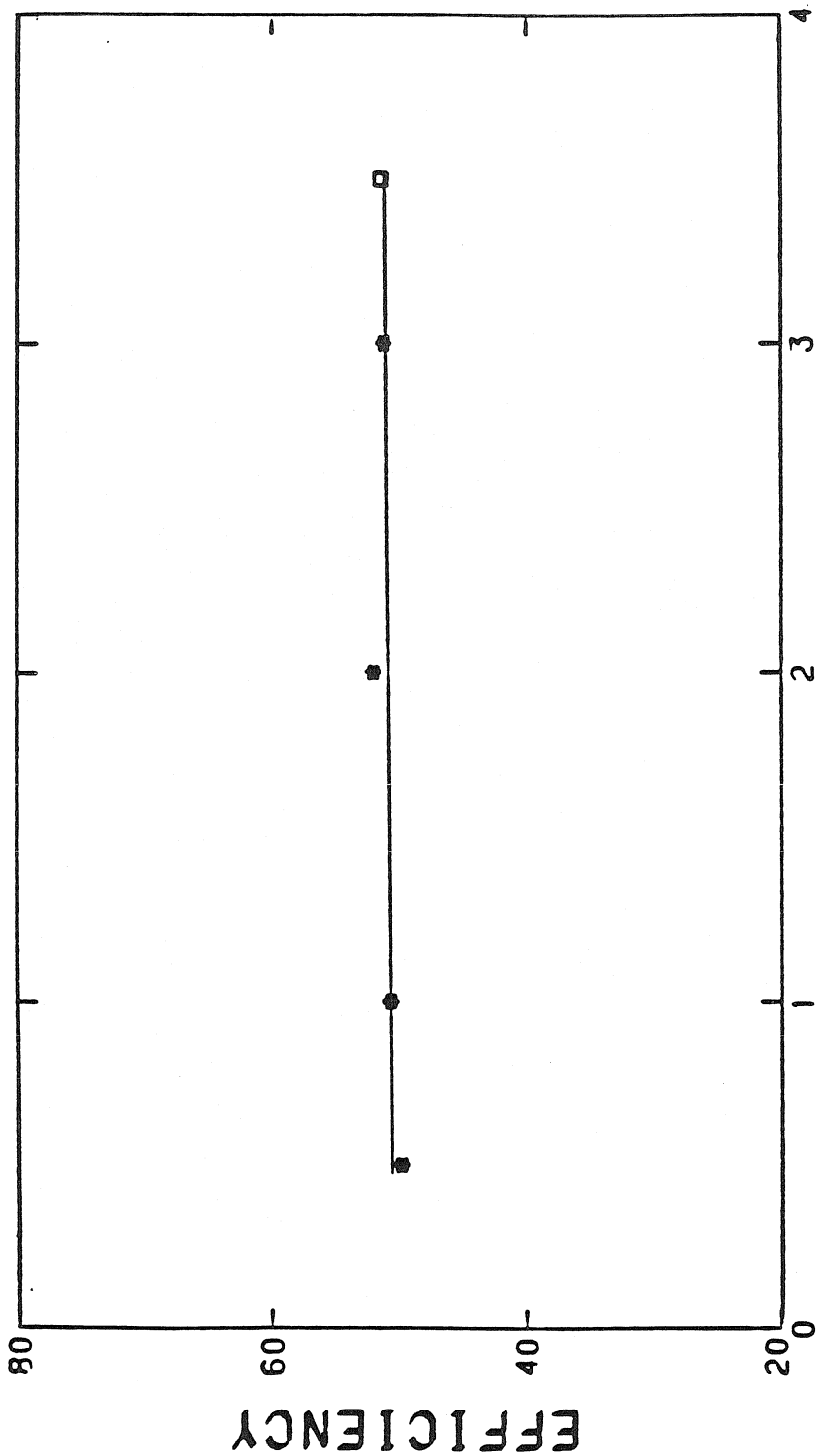

Figure 4.7 Collection efficiency as a function of time for a single stage of the Particle Trap Impactor. (★) Measured by the ROYCO OPC; (□) By Flurometric Analysis

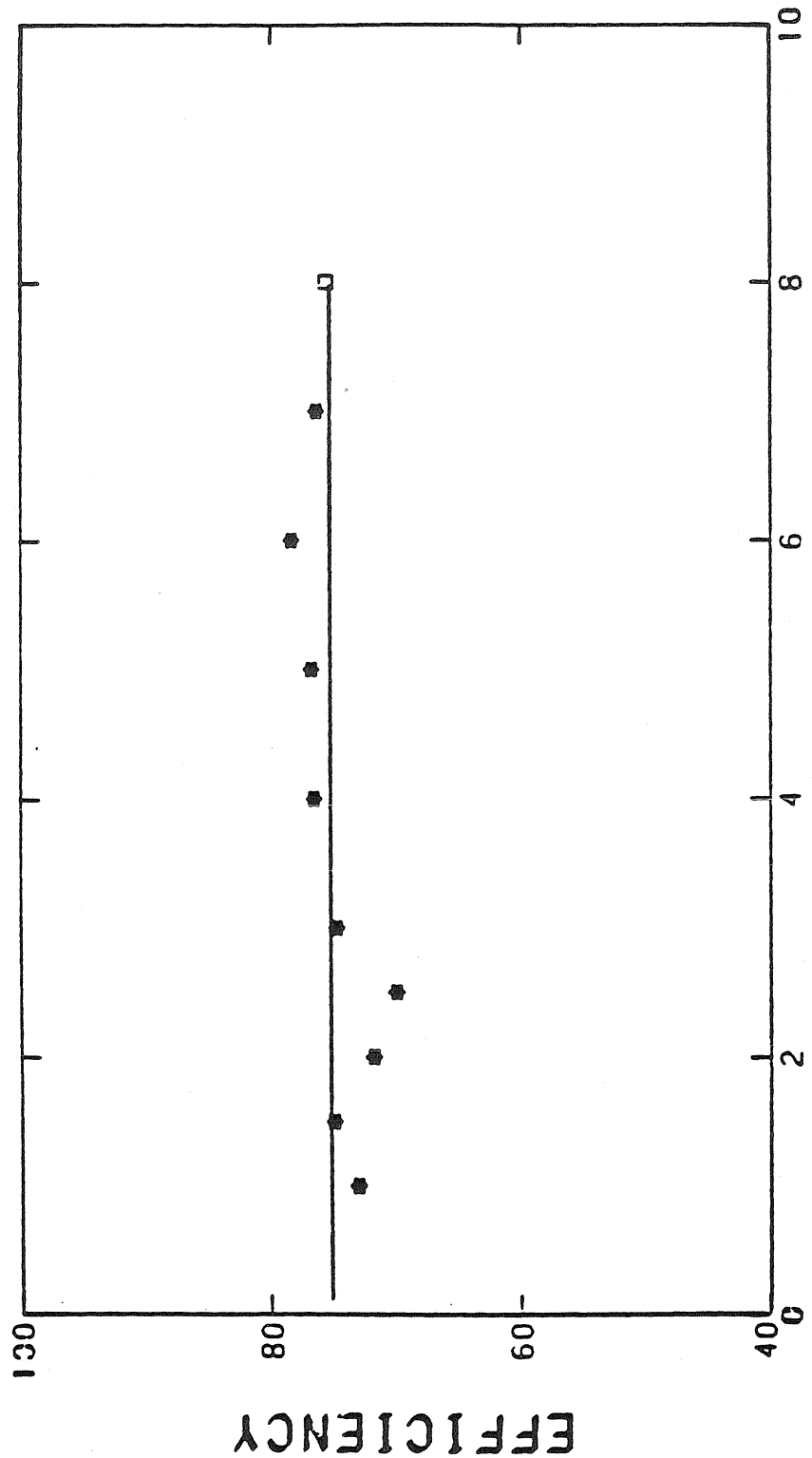

Figure 4.8 Variation of collection efficiency with time for the Particle Trap Impactor. (★) Measured by the ROYCO OPC; (□) Determined by fluorometric analysis at the end of the run.

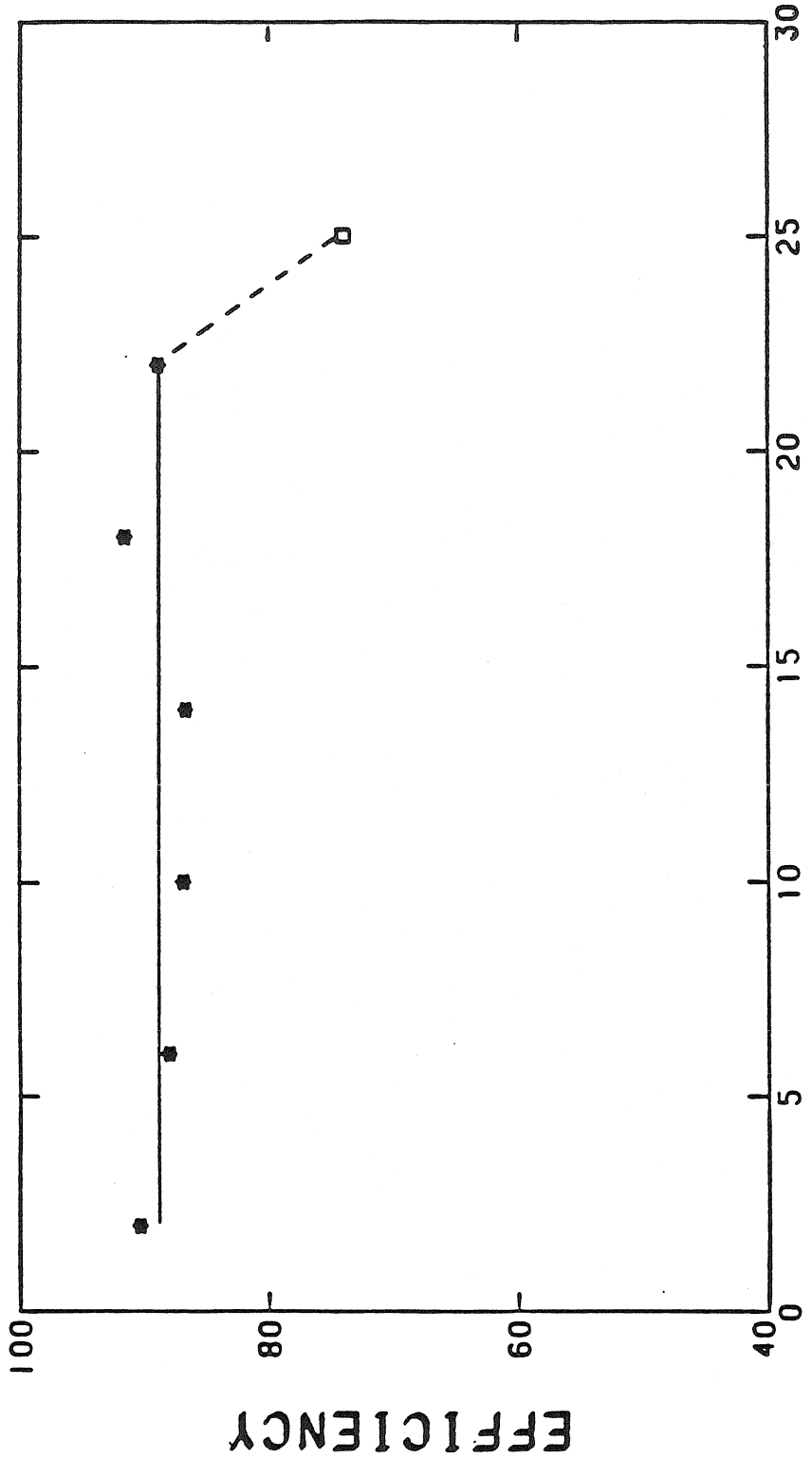

Figure 4.9 Collection efficency as a function of time for the Particle Trap Impactor. (★) Measured by the ROYCO OPC; (□) By fluorometric analysis at end of run.

inherent problems of bounce and reentrainment in conventional impactors have been minimized without the addition of other substrates such as grease. Sampling durations can also be much longer than with greased substrates. Because larger masses can be collected, errors in extraction and subsequent analysis could be reduced. Comparisons of characteristics of such devices with that of conventional impactors indicate that the performance of particle trap devices is nearly as good, although the collection characteristic is slightly less steep, possibly due to reentrainment from the cavity. The performance at high jet velocities was also good. Sharp efficiency-Stokes number characteristics of particle trap impactors clearly require careful alignment of the nozzle and the cavity opening.

There are a number of promising applications for such devices: both as an impactor and as a particle collection device in other industrial processes. They have all the advantages of virtual impactors, but are much simpler to use. A high temperature application is logical because greases in conventional devices cannot withstand the high temperatures. The performance at high temperatures will be discussed in the next chapter.

Nomenclature

D	:	Diameter of nozzle (or jet)
D_0	:	Diameter of cavity opening
D_c	:	Diameter of cylindrical portion in cavity
H	:	Distance from tip of needle to cavity opening
Q_0	:	Secondary (or minor) flow
Q_1	:	Main (or major) flow
Re	:	Reynolds number
S	:	Jet-to-plate spacing
S_c	:	Depth of cavity
St	:	Stokes number

References

(1) Marple, V.A.; Liu, B.Y.H.: Environ. Sci. Technol., 8, 648-654 (1974).

(2) Marple, V.A.; Liu, B.Y.H.; Whitby, K.T.: J. Aerosol Sci., 5, 1-16 (1974).

(3) Biswas, P.; Flagan, R.C: Environ. Sci. Technol., 18, 611-616 (1984).

(4) Rao, A.K.; Whitby, K.T.: J. Aerosol Sci., 9, 77-86 (1978).

(5) Rao, A.K.; Whitby, K.T.: J. Aerosol Sci., 9, 87-100 (1978).

(6) Cheng, Y.S.; Yeh, H.C.: Environ. Sci. Technol., 13, 1392-1396 (1979).

(7) Wesolowski, J.J; John, W.; Duor, W.; Cahill, T.A.; Feeney, P.J.; Wolfe, G.; Flocchini, R.: X-Ray Fluorescence Analysis of Environmental Samples, 121-131, Ann Arbor Science: Ann Arbor (1977).

(8) Lundgren, D.A.: J. Air Poll. Con. Assoc., 17, 225-229 (1967).

(9) Hounam, R.F.; Sherwood, R.J.: Ind. Hyg. J., Mar-Apr, 122-131 (1965).

(10) Conner, W.D.: J. Air Poll. Con. Assoc., 16, 35-38 (1966).

(11) Ravenhall, D.G.,; Forney, L.J.; Jazayeri, M.: J. Colloid Interface Sci., 65, 108-117 (1978).

(12) Schott, J.H; Ranz, W.E.: Environ. Sci. Technol., 10, 1250-1256 (1976).

(13) Marple, V.A.; Chien, C.M.: Environ. Sci. Technol., 14, 976-985 (1980).

(14) Hering, S.V.; Friedlander, S.K.; Collins, J.J.; Richards, L.W.: Environ. Sci. Technol., 13, 184-188 (1979).

CHAPTER 5

THE PARTICLE TRAP: A HIGH TEMPERATURE APPLICATION

5.1 Introduction

The importance of measuring the size distribution in high temperature processes has been outlined in Chapter 1. The cascade impactor is a very appropriate instrument for classification of particles according to size at elevated temmperatures (1). The main problem encountered when using the impactor under stack conditions is to find an impaction substrate that can withstand high temperature and minimize particle bounce.

A number of impactors have been built to operate at high temperature and pressure. Parker, et al. (2) built a single stage high temperature, high pressure impactor. Ceramic fiber substrates were used as impaction plates. Gaskets were used as seals in the impactor. Good agreement between the greased plate and fiber substrate cut diameters were obtained when the impactor was calibrated at room temperature. However, the collection efficiency curves are expected to be less steep in the case of a filter substrate, reducing size resolution (3). Considerable scatter in data was observed, which was attributed to particle bounce. The impactor was operated at considerably low jet velocities; the problem of bounce would be more severe if operated at higher jet velocities.

The MRI in-stack virtual impactor has been described by Woffinden, et al (4). They found wall losses to be considerable. Other limitations of virtual impactors

have been described in Chapter 4.

Newton, et al. (5) designed a high temperature, high pressure cascade impactor. It is a seven stage instrument built of 304 stainless steel. Gold wire (20 mil) was used as an interstage seal. New gold wire was used for each run, the flattened scrap being saved after the run. Six bolts held the entire assembly together. Ungreased stainless steel strips were used as an impactor substrate, thus the impactor had to be operated under restricted conditions to minimize particle bounce, as suggested by Cheng and Yeh (6). The tests were conducted using sticky particles, which also tend to reduce particle bounce.

Novick, et al. (7) have designed a multi-stage virtual impactor with a simpler flow configuration. The instrument is limited to a couple of stages (two), and would have to be used a number of times to obtain the complete size distribution. Also, the pressure needs to be known at a number of locations for accurate flow estimation.

Currently, high temperature sampling in many cases is often done by diluting the aerosol stream to cool it first, and then using a conventional instrument for classification (8, 9, 10). Volatile particles may undergo physical (size) and chemical changes, thus leading to a distorted size distribution.

The particle trap impactor described in Chapter 4 is ideally suited for high temperature applications. The

flat impaction surface is replaced by a quiescent cavity, eliminating the problem of bounce and thus the need to use a sticky substrate. The device has been tested under high temperature conditions by placing the entire unit in a temperature controlled furnace.

5.2 Experimental

The impactor used for the high temperature studies was based on the design of the particle trap impactor described in Chapter 4. A single stage impactor was used for test purposes. Table 5.1 lists various stainless steels and their heat resistivity to intermittent and continuous service (11). The material used for the impactor was SS 446, which can withstand a temperature of 1100 ^{o}C. Annealed copper was used as a gasket material, and, when dimpled, was found to be an effective seal. The unit was leak tested under reasonably high pressures (about 40 to 45 psig). Antiseeze material for high temperature applications, manufactured by Never-Seez Compounds Corporation, was used to prevent seizure of threads. The entire unit was placed in a temperature controlled furnace for testing at high temperatures.

$CaSO_4$ solutions were used to produce monodisperse particles using the TSI model 3030 vibrating orifice aerosol generator. The aerosol was preheated to the temperature of the impactor before sampling.

TABLE 5.1 HEAT RESISTIVITY OF VARIOUS STAINLESS STEELS (11)

Group	Stainless Steel Type Number	Melting Range (°C)	HEAT RESISTIVITY Intermittent Service (°C)	HEAT RESISTIVITY Continuous Service (°C)
Austentic	201	n.a.	816	843
	301	1399-1421	871	927
	304	1399-1454	871	927
	309	1399-1454	982	1093
	310	1399-1454	1038	1149
	316	1371-1399	871	927
Martensitic	410	1482-1532	816	704
Ferritic	442	1427-1510	1037	982
	446	1398-1510	1177	1093

The schematic of the experimental set up is shown in Figure 5.1. A refrigerating unit was used to cool an antifreeze solution, which in turn cooled a tank of water by a heat exchanger coil. This was used to cool the air downstream of the impactor, before it was sampled by the constant volume flow sampler. The same tank of cold water was used to cool the recirculating dilution air.

5.3 Results

The aerosol was sampled upstream and downstream of the impaction stage. To prevent loss of particles by thermophoretic deposition, the sampling tubes were well insulated. The sampled aerosol was mixed with cool dilution air in a 40 liter mixing vessel to reduce its temperature, and then the number concentration was measured by the ROYCO optical particle counter. To characterize the sampling system and ensure that representative number concentrations were obtained, the upstream and downstream number concentrations were measured without the impaction plate in place. This was done at a number of different temperatures and flow rates through the impactor. The results plotted in Figure 5.2 indicate that fairly representative number concentrations are obtained.

Impaction tests were carried out at four different temperatures: 100 ^{o}C, 200 ^{o}, 300 ^{o}C, and 500 ^{o}C. The results are plotted in Figure 5.3, and are compared to the room temperature efficiency-Stokes number characteristic.

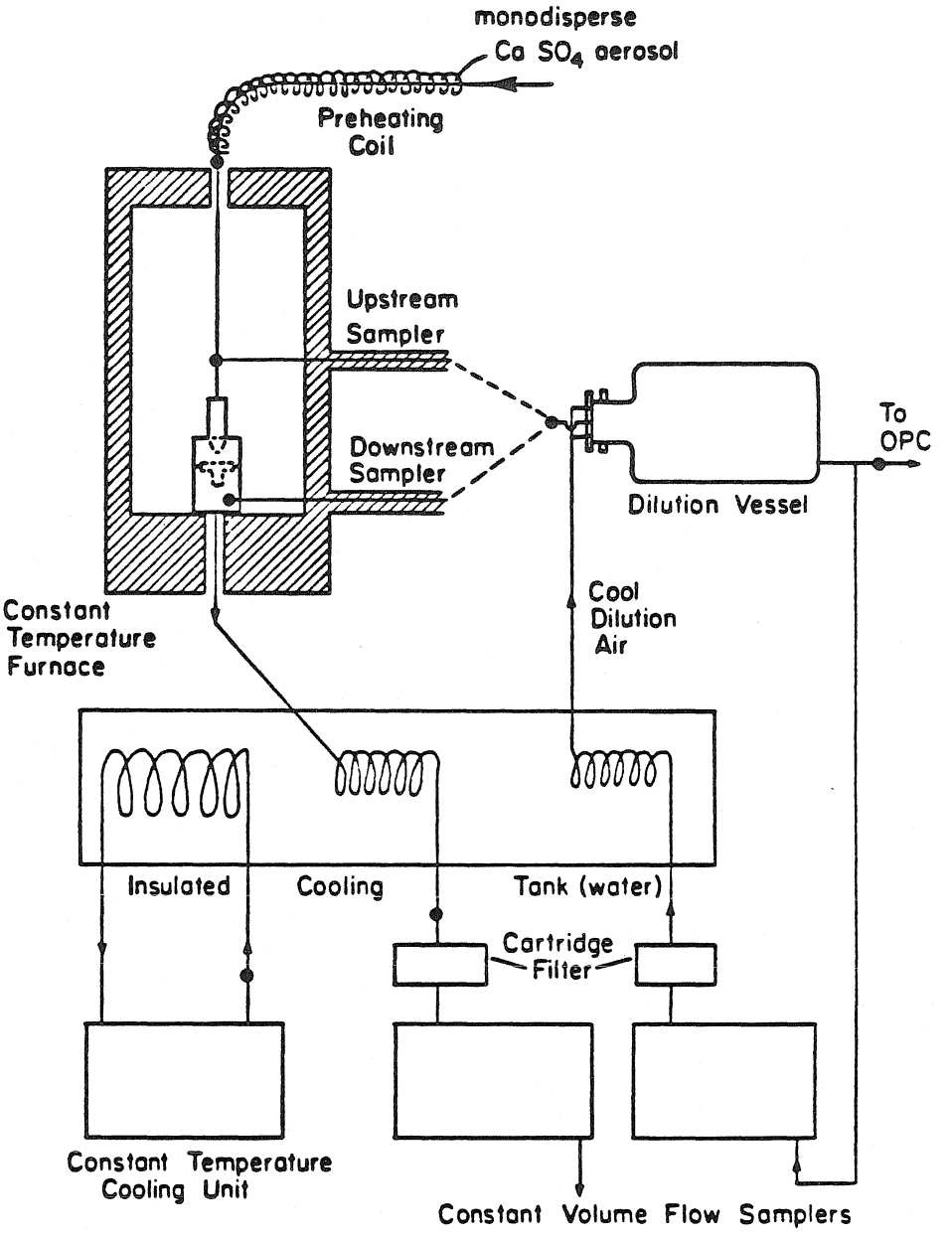

Figure 5.1 Schematic of the experimental set up for the high temperature performance evaluation of the Particle Trap Impactor.

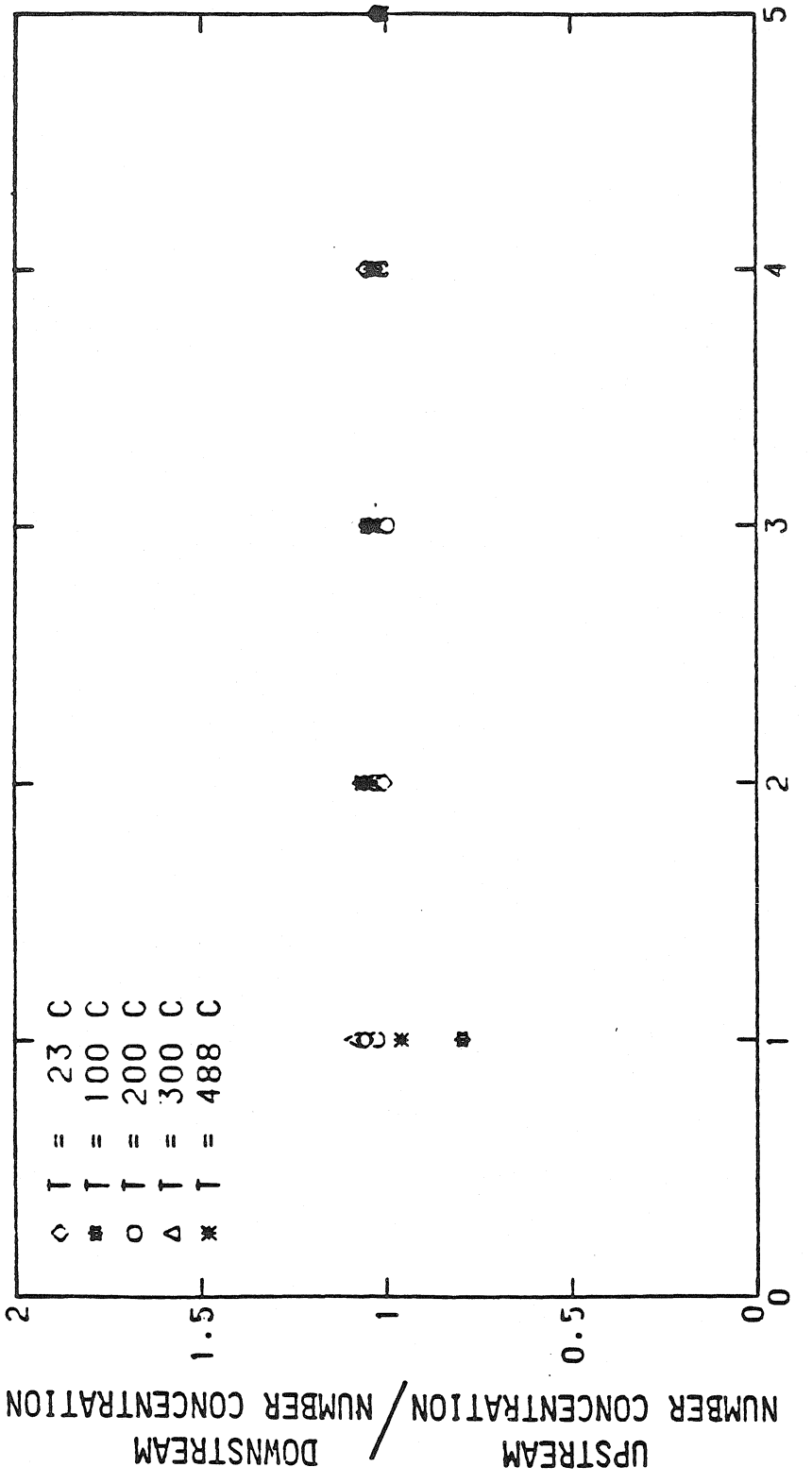

Figure 5.2 Characterizing the sampling system.

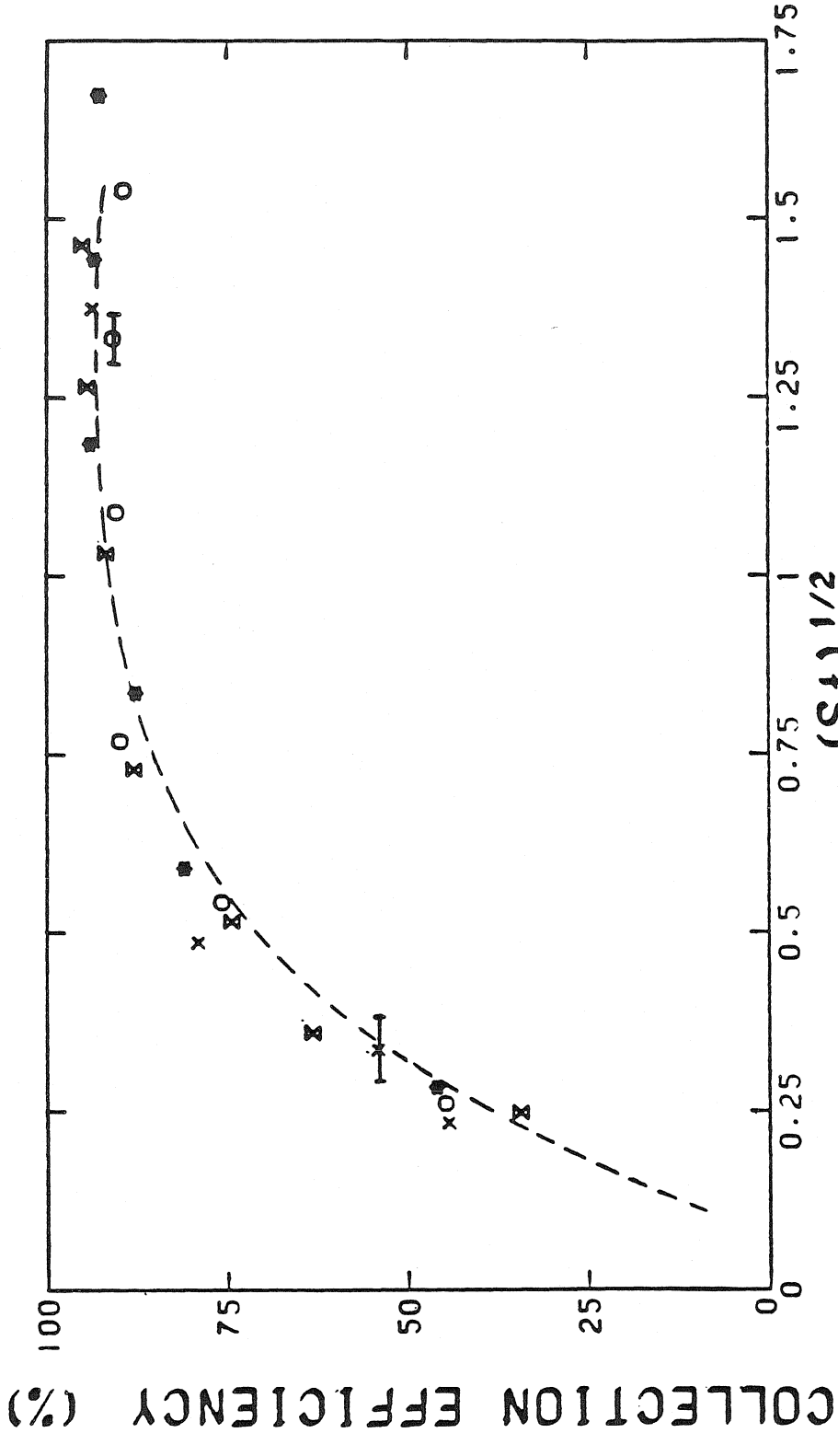

Figure 5.3 Particle Trap Impactor calibration data at different temperatures:
(x) T = 100°C; (o) T = 200°C; (⧗) T = 300°C; (★) T = 500°C.
Dotted curve is the fit to room temperature calibration data.

The performance of the particle trap impactor at high temperatures is found to be good.

5.4 Conclusion

The particle trap impactor is a versatile device, and can be used to obtain very reliable size distribution information. It has many advantages over conventional impactors, some of which were highlighted in the previous chapter. A very good efficiency - Stokes number characteristic is obtained for high temperature operation, which compares well with the room temperature calibration. Due to the use of a cavity as the collection device, large quantities of material could be collected, without re-entrainment being a problem, which would make chemical analysis of the sample rather simple.

References

1) Fissan, H.J.; Bartz, H.: On the sampling of high temperature aerosols, in Aerosols, ed. Liu, B.Y.H.; Pui, D.Y.; Fissan, H.J.; Elsevier, New York (1984).

2) Parker, R.; Calvert, S.; Drehmel, D.; Abbott, J.: J. Aerosol Sci., 12, 297-306 (1981).

3) Marple, V.A.: Development of microorifice impactors; in Aerosols, ed. Liu, B.Y.H.; Pui, D.Y.; Fissan, H.J.; Elsevier, New York (1984).

4) Woffinden, G.J.; Downs, J.L.; Markowski, G.R.; Fegley, M.J.: Environ. Progress, 1, 20-24 (1982).

5) Newton, G.J.; Carpenter, R.L.; Cheng, Y.S.; Barr, E.B.; Yeh, H.C.: J. Colloid Interface Sci., 87, 297-290 (1982).

6) Cheng, Y.S.; Yeh, H.C.: Environ. Sci. Technol., 13, 1392-1396 (1979).

7) Novick, V.J.; Alvarez, J.L.; Appelhans, A.D.: in Aerosols, 143-145, Elsevier, New York (1984).

8) Du, C.J.; Kittleson, D.B.: in Aerosols, 744-748, Elsevier, New York (1984).

9) Carpenter, R.L.; Cheng, Y.S.; Barr, E.B.: in Aerosols, 753-756, Elsevier, New York (1984).

10) Markowski, G.R.; Downs, J.L.; Reese, J.L.: in Aerosols, 757-759, Elsevier, New York (1984).

11) Stainless Steel Fabrication : pp 6-9, Allegheny Ludlum Steel Corporation, Pittsburgh, Pennsylvania (1958).

CHAPTER 6

COAGULATION OF AEROSOLS BY DIFFERENTIAL IMPACTION

6.1 Introduction

Cascade impactors are often used to determine particle size distributions in combustion exhausts where the number concentrations of particles are high, e.g., $10^{14}/m^3$ or greater (1-3). At these concentrations particles may coagulate prior to collection due to differential impaction as large particles cross the trajectories of smaller particles. As they approach the collection substrate large particles may scavenge smaller particles that would normally bypass the stage.

In this chapter the scavenging rate for particles in axisymmetric flow fields is examined. The results are used to determine an upper bound on number concentration for a particular stage of the Marple impactor to keep the fraction of smaller particles scavenged less than about 1%.

6.2 Flow field in the impactor

The flow field of Mercer and Stafford (4) was used for the impingement region of the impactor. Figure 6.1 shows the coordinate system used. The flow is represented as follows:

$$\left.\begin{aligned} u^* &= -x^*/x^*_{in} \\ v^* &= -y^*/2x^*_{in} \end{aligned}\right\} \quad \begin{cases} -x^*_{in} < x^* < 0 \\ y^* < 1+\delta \end{cases}$$

$$u^* = 0 \quad \begin{cases} -x^*_{in} < x^* < 0 \\ y^* > (1+\delta) \end{cases}$$

$$\left.\begin{aligned} u^* &= 1 \\ v^* &= 0 \end{aligned}\right\} \quad -x^*_{in} < x^* < 0 \qquad (6.1)$$

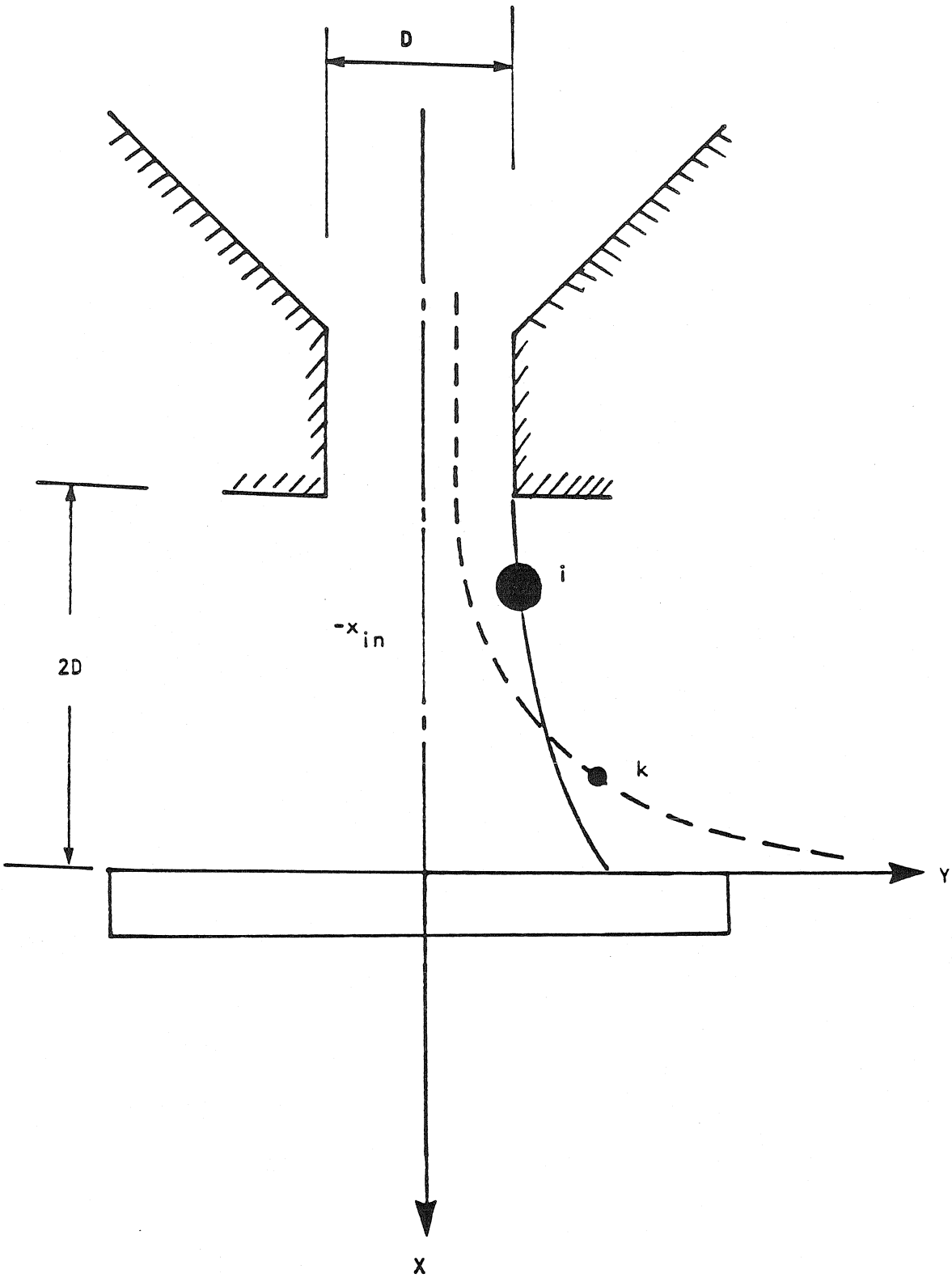

Figure 6.1 Impingement region of impactor showing trajectories of large particle 'i' and small particle 'k'.

where, $u^* = u/U_0$, $v^* = v/U_0$, $x^* = 2x/D$, $y^* = 2y/D$; and U_0 is the jet velocity, D the jet diameter, and $\delta = 2y_{in}/D$.

The force balance equations for the particle in the x and y direction are:

$$\frac{\pi}{6}\rho_p d^3 \frac{d^2x_p}{dt^2} = \frac{3\pi\mu d}{C}\left[u - \frac{dx_p}{dt}\right]$$

$$\frac{\pi}{6}\rho_p d^3 \frac{d^2y_p}{dt^2} = \frac{3\pi\mu d}{C}\left[v - \frac{dy_p}{dt}\right] . \qquad (6.2)$$

Rearranging,

$$\frac{\rho_p C d^2}{18\mu}\frac{d^2x_p}{dt^2} = u - \frac{dx_p}{dt}$$

$$\frac{\rho_p C d}{18\mu}\frac{d^2y_p}{dt^2} = v - \frac{dy_p}{dt} . \qquad (6.3)$$

Multiplying both sides of the equation by $D/2U_0$, and non dimensionalizing with $t^* = 2U_0 t/D$:

$$St \frac{d^2x^*_p}{dt^{*2}} + \frac{dx^*_p}{dt^*} - u^* = 0$$

$$St \frac{d^2y^*_p}{dt^{*2}} + \frac{dy^*_p}{dt^*} - v^* = 0 \qquad (6.4)$$

where, $St = \dfrac{\rho_p C d^2 U_0}{18\,\mu\,(D/2)}$.

The zone of interest is restricted to the impingement region $-x^*_{in} < x^* < 0$ and $y^* < (1 + \delta)$.

The solution of (6.4), using (6.1), is of the form:

$$x_p^* = C_1 e^{m_1 t^*} + C_2 e^{m_2 t^*}$$

$$y_p^* = D_1 e^{n_1 t^*} + D_2 e^{n_2 t^*} \qquad (6.5)$$

where

$$m_1 = \left(-1 + \sqrt{1 - 4\,St/x^*_{in}}\right)/2St$$

$$m_2 = \left(-1 - \sqrt{1 - 4\,St/x^*_{in}}\right)/2St$$

$$n_1 = \left(-1 + \sqrt{1 + 4\,St/2x^*_{in}}\right)/2St$$

$$n_2 = \left(-1 - \sqrt{1 + 4\,St/2x^*_{in}}\right)/2St$$

$$C_1 = \frac{-\left(1 + x^*_{in} m_2\right)}{(m_2 - m_1)}$$

$$C_2 = \frac{1 + x^*_{in} m_1}{m_2 - m_1}$$

$$D_1 = \frac{n_2 y^*_{in}}{n_2 - n_1}$$

$$D_2 = \frac{n_1 y^*_{in}}{n_1 - n_2} \quad .$$

6.3 Scavenging rate in the impingement region of an impactor

Figure 6.2 shows a particle 'i' at location (x_i,y_i) in the impingement region of an impactor stage. The particle velocity $\bar{v}_p$ can be determined from (6.5), and is a function of its location (x_i,y_i) and its Stokes number, $St_i = St(d_i)$. The radius of the sphere of influence is

$$R_{i-k} = (d_i + d_k) / 2 \ . \qquad (6.6)$$

A particle 'k' collides with a particle 'i', when their center to center distance is less than or equal to 'R_{i-k}'.

An approach similar to the computation of coagulation rates in laminar shear flows (5) is used to determine the scavenging rate. The relative velocity of 'k' (w.r.t 'i') normal to the sphere of influence is

$$v_n\,[x,y,St_i,St_k] = (u_k-u_i)\sin\theta - (v_k-v_i)\cos\theta. \qquad (6.7)$$

Consider a large particle 'i' : the flux of 'k' particles into the sphere of influence is

$$F_k = \int_{\theta=0}^{2\pi}\int_{r=0}^{R_{i-k}} N_k v_n h(v_n) r \, dr \, d\theta \qquad (6.8)$$

where,

N_k is the number of 'k' particles per unit volume,

v_n is the relative velocity of 'k' with respect to 'i', normal to the sphere of influence,

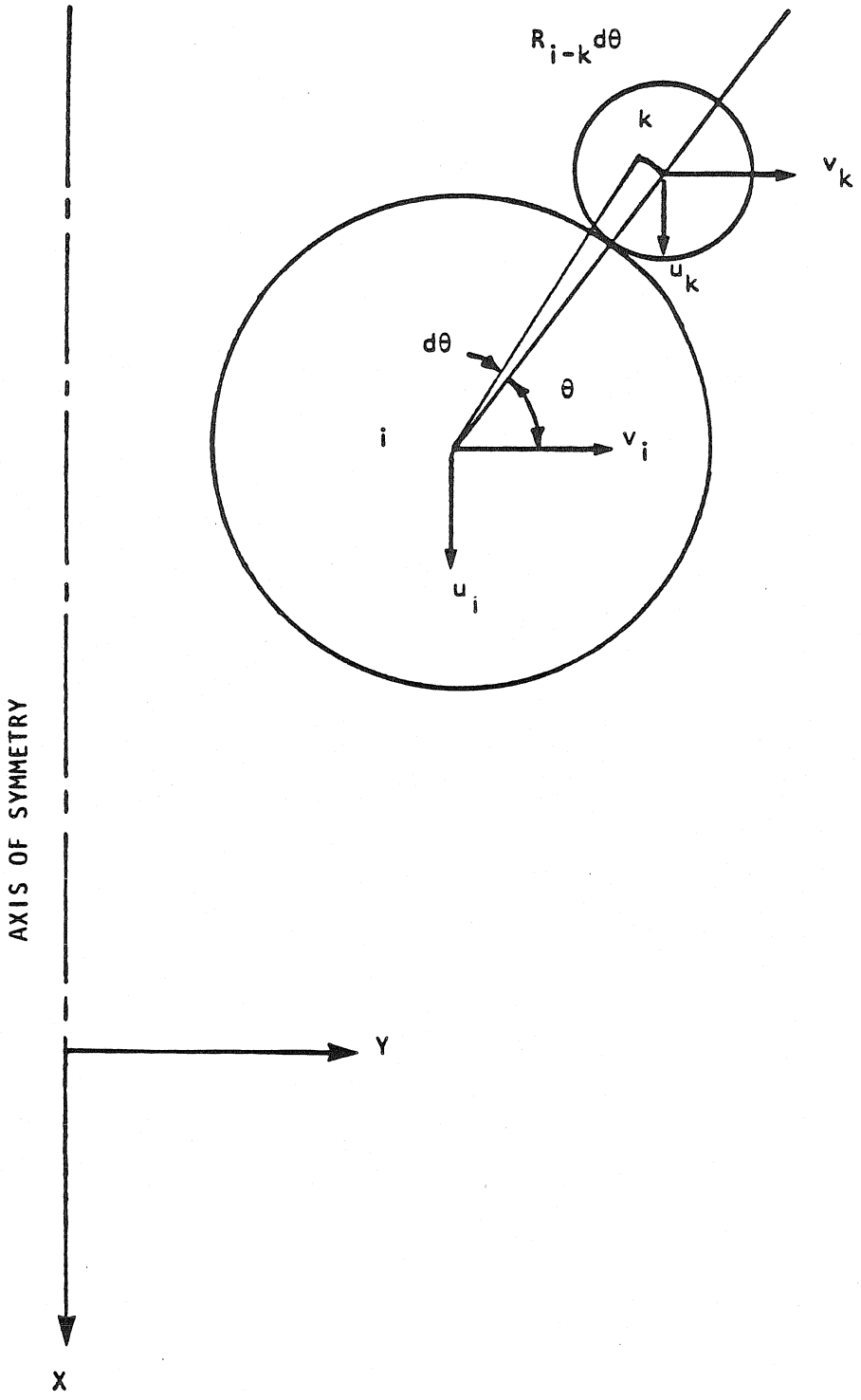

Figure 6.2 Two interacting particles 'i' and 'k' in the flow field.

$h(v_n)$ is the Heaviside function,

$$h(v_n) = 1 \quad \text{for } v_n > 0$$

$$h(v_n) = 0 \quad \text{for } v_n < 0 .$$

Not all 'k' particles approaching the sphere of influence collide with the 'i' particle. The collection efficiency expression developed by Beard and Grover (6) is used, i.e.,

$$Re = \rho v_n d_i/\mu$$

$$G = -0.1007 - 0.358 \ln(Re) + 0.026 (\ln Re)^2$$

$$St_0 = \exp(G)$$

$$St_\Delta = \rho_p d_k^2 v_n C/18\mu d_i$$

$$z = \ln(St_0/St_\Delta)$$

$$H = 0.1465 + 1.302 z - 0.607 z^2 + 0.293 z^3$$

$$y_{co} = (2/\pi) \tan^{-1}(H)$$

$$\eta(St_\Delta) = \eta(x,y,St_i,St_k) = (y_{co} + d_k/d_i)^2/(1 + d_k/d_i)^2 . \qquad (6.9)$$

The collision rate is thus given by

$$\int_{\theta=0}^{2\pi} \int_{r=0}^{R_{i-k}} \eta(St_\Delta) N_k v_n h(v_n)\, r\, dr\, d\theta . \qquad (6.10)$$

A collision frequency function is defined

$$\beta(x,y,St_i,St_k) = \int_0^{2\pi} \int_0^{R_{i-k}} \eta(St_\Delta) v_n(x,y,St_i,St_k) h(v_n)\, r dr\, d\theta. \qquad (6.11)$$

The above is first integrated along a trajectory starting at y_{in}, to obtain the number of collisions with one 'i' particle

$$N_{1-k}(y_{in}) = \int_{-x_{in}}^{0} \frac{N_k\, \beta\, dx}{u_i(St_i)} . \qquad (6.12)$$

The total number of collisions for the particle starting at y_{in} is obtained by multiplying by the volume swept out

$$N_{i-k}\ (y_{in}) = \int_{-x_{in}}^{0}\int^{0} \frac{N_i N_k \beta dx\ 2\pi y(x)\ R_{i-k} dx}{u_i} \quad . \tag{6.13}$$

The total number of collisions in the entire impingement region is obtained by summing over y_{in}, from 0 to D/2, in increments of $2R_{i-k}$:

$$N_{tot} = \sum_{y_{in}=0}^{D/2} \int_{-x_{in}}^{0}\int^{0} \frac{N_i N_k \beta dx\ 2\pi y\ R_{i-k} dx}{u_i} \quad . \tag{6.14}$$

N_k, in reality will be a function of (x,y) due to two effects: Inertial concentration near the plate, and scavenging of particles. The latter can be neglected if the scavenging rate is small, which is desired for unbiased operation of the impactor. For a first-hand estimate, N_k is assumed to be constant in the impingement region. The total number of collisions is

$$N_{tot} = N_i N_k \sum_{y_{in}=0}^{D/2} \int_{-x_{in}}^{0}\int^{0} \frac{\beta dx\ 2\pi y R_{i-k} dx}{u_i} \quad .$$

Non-dimensionalizing with $x^* = 2x/D$, $y^* = 2y/D$, $u^* = u/U_0$, we have

$$N_{tot} = N_i N_k \sum_{y^*_{in}=0}^{1} \int_{x^*_{in}}^{0}\int^{0} \frac{2\pi y^* \beta\ dx^*\ dx^*\ R_{i-k} D^3}{u_i^*\ U_0\ 8} \quad . \tag{6.15}$$

On simplifying,

$$= N_i\ \pi/4\ D^2\ D\ N_k\ \pi/4\ D^2\ D \sum_{y^*_{in}=0}^{1} \int_{x^*_{in}}^{0}\int^{0} \frac{4\beta R_{i-k} y^*\ dx^*\ dx^*}{\pi\ U_0 D^3 u_i^*} \quad . \tag{6.16}$$

The total number of collisions in (6.16) is expressed in terms of a scavenging efficiency

$$\eta_s = \sum_{0}^{1} \int_{x_{in}^*}^{0} \int_{x_{in}^*}^{0} \frac{4\beta R_{i-k} y^* \, dx^* \, dx^*}{\pi D^3 U_0 u_i^*} \quad . \qquad (6.17)$$

6.4 Results

The integral in equation (6.17) is numerically evaluated as a function of the Stokes numbers of particle 'i' and particle 'k', for flow in the impingement region of the Marple impactor. Two factors determine the nature of the η_s - St_k curve: the number of small (k) particles crossing the 'i' particle trajectory increases for decreasing d_k, and the collection efficiency decreases with decreasing d_k. The resultant curve is shown in Figure 6.3.

Using the parameters for the stage under consideration, and the results of Figure 6.3, the maximum number concentrations of 'i' particles to keep scavenging of 'k' particles less than 1% is plotted in Figure 6.4.

6.5 Conclusions

The scavenging rate of particles by differential impaction has been examined for incompressible, continuum regime impactor operation. There are two important factors that have to be considered:

(i) Fraction of fine particles scavenged in the upper stages, i.e., reduction of fines;

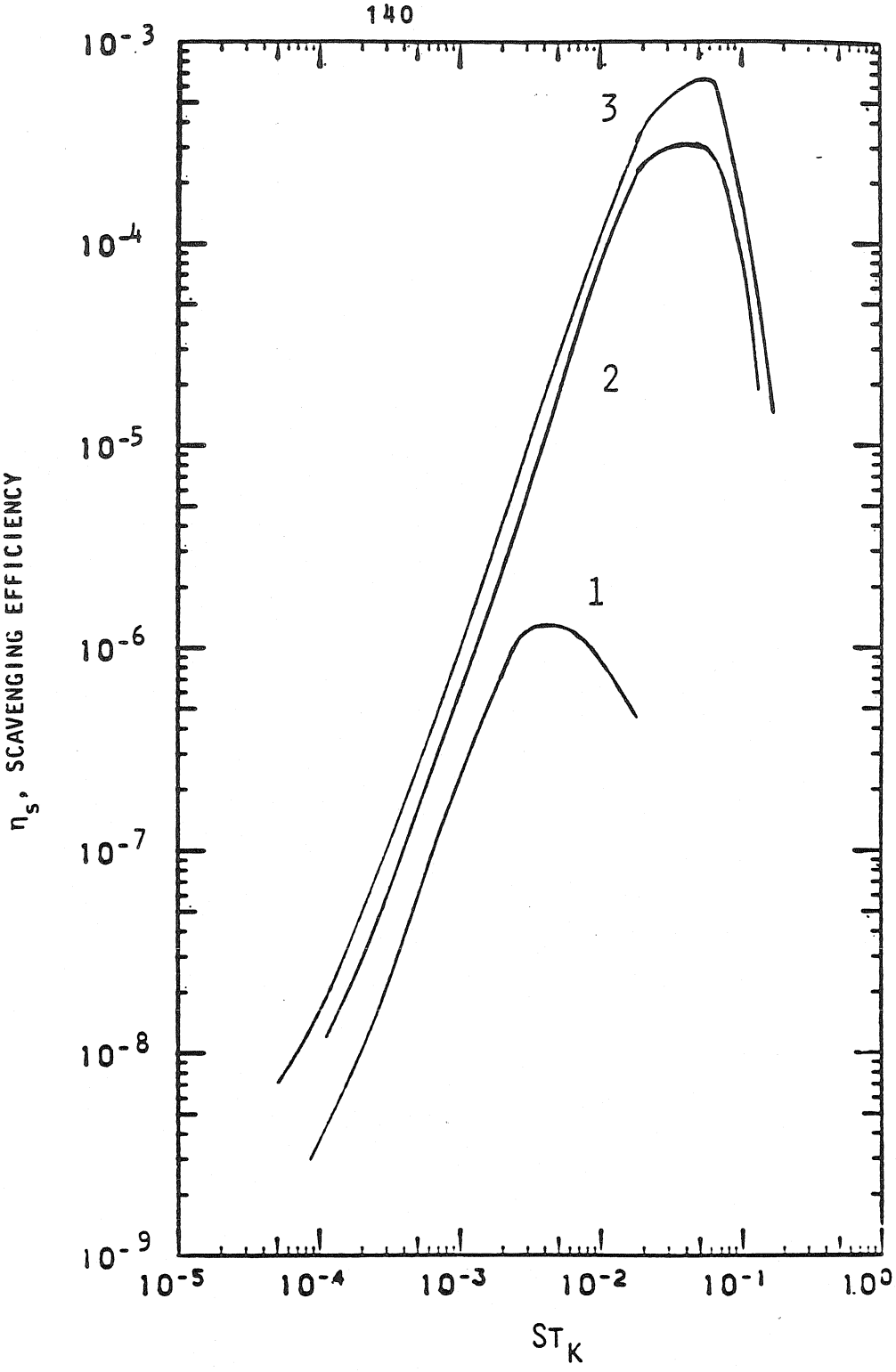

Figure 6.3 Variation of η_s with St_k for a stage of the Marple impactor (D = 4 mm, Q = 3 lpm) for three different values of St_i : (1) $St_i = 2.2\times10^{-2}$; (2) $St_i = 1.7\times10^{-1}$; (3) $St_i = 2.2\times10^{-1}$.

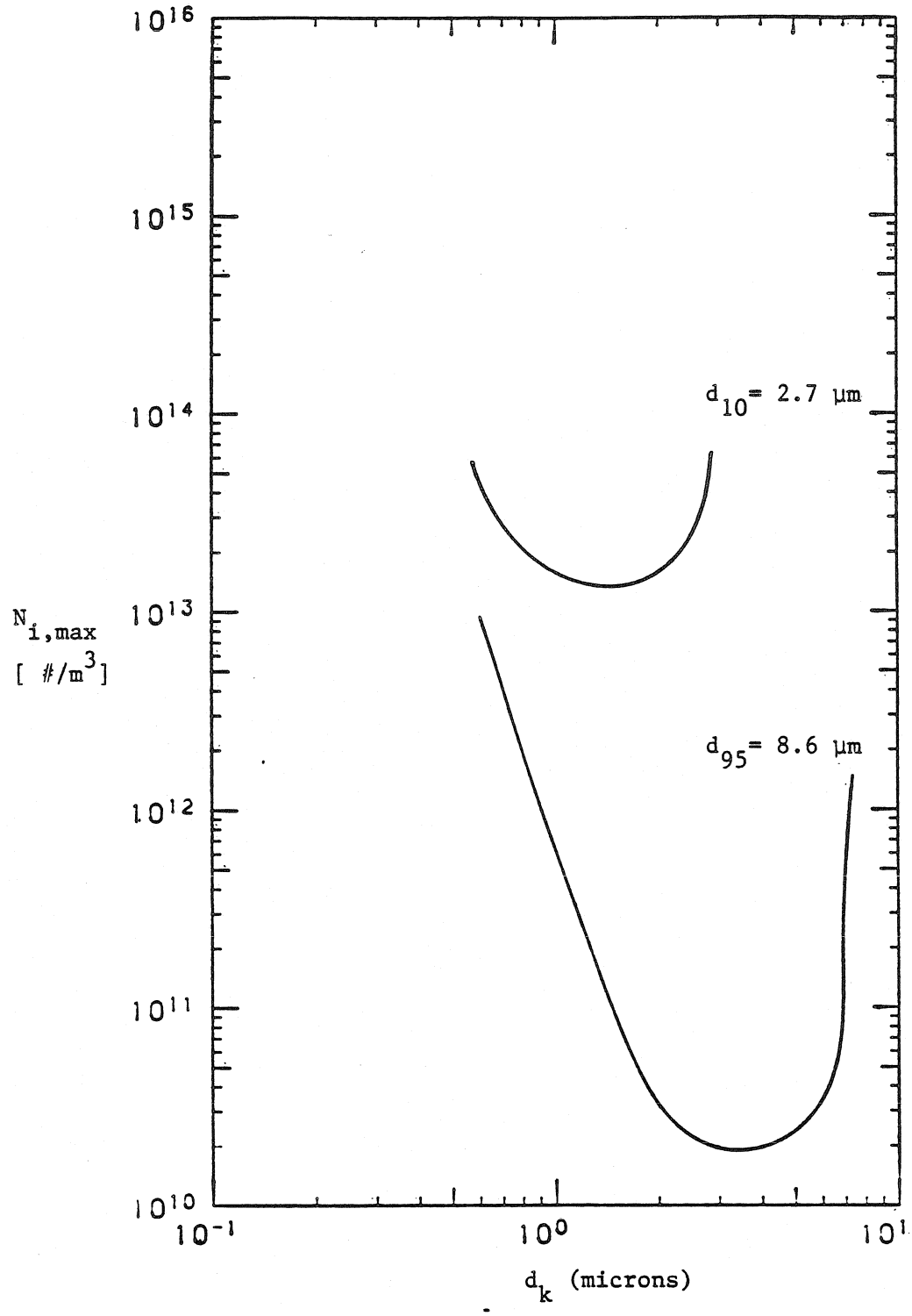

Figure 6.4 Maximum number concentration of 'i' particles so that fraction of 'k' particles scavenged is less than 1%; for the Marple stage, D = 4 mm, Q = 3 lpm. Curves are drawn for d_i corresponding to 10% and 95% efficiency.

(ii) Scavenged particles accounting for a large fraction of the deposited material on the stage of the impactor, i.e., enhancement of coarse particles.

Upperbounds on number concentrations for unbiased sampling have been determined for a particular impactor stage. Actual concentrations in combustion exhausts are as high as 10^{14} #/m^3 (1-3), and this is greater than the upperbounds determined for the stage of the Marple impactor. Thus, dilution maybe be necessary before sampling to obtain unbiased size distributions.

Similar reasoning can be used to develop coagulation rates of aerosols by differential impaction in heat exchangers, gas turbines, and other devices. Fine particles in combustion products may be formed by nucleation or enriched by condensation of vapors, with significant quantities of corrosive species such as sodium or potassium. Appreciable scavenging of these particles would increase the quantity of corrosive species deposited, possibly increasing the corrosion rates of heat exchanger surfaces or gas turbine blades.

Nomenclature

C	Cunningham slip correction factor
d	Particle diameter
D	Jet diameter
h	Heaviside function
N	Number concentration
N_{i-k}	Number of i-k collisions
N_{tot}	Total number of collisions
r	Radial coordinate
R_{i-k}	Radius of sphere of influence
Re	Reynolds number
St	Stokes number
t	Time
u	Velocity in x direction
U_o	Jet velocity
v	Velocity in y direction
x	Coordinate
y	Coordinate

Greek Characters

ρ	Density
θ	Angular coordinate
μ	Viscosity
η	Efficiency

Subscripts/Superscripts

in	Entry condition
n	Normal
p	Particle
s	Scavenging
*	Non-dimensional quantity

References

(1) Carpenter, R.L.; Cheng, Y.S.; Barr, E.B.: in Aerosols, pp. 753-756, eds. Liu, B.Y.H.; Pui, D.Y.H.; Fissan, H.J. (1984)

(2) Markowski, G.R.; Downs, J.L.; Reese, J.L.: in Aerosols, pp. 757-759, eds. Liu, B.Y.H.; Pui, D.Y.H.; Fissan, H.J. (1984)

(3) Kittleson, D.B.: in Aerosols, pp.783-787, eds. Liu, B.Y.H.; Pui, D.Y.H.; Fissan, H.J. (1984)

(4) Mercer, T.T.; Stafford, R.G.: Ann. Occup. Hyg., 12, 41-48 (1969).

(5) Friedlander, S.K.: Smoke, Dust and Haze, John Wiley and Sons: New York (1977).

(6) Beard, K.V.; Grover, S.N.: J. Atmos. Sci., 31, 543-550 (1974).

CHAPTER 7

SUMMARY

7.1 Summary

A number of important questions concerning impactors have been discussed in this work. First, the operation of impactors under compressible flow conditions was discussed. The results of extensive calibration tests indicated that impactors can be operated under high velocity conditions. The same scaling criteria as incompressible impactors are valid, provided the fluid properties are evaluated at the stagnation point condition on the plate. Procedures for predicting the performance of high velocity impactors and designing them were developed.

The virtual impactor was modified to develop a particle trap impactor. The complicated flow control problem was avoided by eliminating the minor flow through the collection cavity. A number of different parameters were varied to arrive at an optimal combination. This impactor was tested at ambient conditions, and the performance was as good as conventional impactors with greased plates. Sampling durations can be much longer for these particle trap impactors without reentrainment being a serious problem. The impactor can be readily operated at high temperatures, and the performance was found to be very good under such conditions.

The distortion of size distributions by aerosol sampling instruments due to particle size changes was considered. The problem arises due to the change of

pressure and temperature in the instrument, and/or the presence of vapor absorbing or desorbing surfaces. Predictions indicated this to be a serious problem for sampling under atmospheric conditions. The biases are most pronounced for small particles at high relative humidities or near the deliquescent point of the aerosol. Controlled experiments demonstrated this effect for a number of instruments like the low pressure impactor, conventional cascade impactors, and optical particle counters. Some of the problems of particle size changes within the instruments could be readily corrected by minor modifications or restriction of operating conditions, while others such as pressure effects in low pressure impactors are inherent to instrument design.

The final part of the work looked at the problem of coagulation of aerosols by differential impaction. The coagulation rate was calculated in the impingement region of the impactor. A critical number concentration can be determined above which a large fraction of small particles are scavenged by bigger ones. This could also be applied to other flow geometries such as in heat exchangers and gas turbines to determine the particulate deposition rate due to differential impaction.

7.2 Applicability

The following list summarizes the applicability of this work:

1) A basis for estimating impactor performance at conditions other than those for which calibration data are available and for designing high-velocity impactors.

2) The possibility of distortion of size distributions due to particle growth or evaporation in a number of commonly used aerosol sampling instruments.

3) The development of a particle trap impactor that can be used to sample aerosols for long durations and/or at high temperatures, or that can be used as a particle collection device in other industrial processes.

4) The computation of coagulation rates of aerosols by differential impaction in different flow geometries (such as impactors, heat exchangers, gas turbines) to give important information about particle scavenging rates.

APPENDIX A

A.1 CORRECTION TERM TO ACCOUNT FOR VAPOR TRANSPORT IN THE TRANSITION REGIME

A number of review papers (1,2) have been written; this section lists the various formulae to compute the correction factor. A comparison of the different expressions is also done for a water vapor-air system.

In the continnum regime, the rate of diffusional condensation is given by:

$$J_c = \frac{D_{ij}(p_\infty - p_d)}{2kdT} \qquad \text{(A.1.1)}$$

and, in the free molecule regime by:

$$J_k = \frac{\alpha(p_\infty - p_d)}{(2\pi m_i kT)^{1/2}} \quad . \qquad \text{(A.1.2)}$$

If the non-continnum effects are assumed to be limited to a region ' Δ ' beyond the droplet surface, then, using flux matching:

$$\frac{J}{J_c} = \frac{\lambda_i \bar{C}_i \beta}{4D_{ij}} \left[\frac{1 + Kn\Delta/\lambda_i}{Kn + Kn^2\Delta/\lambda_i + \bar{C}_i \beta \lambda_i / 4D_{ij}} \right] \quad . \qquad \text{(A.1.3)}$$

Two expressions for Δ are considered:

$$\text{Bradley:} \qquad \Delta = (1+z)^{1/2} \lambda_i \qquad \text{(A.1.4)}$$

$$\text{Wright:} \qquad \Delta = 2D_{ij}/\bar{C}_i \quad . \qquad \text{(A.1.5)}$$

Fuchs and Sutugin obtained the following relation:

$$\frac{J}{J_c} = \frac{1 + Kn_{F-S}}{1 + 1.7104\ Kn_{F-S} + \frac{4}{3} Kn_{F-S}^2} \qquad \text{(A.1.6)}$$

with $Kn_{F-S} = \frac{2\lambda_{F-S}}{d}$; and λ_{F-S} defined as $\frac{3D_{ij}}{\bar{C}_i}$.

A rigorous treatment of the Boltzman's equations led to Sitarski and Nowakowski obtaining a relation, which was later modified by Davies, et al. (1)

$$\frac{J}{J_c} = \frac{1 + \frac{3\beta(1+z)^2 Kn}{4(3+5z)}}{\frac{4(9+10z)\Omega_D}{15\pi(1+z)^2} + Kn\,\frac{\beta(1+2z)}{\pi(3+5z)} + \frac{1}{2z} + \frac{9(1+z)^2 Kn^2}{8(3+5z)}} \cdot \frac{\beta\lambda_i \bar{c}_i}{4D_{ij}} \qquad (A.1.7)$$

Table A.1.1 is a listing of the formulae to evaluate properties of the gas based on the kinetic theory. Table A.1.2 lists the various expressions for the correction factors. Table A.1.3 compares the values of the different correction factors for a water vapor-air system. The results indicate there is reasonable agreement amongst the first three formulae; the modified Sitarski equation, though accurate at the continuum regime limit, does not converge to the right limit in the free molecule regime.

TABLE A.1.1 PROPERTIES OF A VAPOR-GAS MIXTURE (KINETIC THEORY OF GASES)

1) Mean Free Path

$$\lambda_{VAPOR} = \lambda_i = \frac{1}{\sqrt{2}\, n_i\, \pi\sigma_{ii}^2 + (\sqrt{1+z})\, n_j\, \pi\sigma_{ij}^2}$$

$$\lambda_{GAS} = \lambda_j = \frac{1}{\sqrt{2}\, n_j\, \pi\sigma_{jj}^2 + (\sqrt{1+z^{-1}})\, n_i\, \pi\sigma_{ij}^2}$$

where,

$$n_i = \frac{P_i}{kT} \quad , \quad n_j = \frac{P_j}{kT}$$

$$\sigma_{ij} = (\sigma_i + \sigma_j)/2 \; ; \quad z = m_i/m_j$$

2) Kinetic Velocity

$$\bar{c}_i = \left(\frac{8kT}{\pi m_i}\right)^{1/2}$$

3) Diffusion Coefficient

$$D_{ij} = \frac{1.86 \times 10^{-7}}{\sigma_{ij}^2 \Omega_D P} \sqrt{T^3\left(\frac{1}{M_i} + \frac{1}{M_j}\right)} \qquad [m^2/sec]$$

TABLE A.1.2 CORRECTION FACTORS (= J/J_c)

1) BRADLEY

$$\frac{J}{J_c} = \frac{\lambda_i \bar{C}_i \beta}{4D_{ij}} \left[\frac{1 + Kn\Delta/\lambda_i}{Kn + Kn^2\Delta/\lambda_i + \bar{C}_i \beta \lambda_i / 4D_{ij}} \right]$$

$$Kn = \frac{2\lambda i}{d} \qquad \Delta = (1+z)^{1/2} \lambda_i$$

2) WRIGHT

$$\frac{J}{J_c} = \frac{\lambda_i \bar{C}_i \beta}{4D_{ij}} \left[\frac{1 + Kn\Delta/\lambda_i}{Kn + Kn^2\Delta/\lambda_i + \bar{C}_i \beta \lambda_i / 4D_{ij}} \right]$$

$$Kn = \frac{2\lambda i}{d} \qquad \Delta = 2D_{ij}/\bar{C}_i$$

3) FUCHS - SUTUGIN

$$\frac{J}{J_c} = \frac{1 + Kn_{F-S}}{1 + 1.7104\ Kn_{F-S} + \frac{4}{3} Kn^2_{F-S}}$$

with $Kn_{F-S} = \frac{2\lambda_{F-S}}{d}$; and λ_{F-S} defined as $\frac{3D_{ij}}{\bar{C}_i}$

4) MODIFIED SITARSKI EQUATION

$$\frac{J}{J_c} = \frac{1 + \frac{3\beta(1+z)^2 Kn}{4(3+5z)}}{\frac{4(9+10z)\Omega_D}{15\pi(1+z)^2} + Kn\,\frac{\beta(1+2z)}{\pi(3+5z)} + \frac{1}{2z} + \frac{9(1+z)^2 Kn^2}{8(3+5z)}} \cdot \frac{\beta\lambda_i \bar{c}_i}{4D_{ij}}$$

TABLE A.1.3 COMPARISON OF CORRECTION FACTORS

Water Vapor - Air System P_{vap} = 0.03 atm
P = 1.0 atm, T = 298 °K

Knudsen # (Kinetic theory)	Knudsen # (F-S)	<----------J/J_c----------> Bradley	Wright	F-S	Davies
0.010	0.0175	0.9894	0.9884	0.9876	0.9977
0.020	0.0349	0.9787	0.9767	0.9751	0.9865
0.050	0.0873	0.9464	0.9421	0.9378	0.9535
0.100	0.1747	0.8929	0.8861	0.8770	0.9007
0.200	0.3493	0.7919	0.7832	0.7666	0.8043
0.500	0.8734	0.5632	0.5566	0.5337	0.5832
1.000	1.7467	0.3612	0.3583	0.3410	0.3720
2.000	3.4935	0.2024	0.2017	0.1933	0.1965
5.000	8.7336	0.0849	0.0848	0.0828	0.0719
10.000	17.4673	0.0428	0.0428	0.0422	0.0330
Knudsen # (Kinetic theory)	Knudsen # (F-S)	<----------J/J_k----------> Bradley	Wright	F-S	Davies
0.010	0.0175	0.0230	0.0230	0.0230	0.0232
0.020	0.0349	0.0456	0.0455	0.0454	0.0459
0.050	0.0873	0.1102	0.1097	0.1092	0.1110
0.100	0.1747	0.2080	0.2064	0.2043	0.2098
0.200	0.3493	0.3688	0.3648	0.3571	0.3747
0.500	0.8734	0.6559	0.6482	0.6215	0.6791
1.000	1.7467	0.8411	0.8345	0.7943	0.8665
2.000	3.4935	0.9429	0.9394	0.9005	0.9152
5.000	8.7336	0.9885	0.9876	0.9637	0.8370
10.000	17.4673	0.9969	0.9966	0.9829	0.7685

Nomenclature

c	Kinetic velocity
d_p	Particle diameter
D_{ij}	Binary diffusion coefficient
k	Boltzmann Constant
Kn	Knudsen number
J	Rate of vapor transport
m	Molecular mass
M	Molecular weight
P	Pressure
T	Temperature
z	Ratio of molecular masses

Greek Characters

α	Evaporation coefficient
β	Parameter $[= \alpha/(2-\alpha)]$
Δ	Position at which fluxes are matched
λ	Mean free path
Ω_D	Collision integral for mass diffusion

References

1) Davies, E.J.: Aerosol Sci. Technol., 2, 121-144 (1983).

2) Davies, E.J.; Ravindran, P.; Ray, A.K.: Chem. Eng. Commun., 5, 251-268 (1980).

APPENDIX B.1 LISTING OF "CASCAD.FOR"

```
FORTRAN IV     V02.5-9

      c  PROGRAM:   CASCAD.FOR
      c             ----------
      c  Determines the cutoff sizes of the stages of a multistage
      c  impactor
      c
      c  REFERENCE: Biswas, P.; Flagan, R.C.: Environ. Sci. Technol.,
      c             18, 611-616, (1984).
      c  BRIEF DESCRIPTION:
      c
      c     * All the data is read in from the data files and the
      c       the terminal
      c     * Then, all units are changed to S.I. units
      c     * Depending on whether operation is subsonic or sonic
      c         the following is implented
      c    IF SUBSONIC:
      c          . Flow rate is specified, which is first converted to a
      c       mass flow rate, then a dimensionless mass flow rate for
      c       the first stage.
      c       . Subroutine CASDIS is called to determine the discharge
      c       coefficient of stage 1.  Using the value of Cd the isen-
      c       tropic flow rate is determined, and then the pressure
      c       ratio r is computed.  Knowing r for stage 1 the pressure
      c       upstream of stage is computed.  The process is repeated
      c       till the pressure upstream of each stage is determined.
      c
      c    IF SONIC:
      c
      c       Pressure downstream of the impactor is specified.  An
      c       initial guess of the flow rate is made, and calculations
      c       analogous to the subsonic case are carried out.  The
      c       computed downstream pressure is then compared to that
      c       specified; if different, a new flow rate is assumed and
      c       the entire procedure is repeated till a match in the
      c       downstream pressures are obtained. (See LCALCO.FTN)
      c
      c
      c
      c
      c
      c       After the pressures are known upstream of each stage, the
      c       stagnation point pressure is determined by multiplying by
      c       the factor read in from data file CASGEO.DAT
      c
      c       The property values are determined at the stagnation point
      c       conditions, and using the value of critical Stokes number
      c       the cut off sizes are determined.
      c
      c-------------------------------------------------------------------
      c
      c  DATA FILES REQUIRED:
      c
      c       CASPRO.DAT   : Contains the properties of carrier gas under
      c                      standard conditions, properties of the aerosol
      c                      (RHP), and the critical Stokes number
```

```
c
c     CASGEO.DAT    : Geometric data for the multistage impactor
c
c     Current files contain data for air (carrier gas) and the
c     Marple impactor (six stage).  Print out files for further
c     description.
c
c-----------------------------------------------------------------------
c
c  SUBROUTINES REQUIRED:
c
c     SUBROUTINE CASDIS ( MD,LJ,AI,PI,RN,TD,CD,PCD,MACH)
c
c         Computes the discharge coefficient for the impactor
c         under question.
c
c-----------------------------------------------------------------------
c
c
c  LIST OF VARIABLES:
c
c     A(I)  : Area of nozzle in stage i
c     DJ(I) : Jet diameter for stage i, read in mm from data file
c                   CASGEO.DAT
c     DP50(I): Diameter of particles collected with 50 % efficiency
c          in stage i
c     GAM   : Ratio of specific heats for carrier gas.
c     JUMP  : Factor that decides if full routine CASDIS
c         should be executed; or only a part of:
c         JUMP = 0  : exexcute full routine
c         JUMP = 1  : only compute TD (jet temperature)
c     MAC(I): Mach number for nozzle in stage i
c     MD    : Mass flow rate of carrier gas
c     MR(I) : Dimensionless mass flow rate for stage i
c     N     : Total number of stages
c     P(I)  : Pressure upstream of stage i
c     PI    : Inlet pressure (Read in mm of Hg)
c     QO    : Volumetric flow rate in lpm at TQ, PQ
c     R(I)  : Pressure ratio across stage i
c     RGAS  : Gas Constant read in from CASPRO.DAT in SI units
c     RKN50(I): Knudsen number based on d50 for stage i
c     RLAMO : Mean free path of gas at standard conditions
c     RLJ(I): Throat length; read in from CASGEO.DAT in mm
c     RHO   : Density of carrier gas; read in from CASPRO.DAT
c         in SI units
c     RHP   : Density of aerosol particles (read in SI units)
c     RINT  : Factor that determines ratio of upstream pressure
c         to the stagnation pressure
c         X = SLOPE * r + RINT
c     SLOPE : Factor that determines ratio of upstream pressure
c         to stagnation point pressure
c     T(I)  : Temperature upstream of stage i
c     TI    : Inlet temperature (K)
c     TQ    : Temperature at which Q is measured (K)
```

```
c     VISCO : Dynamic viscosity of carrier gas (SI units)
c-------------------------------------------------------------------
c-------------------------------------------------------------------
c*******************************************************************
c-------------------------------------------------------------------
c-------------------------------------------------------------------
C
c
c
      IMPLICIT DOUBLE PRECISION(A-H,L-M,O-Z)
      INTEGER I,J,K,N
      DIMENSION P(10),T(10),DJ(10),RLJ(10),A(10),R(10),MAC(10),
     1  DIS(10),FPR(1000),F(1000),MR(10),DP50(10),RKN50(10),IK(10),
     1  ISON(10)
      COMMON PO,TO,RHO,VISCO,GAM,RGAS
c
c  Assigning devices and input/output files.
c
      OPEN (UNIT = 1, NAME = 'CASPRO.DAT', TYPE = 'OLD')
      OPEN (UNIT = 2, NAME = 'CASGEO.DAT', TYPE = 'OLD')
      OPEN (UNIT = 3, NAME = 'CASOUT.DAT', TYPE = 'NEW')
      CALL ASSIGN (5, 'TT:')
      CALL ASSIGN (6, 'TT:')
c
c  Reading in properties of carrier gas and aerosol particles
c  from CASPRO.DAT
c
      READ(1,10) PO, TO, RHO, VISCO, RLAMO, RGAS, GAM, DUMMY
      READ(1,10) RHP, ST50
10    FORMAT (2D15.8)
c
c  Reading in Impactor geometrical parameters from 'CASGEO.DAT'
c
      READ(2,20) N
20    FORMAT(I3)
      READ(2,30) (DJ(I),RLJ(I), I = 1, N)
30    FORMAT(2D14.5)
      READ(2,40) TI,PI,TATM,PATM
      READ(2,40) TQ,PQ,QO,SONIC
      READ(2,40) SLOPE, RINT, DUM, DUM
40    FORMAT(4D14.5)
c
c  Unit Conversion, to SI units
c
      PATM = PATM * 13600. * 9.81 / 1000.
      PO   = PO   * 13600. * 9.81 / 1000.
      PI   = PI   * 13600. * 9.81 / 1000.
      PQ   = PQ   * 13600. * 9.81 / 1000.
c
        DO 50 J = 1, N
        DJ(J)  = DJ(J)  / 1000.
        RLJ(J) = RLJ(J) / 1000.
50      CONTINUE
c
```

```
      RLAMO = RLAMO / 1.D06
      QM3S  = QO    / 60000.
c
c
c
c  Density at which flow rate is specified
      RHQ = RHO*TO*PQ/(TQ*PO)
c  Density at the inlet
      RHI = RHO*TO*PI/(TI*PO)
c  Check whether operation is subsonic or sonic
c
      IF (SONIC.GT.0.0) GO TO 201
c
      EPSI=0.001
      IGUESS = 0
      JUMP=0
      ISQ=0
      T(1)=TI
      P(1)=PI
      MD=QM3S*RHQ
c
c
      DO 130 I=1,N
      A(I)=3.1416*(DJ(I)**2)/4.
      MR(I)=MD*DSQRT(RAIR*T(I))/(A(I)*P(I))
      IF(MR(I).GE.0.6847.AND.SONIC.LE.0.0) GO TO 60
        GO TO 80
60      WRITE(6,70) I
70      FORMAT(/,' OPERATION MODE SPECIFIED SUBSONIC'/,
     !           ' WHICH IS INCORRECT;'/,
     !           ' UNDER SPECIFIED CONDITIONS, STAGE',I4,/,
     !           'IS CHOKED. RERUN WITH SONIC CONDITIONS')
      STOP
80    IF(I.EQ.1) RN=0.98
        IF(I.NE.1) RN=R(I-1)
        NEWTON=0
90      NEWTON=NEWTON+1
        ISQ=0
        CALL CASDIS (MD,RLJ(I),A(I),P(I),RN,TD,CD,PCD,MACH)
        X1=GAM/(GAM-1.)
        X2=(2./(GAM+1.))**X1
        HOLD=DSQRT(2.*X1*(1.-RN**(1./X1)))
      IF(RN.GT.X2) G=RN**(1./GAM)*HOLD
          IF(RN.LE.X2) G=(2./(GAM+1.))**(1./(GAM-1.))*DSQRT
     !  (2.*GAM/(GAM+1.))
      IF(RN.LE.X2) ISQ=1
      IF(RN.GT.X2) PG=HOLD/(GAM*RN**(1./X1))-1./HOLD
      IF(RN.LE.X2) PG=0.0
      FN=CD*G-MR(I)
        PFN=PCD*G+CD*PG
        IF(DABS(PFN).LT.1.D-20) GO TO 100
      RN1=RN-FN/PFN
100   IF(DABS(RN1-RN).LT.EPSI)GO TO 120
      IF(RN1.GE.1.00.OR.RN1.LT.0.0) RN1=0.9999999
```

```
      RN=RN1
      IF(NEWTON.LT.1000) GO TO 90
      WRITE (6,110)
110   FORMAT(' NEWTON ITERATIONS FOR FINDING R',/,
     !  ' HAS NOT CONVERGED AFTER 1000 ITERATIONS')
      STOP
120   R(I)=RN1
      DIS(I)=CD
      ISON(I)=ISQ
      MAC(I)=MACH
      P(I+1)=P(I)*R(I)
      T(I+1)=T(I)
130   CONTINUE
      WRITE(3,140)(DJ(I),RLJ(I),DIS(I),R(I),MAC(I),ISON(I),I=1,N)
      WRITE(3,150)(P(I),T(I),I=1,N+1)
140   FORMAT(5F12.8,I6)
150   FORMAT(2F15.3)
c
c  This part calculates DP50:THE CUTOFF DIAMETER given ST50
c  and the stagnation point conditions.  The upstream stagn-
c  ation pressures are multiplied by the respective factor
c  to determine the stagnation point condition.
c
c
        DO 160 IJ =1, N
        IF (R(IJ).GE. 0.35) GO TO 160
        X = SLOPE * R(IJ) + RINT
        P(IJ) = X * P(IJ)
160     CONTINUE
c
      DPG=0.1D-06
      EPSI=1.D-08
      DO 190 I=1,N
      VISC=VISC0*(T(I)/T0)**0.7
      JUMP=1
      RLAM=RLAM0*(VISC/VISC0)*(P0/P(I))*DSQRT(T(I)/T0)
c
c  Calling CASDIS only to compute the jet Temperature
c
      CALL CASDIS (MD,RLJ(I),A(I),P(I),R(I),TD,CD,PCD,MACH)
      VJ=MD*P0*TD/(A(I)*R(I)*P(I)*RH0*T0)
      ICOUNT=0
      IF(I.NE.1) DPG=DP50(I-1)
      DP=DPG
170   FDP=DP**2.+2.*RLAM*DP*(1.257+0.4*DEXP(-0.55*DP/RLAM))-18.
     1  *VISC*DJ(I)*ST50/(RHP*VJ)
      DFDP=2.*DP+2.*RLAM*(1.257+0.4*DEXP(-0.55*DP/RLAM))+
     1  2.*RLAM*DP*(0.4*DEXP(-0.55*DP/RLAM))*(-0.55/RLAM)
      DPN=DP-FDP/DFDP
      IF(DABS(DPN-DP).LT.EPSI) GO TO 180
      DP =DPN
      ICOUNT=ICOUNT+1
      IF(ICOUNT.GT.75) GO TO 180
      GO TO 170
```

```
180   DP50(I)=DP*1.D06
      IK(I)=ICOUNT
      RKN50(I)=2.*RLAM/DP
190   CONTINUE
      WRITE(3,200) (DP50(I),RKN50(I),IK(I),I=1,N)
200   FORMAT(2F10.4,I4)
c
c  See program LCALCO.FTN for sonic calculations
201   DUMMY = 0.0
c
      STOP
      END
```

```
c
c
c-----------------------------------------------------------------
c
c     SUBROUTINE: CASDIS
c  This subroutine calculates the discharge coefficient.
c
c  INPUTS TO THE SUBROUTINE:
c     MD:     Mass flow rate
c     LJ:     Throat length (=RLJ(I) in main program)
c     AI:     Area of stage i (= A(I) in main program)
c     PI:     Pressure upstream of stage i (=P(I) in main)
c     RN:     Pressure ratio across stage
c     TD:     Throat temperature (computed in subroutine)
c     CD:     Discharge coefficient
c     PCD:    Derivative of the discharge coefficient wrt REDLJ
c     MACH:   Mach number of the stage (Double Precision)
c     TI:     Upstream Temperature (= T(I) in main program)
c
c  METHODOLOGY:
c
c     From equation (11), EST,18,611-616; we have
c     TD = TI - U1**2/2Cp
c         where Cp = GAM*RGAS/(GAM-1)
c     also, U1 = MD/(RH1*AI)
c          = MD*RGAS*TD/(Pi+1*AI)
c       Combining we have
c     TD = TI - ((MD*RGAS*TD)/(Pi+1*AI))**2 * GAM*RGAS/(GAM-1)
c     rearranging, with Pi+1 = RN*PI
c
c     (MD*RGAS)**2 *(GAM-1)/(2*GAM*RGAS) TD**2 + (AI*PI*RN)**2*TD
c                          - (AI*PI*RN)**2*TI  = 0.
c
c     Solve quadratic in TD
c     where A= (MD*RGAS)**2*(GAM-1)/(2.*GAM*RGAS
c           B = (AI*PI*RN)**2
c           C = -(AI*PI*RN)**2*TI
c     and, as TD is always greater than 0.
c     TD = (DSQRT(B**2-4.*A*C) - B)/ (2. *A)
c
c-----------------------+++++++++++++++-----------------------------
c
0001        SUBROUTINE CASDIS (MD,LJ,AI,PI,RN,TD,CD,PCD,MACH)
0002      IMPLICIT DOUBLE PRECISION(A-H,L-M,O-Z)
0003      INTEGER I,J,K,N
0004      COMMON PO,TI,RHO,VISCO,GAM,RGAS
      c
      c  Computing A, B, C as described above to determine TD, the
      c  thraot area temperature
      c
0005      A = (MD*RGAS)**2 * (GAM-1.) / ( 2. *GAM*RGAS)
0006      B = (AI * PI * RN ) **2
0007      C = -(AI * PI * RN ) **2 * TI
0008      TD=(DSQRT(B**2.-4.*A*C)-B)/(2.* A)
```

```
0009          MACH = MD * RGAS * TD/(RN*PI*AI*DSQRT(GAM*RGAS*TD))
0010            IF(MACH.LE.1.0) GO TO 10
0012            MACH=1.0
0013            TD=(MACH)**2*B*GAM*RAIR*(RHO*TI)**2/(MD*PO)**2
      c
      c  REDLJ = Re * (D/L)
      c
0014  10      REDLJ=(4.*MD/(3.1416*LJ*VISCO))/(TD/TI)**0.7
      c
0015          IF (JUMP.EQ.1) RETURN
      c
      c  CD is the discharge coefficient; following expression
      c  has been obtained by fitting exptl. data from the
      c  paper by Biswas and Flagan.
      c
0017          IF(REDLJ.LT.1000.) CD=0.310*(REDLJ)**0.159
0019          IF(REDLJ.GE.1000.) CD=0.930
      c
      c  PCD is the derivative of the discharge coefficient
      c
0021          IF(REDLJ.LT.1000.) PCD=0.310*0.159*(REDLJ)**(0.159-1.)
0023          IF(REDLJ.GE.1000.) PCD=0.0
0025          RETURN
0026          END
```

CASPRO.DAT

```
760.0, 295.0              !PO(mm Hg),TO(K)
1.177, 1.843D-05          !RHO(kg/m**3),VISCO(kg/m-sec)
0.065, 286.7              !RLAMO(micron),RGAS(S.I.)
1.400, 0.0                !GAM,DUMMY
1000., 0.0875             !RHP(kg/m**3),ST50
```

CASGEO.DAT

```
  6                                  ! Total # of stages
8.000, 8.382                         ! Diameter, throat length (mm) Stage 1
6.000, 5.918                         !   "         "     ; Stage 2
4.000,12.294                         !   "         "     ; Stage 3
2.500,11.354                         !   "         "     ; Stage 4
1.500, 9.779                         !   "         "     ; Stage 5
1.000,10.033                         !   "         "     ; Stage 6
295.0, 745.0, 295.0, 745.0
295.0, 745.0,   3.0, -1.00
2.750, 0.055, 0.0, 0.0
```

APPENDIX B.2 LISTING OF "GROWTH.FOR"

```
c       PROGRAM  GROWTH.FOR
c**********************************************************************
c
c       LIST OF VARIABLES:
c
c
c----------------------------------------------------------------------
c
c  This program calculates the diameter of a humid aerosol particle
c  at the end of a time period (TF).  Inputs to the program are:
c       DP  :    Dry particle diameter (microns)
c       RHI :    Inlet Relative Humidity (fraction)
c       TEMP:    Temperature (C)
c       RH  :    Ambient Relative Humidity at which growth/shrinkage occurs
c       TF  :    Time Duration (secs) for which growth/shrinkage occurs
c
c  Uses Subroutines PSAT.FOR, SIZE.FOR and PSAT.FOR
c
c
c
c----------------------------------------------------------------------
c
        IMPLICIT DOUBLE PRECISION (A-H,M,O-Z)
        INTEGER IFILE(20), OFILE(20)
        DIMENSION DP(50), DIN(50), DFIN(50), RHS(50), RHSIN(50)
        EXTERNAL RHOS, SIGMA
        COMMON A/RK,RNAV,RHOA,RHOW,MWA,MWW,VM,RHDEL,RHC/
c
c  Assigning home terminal or logged on terminal to '5' and '6'
c  TT: on the PDP-11
c
        CALL ASSIGN (5,'TT:')
        CALL ASSIGN (6,'TT:')
c
c  Now assigning the input and output file names
c
        WRITE  (6,10)
10      FORMAT (' READ IN INPUT DATA FILE NAME: ')
        READ   (5,20) IFILE
20      FORMAT ( 20A2)
        WRITE  (6,30)
30      FORMAT (' READ IN OUTPUT FILE NAME: ')
        READ   (5,20) OFILE
c
        OPEN (UNIT = 1, NAME = IFILE, STATUS = 'OLD')
        OPEN (UNIT = 2, NAME = OFILE, STATUS = 'NEW')
c
c  NTOT is the number of diameters
c  NDP  is the number of conditions
c
        READ   (1,40) NTOT, NDP
40      FORMAT ( 2I4)
```

```
c  DP is the dry particle diameter in microns
c
      READ   (1,50) (DP(I), I = 1, NTOT)
50    FORMAT (10D10.4)
c
c  RHI is the inlet relative humidity; TIN the inlet temperature
c  in K, PIN the inlet pressure in mm Hg.
c
      READ   (1,60) RHI, PIN, TIN
60    FORMAT (3D10.5)
c
c
c
c  Do the outer loop NDP times for different relative humidities
c
      DO 140 J = 1, NDP
         READ   (1, 70) P, T, RH, TIME
70       FORMAT (4D10.4)
c
         IF ( RH.LT.RHDEL.AND.RHI.LT.RHDEL) GO TO 120
         IF ( RH.LT.RHC) GO TO 120
c
c  Compute saturation pressure
c
         CALL PSAT ( T, PS)
c
         CON1 = 4. * 1.334D15 * DIFF(T) * VM * PS / (RK*T)
c
      DO 110 I = 1, NTOT
c
c  If the inlet humidity is greater than the deliquescent point;
c  RHDEL; then the inlet particle is wet or in droplet form,
c  and the initial size or the inlet size is compute from the
c  dry particle diameter, DP, using subroutine SIZE.
c
            IF (RHI.LT.RHDEL) GO TO 75
            CALL SIZE (RHI,TIN,DP(I),D0,WT0)
            GO TO 80
c
c  If inlet humidity is less than the deliquescent humidity,RHDEL,
c  then the inlet particle is dry.  But if RH is greater than the
c  the deliquescent point, then a wet size is computed at the
c  deliquescent humidity, RHDEL, and the time reduced by a corr-
c  esponding factor, CTIM, required to transport the amount of
c  water to saturate the dry particle.
c
75          CALL KNFS ( DP(I), P, T, RKNFS)
            CORR = (1. + RKNFS)/(1. + 1.71*RKNFS + 1.333*
     !                 RKNFS**2)
            CALL SIZE ( RHDEL, T, DP(I), D0, WT)
c
c  If the initial humidity is less than the RHDEL, but the final
c  relative humidity greater than RHDEL, then compute time reqd.
c  to form droplet at size in equilibrium with RHDEL by determin-
c  ing time by using vapor transport rate to RHD = 0.
```

```
                CTIM = (DO-DP(I))*DP(I)/(CON1*CORR*(RHDEL-0.))
                IF (CTIM.GE.TIME) GO TO 120
                TFS = TIME -CTIM
80              TIC = 0.0
                IF (RHI.GE.RHDEL) TFS = TIME
                IF (RHI.GE.RHDEL) DO  = DP(I)
                IF (RHI.LT.RHDEL) RHT = RHDEL
                IF (RHI.GE.RHDEL) RHT = RHI
c
c  Here the inlet diameter is stored in DIN(I) and the inlet density
c  in RHSIN(I).  I varies from 1 to NTOT for each J (1 to NDP).
c
                IF (RHI.GE.RHDEL)  DIN(I)  = DO
                IF (RHI.GE.RHDEL) RHSIN(I) = RHOS(WTO,TIN)
                IF (RHI.LT.RHDEL)  DIN(I)  = DP(I)
                IF (RHI.LT.RHDEL) RHSIN(I) = RHP
c
90              CALL KNFS( DO, P, T, RKNFS)
                CORR = (1. + RKNFS)/(1. + 1.71*RKNFS + 1.333*
     !                  RKNFS**2)
                D1 = DO + DTIM*CON1*(RH-RHT)*CORR/DO
                RNV = PI * (D1*1.D-04)**3 / 6.
                RMO = 1000. * RNA / RNV
                C2  = RMO *MWA
                WT  = (DSQRT(B**2 + 0.4*A*C2)-B)/(2.*A)
                RNM = WT*1000. / ((100.-WT)*MWA)
                AW  = ACT (RNM)
                IF ( AW . LT. 0.0 ) AW = 0.0
                IF ( AW . GT. 1.0 ) AW = 1.0
                RHT = AW * DEXP(4.*SIGMA(WT,T)*VM/(RK*(D1*1.0D-04)*T)
c
                TIC = TIC + DTIM
                IF ( TIC.GT.TFS ) GO TO 100
                DO = D1
                GO TO 90
100             DFIN (I) = D1
                RHS  (I) = RHOS(WT,T)
                GO TO 110
c
c Following is done if the particles are dry
c
120             DUM = 0.0
                DFIN(I) = DP(I)
                RHS (I) = RHP(I)
c
110             CONTINUE
c
c  Storing the results for one value of NDP in the output file
```

```
c
      WRITE(2,130) NDP, RHI, RH, P, T, TIME
130   FORMAT(//, ' CONDITION',I4,/,
     !           ' INLET  RELATIVE  HUMIDITY : ',D10.3,/,
     !           ' AMBIENT RELATIVE HUMIDITY : ',D10.3,/,
     !           ' AMBIENT PRESSURE (mm Hg.) : ',D10.3,/,
     !           ' AMBIENT TEMPERATURE       : ',D10.3,/,
     !           ' TIME FOR GROWTH (secs)    : ',D10.3)
      WRITE(2,133)
133   FORMAT(///,'    DP          DIN          RHSIN       DFIN
     !    RHS',//)
      WRITE(2,135) (DP(I),DIN(I),RHSIN(I),DFIN(I),RHS(I),I=
     !  1, NTOT)
135   FORMAT (5D15.5)
c
140   CONTINUE
c
c
c
      STOP
      END
c
c This subroutine computes the Knudsen number. Passed from the
c main program are diameter D (microns), Temperature(T) in Kelvin
c The value of pressure is read in. Default value is 1 atm.
      SUBROUTINE KNUDS(D,P,T,RKN)
      IMPLICIT DOUBLE PRECISION (A-H,O-Z)
      RLAMO=0.065
      PO=760.
      TO=298.
      RLAMDA=RLAMO*(PO/P)*(T/TO)**1.2
      RKN=2.*RLAMDA/D
      RETURN
      END
```

```
c  PROGRAM SIZE.FOR
c*****************************************************************
c
c This subroutine calculates the diameter of a
c particle in equilibrium with an environment @ relative
c humidity RH and temperature TEMP (K).  The dry particle
c diamter is DP in meters.
c
c
c       LIST OF VARIABLES:
c
c
c-----------------------------------------------------------------
c
        SUBROUTINE SIZE(RH,TEMP,DP,DF,WT)
        IMPLICIT DOUBLE PRECISION (A-H,M,O-Z)
        EXTERNAL FUNCTION RHOS, SIGMA, ACT, RMT
        COMMON A/RK,RNAV,RHOA,RHOW,MWA,MWW,VM,RHDEL,RHC/
c
c
        PI = 3.14156
c
c  Subroutine PROP is called to transfer variables in
c  Common block A.
c
        IF ( RH.LT.RHDEL) GO TO 1005
c
c
c MA= mass of solute, RNA= moles of solute
c MS= mass of solution, MW= mass of solvent=MS-MA
c
        MA=PI*DP**3*RHOA/6.
        RNA=MA/MWA
c
c
c Actual iteration begins: RM(molality of soln)
c is the parameter that is varied. The droplet diameter
c is computed in two ways: by determining the molarity(RMO)
c of the soln and then using RNA to determine the volume of
c the solution (VOLS) and then the diameter (D1).  The second
c way is to use the equilibrium relation (water vapor pressure
c balance) to determine D2.  If the values match, convergence has
c been obtained.  Otherwise, the mean of D1 and D2 is used to find
c a new molality (RM2) and the iteration is continued.
c
        ICOUNT=0
        DF = 0.622 * RH * DP / (1.-RH)
        SIG=SIGMA(WT,TEMP)
        TOL = 0.1D-09
        GO TO 1003
1000    WT = 100. * RM * MWA / (1000. + RM*MWA)
        RMO = 1000. * RHOS(WT,TEMP) * RM / (1000.+MWA*RM)
        VOLS = RNA / RMO*1000.
        D1=(6. * VOLS / PI)**(1./3.)
```

```
c Calculation of D2
c
c
        AW = ACT(RM)
        IF(AW . GE . 1.00) AW=1.00
        D2=4. * SIG * VM / (RK*TEMP*DLOG(RH/AW))
        IF (DABS(D1-D2).LE.TOL) GO TO 1001
        DF = (D1+D2)/2.
1003    AW2 = RH/ DEXP(4.*SIG*VM/(DF*RK*TEMP))
        IF(AW2.GE.1.00)AW2=1.000
        RM2 = RMT(AW2)
        ICOUNT=ICOUNT+1
        IF (ICOUNT.GE.100) GO TO 1002
        RM=RM2
        GO TO 1000
1001    D1  = D1*1.D04
        D2  = D2*1.D04
        DF  = DF*1.D04
        TOL = TOL*1.D04
        DP  = DP*1.D04
c
        IF (RH.GE.RHDEL) GO TO 1004
1005    DF = DP * 1.D04
        D1 = DP * 1.D04
        D2 = DP * 1.D04
        DP = DP * 1.D04
        TOL=TOL*1.D04
        ICOUNT=0
c
1004    WRITE(6,102) DP,D1,D2,TOL,ICOUNT
102     FORMAT(/,' DP,D1,D2,TOL,ICOUNT:',4D15.4,/,I3)
        RETURN
1002    WRITE(6,103) ICOUNT,D1,D2,TOL
103     FORMAT(/,' FAILURE TO CONVERGE:',I3,3F10.7)
        RETURN
        END
```

```
c
c-----------------------------------------------------------
c-----------------------------------------------------------
c  This is a combination of programs containing the property
c  data and other function subroutines that compute the
c  properties.  Currently, it is set up for ammonium sulfate
c  solution in water.
c
c       LIST OF VARIABLES:
c    MWW    : Molecular Weight of solvent
c    MWA    : Molecular weight of solute
c    RK     : Boltzmann's constant (C.G.S. units)
c    RNAV   : Avogardo number      (  "      "  )
c    RHDEL  : Deliquescent point of ammonium sulfate
c    RHC    : Crystallisation humidity
c    RHOA   : Density of solute
c    RHOW   : Density of solvent
c-----------------------------------------------------------
c
       SUBROUTINE PROP(X)
       IMPLICIT DOUBLE PRECISION(A-H,M,O-Z)
       COMMON A/RK,RNAV,RHOA,RHOW,MWA,MWW,VM,RHDEL,RHC/
c
       RK   = 1.38054D-16
       RNAV = 6.023D23
       RHOA = 1.769
       RHOW = 1.000
       MWA  = 132.14
       MWW  = 18.00
       VM   = MWW / (RHOW*RNAV)
c
       RHDEL = 0.81
       RHC   = 0.35
c
       RETURN
       END
c
c*************************************************************
c
c  This routine computes the density of an ammonium sulfate
c  solution, given the weight percent of ammonium sulfate
c  and the temperature.
c
c       LIST OF VARIABLES:
c
c       A       : Parameter used to compute the density
c       B       : Parameter used to compute the denisty
c       ITEMP   : Integer form of temperature (C)
c       RHOS    : Density of solution in gm/cc
c       TEMP    : Temperature in kelvin
c
c-----------------------------------------------------------
```

```
c
      FUNCTION RHOS ( WT, TEMP )
      ITEMP = (TEMP-273.15)/10.0
      ITEMP = ITEMP + 1
      IF ( ITEMP.LT.1) ITEMP = 1
      IF ( ITEMP.GT.4) GO TO 10
      GO TO(1,2,3,4) ITEMP
1     A = 0.00581
      B = 1.00351
      GO TO 12
2     A = 0.00574
      B = 1.00248
      GO TO 12
3     A = 0.005695
      B = 1.0003656
      GO TO 12
4     A = 0.005665
      B = 0.99746
      GO TO 12
10    WRITE(6,11) ITEMP
11    FORMAT(/, ' SOMETHING IS WRONG!',I4)
      RETURN
12    RHOS = A * WT + B
      RETURN
      END
c
c*********************************************************************
c
c  This computes the surface tension of an ammonium sulfate
c  solution in dynes/cc
c
      FUNCTION SIGMA (WT, TEMP)
      SIGMA = 2.162*WT +0.014
      RETURN
      END
c
c*********************************************************************
c
c  This function computes the activity of an ammonium sulfate
c  solution
      FUNCTION ACT(RM)
      ACT = -0.0381*RM + 1.0011
      RETURN
      END
c
c
c*********************************************************************
c
c  This function computes the molality of the ammonium sulfate
c  solution, given its activity.
      FUNCTION RMT(AW)
      RMT = ( 1.0011 - AW ) / 0.0381
      RETURN
      END
```

APPENDIX B.3 LISTING OF "COAG.FOR"

```
c  PROGRAM  COAG.FOR
c  This program computes the collision rates of two spherical
c  particels in any supplied flow field. Uses the laminar shear
c  model for coagulation of particles.
c
c-------------------------------------------------------------
c     LIST OF SUBROUTINES:
c
c  1)   VELPAR : Computes of x, and y components of particle
c                velocity as a function of time.
c
c  2)   VELLOC : Computes the x, and y components of particle
c           velocity; now as a function of the location of
c           the particle.
c
c  3)   PROPTY : Supplies the properties of the gas and the
c           particle.
c-------------------------------------------------------------
c
c     LIST OF FUNCTION SUBPROGRAMS:
c
c  1)   C(RKN)      :      Cunningham slip correction factor as a
c                  function of the Knudsen no., RKN
c  2)   RLAM(P,TK)  :      Mean free path in carrier gas at pressure
c                  P, and temperature TK
c  3)   RHO (TK,P)  :      Density of carrier gas at pressure P, and
c                  temperature, TK
c  4)   VISC(TK)    :      Viscosity of carrier gas at temperature, TK
c
c-------------------------------------------------------------
c
c     INPUT FILE :  COAG.INP
c
c  The inputs are:
c             DT    : Integration time increment (secs)
c             DELTHE: Integration angle increment (rads)
c             DJ    : Jet diameter (mm)
c                   DPI   : Diameter of particle that is
c                     scavenging particles (microns)
c             DPK:  : Diameter of scavenged particles
c             P     : Pressure (mm Hg.)
c             TK    : Temperature (K)
c             THETA : Total theta (rads == 360 degrees )
c             TMAX  : Maximum time particle 'i' stays in
c                     impingement region ( greater than
c                     the residence time)
c                 UO    : Jet velocity (m/s)
c             XIN   : Inlet position of particle (x coord)
c             YIN   : Inlet position of particle (y coord)
c
c-------------------------------------------------------------
c
c     LIST OF VARIABLES:
c
```

```
c     ABVI   :  Magnitude of velocity of particle 'i'
c          = DSQRT (UPI**2 + VPI**2)
c     ABVK   :  Magnitude of velocity of particle 'k'
c     EFFNCY :  Efficiency of coagulation
c     NRUN   :  Total number of times computation is to be
c          done
c     PAR1   :  Value of inner integral (See Chapter 5b)
c     PARE1  :  Value of inner integral with coagulation
c          efficiency = 1.
c     PAR2   :  Value of total integral (see Chapter 5b)
c     PARE2  :  Value of total integral with coagulation
c          efficiency = 1.
c     PI     :  Constant = 3.1412
c     R      :  Sum of particle radii [ = (DPI+DPK)/2. ]
c     RHP    :  Particle density
c     TMAX   :  Residence time of particle 'i'
c     UDEL   :  = (ABVI - ABVK)
c     UPI    :  x component of velocity of 'i'
c     UPK    :  x component of velocity of 'k'
c     VPI    :  y component of velocity of 'i'
c     VPK    :  y component of velocity of 'k'
c     XPI    :  x coord of location of 'i'
c     XR     :  x coord of location of 'k'
c     YPI    :  y coord of location of 'i'
c     YR     :  y coord of location of 'k'
c
c-----------------------------------------------------------------
c-----------------------------------------------------------------
C  Main program to find particle collision rates in the impigement
C  region of the impactor
      IMPLICIT DOUBLE PRECISION (A-H,O-Z)
      COMMON /A/ P, TK
      COMMON /B/ PI, RHP
      EXTERNAL C, RHO, VISC, RLAM
c
c
      CALL ASSIGN (1, 'COAG.INP')
      CALL ASSIGN (2, 'COAG.OUT')
      CALL ASSIGN (6,'TT:')
c
c  NRUN = number of times the do loop is executed
c
      READ (1,90) NRUN
90    FORMAT(I3)
c
c
c  Now reading in the input parameters
c  These are not varied in the DO loop
c
      READ (1,95)  UO, XIN, DJ
      READ (1,95)   P, TK, TMAX
      READ (1,95)  DT, DELTHE, THETA
95    FORMAT (3D20.5)
c
```

```
c  Convert all units to S.I.
c
      XIN = XIN / 1000.
      DJ  = DJ / 1000.
      P   = P * 13600. * 9.81 / 1000.
C
      DO 1000 IRUN = 1, NRUN
c
c  inputs that can be varied
c
      READ (1,100) DPI, DPK, YIN
100   FORMAT (3D20.5)
c
      CALL PROPTY (DUMMY)
c
c  Convert all units to S.I.
      YIN = YIN / 1000.
      DPI = DPI * 1.0D-06
      DPK = DPK * 1.0D-06
c
c
      XIN=DJ
      R  = (DPI + DPK)/2.0
c
c  Residence of particle 'i' is input to some high enough value
c  The integration is continued only till the scavenging particle
c  is in the impaction zone. A check is made before incrementing the
c  time.
c
      WRITE(2,101) DJ, UO, YIN, DELTHE, DT, TMAX, DPI, DPK
101   FORMAT(////,' Jet Diameter, DJ   (m)            :',D10.3,/,
     !           ' Jet   Velocity, UO   (m/s)        :',D10.3,/,
     !           ' Inlet y coord;  non dimensional          ',/,
     !           '     wrt jet radius, YIN (=2y/dj)  :',D10.3,/,
     !           ' Angle increment, DELTHE (radians) :',D10.3,/,
     !           ' Time step, DT     (secs)          :',D10.3,/,
     !           ' Residence  Time,  TMAX  (secs)    :',D10.3,/,
     !           ' Scavenging particle size, DPI (m) :',D10.3,/,
     !           ' Scavenged  particle size, DPK (m) :',D10.3,//)
c
c  Printing headings for the output file
      WRITE (2,103)
      WRITE(2,102)
102     FORMAT('    TIME       XPI(mm)       YPI(mm)  ABVI(m/s)',
     !  '     ABVK(m/s)     PARE1       PARE2        PAR1',
     !  '       PAR2(m**3)')
      WRITE (2,103)
103   FORMAT('-----------------------------------------',
     !  '-----------------------------------------',
     !  '------------------')
c
C  Inner Integration Loop
c
c  Initialising PAR2, TIME, ICOUNT, PAR1, and THETA
```

```
c
      PAR2=0.
      TIME=0.
      ICOUNT=0
1     PAR1=0.
      THETA=0.7854
c
c  Calling VELPAR to determine scavenging particle 'i' velocity
c  at time = TIME.
      CALL VELPAR(TIME,U0,DPI,DJ,XIN,YIN,UPI,VPI,XPI,YPI)
c
c
c
      ABVI=DSQRT(UPI**2+VPI**2)
      ICOUNT=ICOUNT+1
c
c  Determining position of particle 'k' (XR,YR) wrt particle 'i'
c
2     XR=XPI+R*DCOS(THETA)
      YR=YPI+R*DSIN(THETA)
c
c  Now calling VELLOC to determine velocity of particle 'k'
c  whose position in the flow field is known
c
      CALL VELLOC(XR, YR, U0, DPK, DJ, XIN, TIME, UPK, VPK)
c
      ABVK=DSQRT(UPK**2+VPK**2)
c
c  Computing the efficiency of coagulation when particles i and k
c  approach each other on a collision path
      UDEL = DABS(ABVI-ABVK)
c  Function subroutine EFFNCY returns value of efficiency
c  For comparison purposes, also computed with efficiency of
c  unity. Called PARE1.
c
c  Only have a flux if net velocity is inwards, towards particle
c  i (see Chapter 6)
c
      APOS = (UPK-UPI)*DSIN(THETA) - (VPK-VPI)*DCOS(THETA)
      IF(APOS.GT.0.0) PAR1=PAR1+APOS*R*DELTHE*2.0*PI*YR
     !                          *EFFNCY(DPI,DPK,UDEL)
      IF(APOS.GT.0.0) PARE1=PARE1+APOS*R*DELTHE*2.*PI*YR
      THETA=THETA+DELTHE
      IF(THETA.LT.6.283) GO TO 2
c
c  Outer Integration Loop
c
      PAR2 = PAR2 + PAR1 *DT
      PARE2=PARE2 + PARE1*DT
c
      XPIP = XPI * 1.0D03
      YPIP = YPI * 1.0D03
c
      WRITE(2,104) TIME,XPIP,YPIP,ABVI,ABVK,PARE1,PARE2,PAR1,PAR2
```

```
104     FORMAT(G10.4,2X,F10.4,2X,F10.4,2X,G10.4,2X,G10.4,2X,
     !  G10.4,2X,G10.4,2X,G10.4,2X,G10.4)
       TIME=TIME+DT
       IF(TIME.GT.TMAX) GO TO 1000
       IF(XPI.GE.0.0.OR.YPI.GE.(DJ/2.+YIN)) GO TO 1000
       GO TO 1
1000   CONTINUE
       STOP
       END
```

```
C
C-----------------------------------------------------------------------
C***********************************************************************
C-----------------------------------------------------------------------
c
c  SUBROUTINE VELPAR
c
c  This subroutine calculates the particle velocity at time 't'
c  after entry into the impaction region. Flow field based on
c  Mercer and Stafford, Ann. Occ. Hyg., Vol 12, pp 41-48 (1969).
c
c
c          c               c
c           c             c
c            c           c
c             c         c
c              c        c
c              c        c
c              c        c
c              c        c
c              c        c
c              c        c          ^
c                                  !
c                <-DJ->            !
c                                  ! 2 (DJ)
c                                  !
c                                  !
c          ccccccccccc!ccccccccccc---V------> y
c                     !
c                     !
c                     !
c                     !
c                     !
c                     !
c                     !
c                     V
c
c                     x
c
c
c-----------------------------------------------------------------------
c
c     LIST OF VARIABLES:
c
c     DJ   :  Jet diameter
c     DP   :  Diameter of particle whose velocity is
c             desired
c     P      :  Pressure
c     T    :  Time at which particle velocity is desired
c     TK     :  Temperature
c     TST    :  non dimensional time
c     UO   :  Jet velocity
c     UP   :  x component of particle velocity
c     UPST   :  non dimensional velocity of particle
c     VP     :  y component of particle velocity
```

```
c     VPST    :  non dimensional y component of velocity
c     XIN :  Inlet coords of particle
c     XP      :  x coordinate of particle
c     XST     :  Nondimensional particle coordinate
c     YIN     :  Inlet coords of particle
c     YP  :  y coordinate of particle
c     YST     :  Nondimensional y coordinate of particle
c     YSTIN   :  Nondimensional inlet coords of particle
c            ( = 2*YIN/DJ)
c-----------------------------------------------------------------
c
c       EQUATIONS:
c
c     ( For details and derivations see Chapter 6 )
c     Relations are for particle motion in the impingement region
c     of the impactor; flow field based on Mercer & Stafford (see
c     Chapter 5b).
c
c     Particle position coordinates as a function of time:
c
c     XST  = C1*DEXP(RM1*TST) + C2*DEXP(RM2*TST)
c     YST  = D1*DEXP(RN1*TST) + D2*DEXP(RN2*TST)
c
c     Can differentiate these with respect to time for obtaining
c     particle velocity expressions
c
c-----------------------------------------------------------------
c
      SUBROUTINE VELPAR(T,U0,DP,DJ,XIN,YIN,UP,VP,XP,YP)
      IMPLICIT DOUBLE PRECISION (A-H,O-Z)
      EXTERNAL VISC,RHO,RLAM
      COMMON /A/ P, TK
      COMMON /B/ PI, RHP
c
c  AID is a subroutine containing the list of common statements
c  to both VELPAR and VELLOC
c
      CALL AID(T,U0,DP,DJ,XIN,TST,RM1,RM2,RN1,RN2,C1,C2)
c
      YSTIN=2.*YIN/DJ
      D1=RN2*YSTIN/(RN2-RN1)
      D2=RN1*YSTIN/(RN1-RN2)
      XST=C1*DEXP(RM1*TST)+C2*DEXP(RM2*TST)
      YST=D1*DEXP(RN1*TST)+D2*DEXP(RN2*TST)
      UPST=C1*RM1*DEXP(RM1*TST)+C2*RM2*DEXP(RM2*TST)
      VPST=D1*RN1*DEXP(RN1*TST)+D2*RN2*DEXP(RN2*TST)
      XP=DJ*XST/2.
      YP=DJ*YST/2.
      UP=U0*UPST
      VP=U0*VPST
      RETURN
      END
```

```
C
C
C**********************************************************************
c
c  SUBROUTINE VELLOC
c
c  This subroutine computes the particle velocity, given the (X,Y)
c  coordinates of the particle.  From the 'X' equation, it iteratively
c  solves for 'T'; and gets 'YIN' using the 'Y' equation.  Then the
c  velocity is found in the same manner as in 'VELPAR'
c
c
c     LIST OF VARIABLES
c
c     DJ   :  Jet diameter
c     DP   :  Diameter of particle whose velocity is
c             desired
c     DFTST    :  Value of derivative of iterated expression
c     FTST     :  Value of iterated expression for previous value
c             of TST
c     ICOUNT   :  Iteration number count { max value set to 50 at
c             the present (can be changed); iterations stop
c             after ICOUNT exceeds 50 }
c     P        :  Pressure
c     T    :  Time at which particle velocity is desired
c     TK       :  Temperature
c     TST      :  non dimensional time
c       TSTN     :  Current value of non dimensional time in the
c             Newton iteration loop
c     UO   :  Jet velocity
c     UP   :  x component of particle velocity
c     UPST     :  non dimensional velocity of particle
c     VP       :  y component of particle velocity
c     VPST     :  non dimensional y component of velocity
c     XIN  :  Inlet coords of particle
c     XR       :  x coordinate of particle
c     XST      :  Nondimensional particle coordinate
c     YIN      :  Inlet coords of particle
c     YR   :  y coordinate of particle
c     YST      :  Nondimensional y coordinate of particle
c     YSTIN    :  Nondimensional inlet coords of particle
c             ( = 2*YIN/DJ)
c
c----------------------------------------------------------------------
c
        SUBROUTINE VELLOC( XR, YR, UO, DP, DJ, XIN, T, UP, VP)
      IMPLICIT DOUBLE PRECISION(A-H,O-Z)
      EXTERNAL RHO, VISC, RLAM
      COMMON /A/ P,TK
      COMMON /B/ PI, RHP
c
c  List of common statements in subroutine AID
c
      CALL AID(T,UO,DP,DJ,XIN,TST,RM1,RM2,RN1,RN2,C1,C2)
```

```
c
      XPST=2.*XR/DJ
      YPST=2.*YR/DJ
C  Newton Iteration Loop to find 'TST'
      ICOUNT=0
1     FTST=C1*DEXP(RM1*TST)+C2*DEXP(RM2*TST)-XPST
        DFTST=C1*RM1*DEXP(RM1*TST)+C2*RM2*DEXP(RM2*TST)
      TSTN=TST-FTST/DFTST
      IF(DABS(TSTN-TST).LE.1.D-03) GO TO 3
      ICOUNT=ICOUNT+1
      IF(ICOUNT.GE.50) GO TO 2
      TST=TSTN
      GO TO 1
2     TYPE 100,ICOUNT,TST,TSTN
100   FORMAT(' ICOUNT,TST,TSTN:',I5,2G14.7)
3     YSTIN=YPST*(RN2-RN1)/(RN2*DEXP(RN1*TSTN)-RN1*DEXP(RN2*TSTN))
      D1=RN2*YSTIN/(RN2-RN1)
      D2=RN1*YSTIN/(RN1-RN2)
      UPST=C1*RM1*DEXP(RM1*TSTN)+C2*RM2*DEXP(RM2*TSTN)
      VPST=D1*RN1*DEXP(RN1*TSTN)+D2*RN2*DEXP(RN2*TSTN)
      UP=U0*UPST
      VP=U0*VPST
      RETURN
      END
```

```
C
C
C*********************************************************************
c
c
c  SUBROUTINE AID
c
c  This is the common set of statements called by both 'VELPAR' and
c  'VELLOC'.
c
c
c     LIST OF VARIABLES
c
c     C   :  Slip correction factor (external function)
c     C1  :  Parameters needed to calculate velocity (see VELPAR)
c     C2  :                  -do-
c     DJ  :  Jet diameter
c     DP  :  Particle diameter
c     P   :  Pressure
c     RLAM    :  Mean free path (external function)
c     RM1 :  Parameters to calculate velocity (see VELPAR)
c     RM2 :                      -do-
c     RN1 :                      -do-
c     RN2 :                      -do-
c     T   :  Time
c     TK  :  Temperature
c     TST :  Non dimensional time (= 2*U0*T/DJ)
c     XIN :  Inlet location of particle
c     XSTIN       :  Non dimensional inlet location
c     VISC    :  Viscosity of carrier gas (external function)
c
c---------------------------------------------------------------------
c
      SUBROUTINE AID(T,U0,DP,DJ,XIN,TST,RM1,RM2,RN1,RN2,C1,C2)
      IMPLICIT DOUBLE PRECISION(A-H,O-Z)
      COMMON /A/ P, TK
      COMMON /B/ PI, RHP
      EXTERNAL C, VISC, RLAM
      TST= 2.*T*U0/DJ
      XSTIN=2.*XIN/DJ
      RKN = 2. * RLAM(P,TK) / DP
      A=RHP*C(RKN)*U0*DP**2/(18.*VISC(TK)*(DJ/2.))
      RMH=DSQRT(1.-4.*A/XSTIN)
      RNH=DSQRT(1.+2.*A/XSTIN)
      RM1=(-1.+RMH)/(2.*A)
      RM2=(-1.-RMH)/(2.*A)
      RN1=(-1.+RNH)/(2.*A)
      RN2=(-1.-RNH)/(2.*A)
      C1=(1.+XSTIN*RM2)/(RM1-RM2)
      C2=(1.+XSTIN*RM1)/(RM2-RM1)
      RETURN
      END
```

```
C
C
C*************************************************************************
C
C
C  FUNCTION  C(RKN)
C
c
c This calculates the value of the Cunningham slip correction factor.
c
c
      FUNCTION C(RKN)
      IMPLICIT DOUBLE PRECISION (A-H,O-Z)
      A1=1.257
      A2=0.400
      A3=0.550
      C=1.+RKN*(A1+A2*DEXP(-2.*A3/RKN))
      RETURN
      END
```

```
C
C
C
C*****************************************************************
C
C  FUNCTION EFFNCY
c
c
c  This function computes the efficiency of coagulattion of
c  two spherical particles, which are on a collision path.
c  Reference :  Beard, K.V. and Grover, S.N.: J. Atmos. Sci.,
c               31, 543-550, (1974).
c-----------------------------------------------------------------
c     LIST OF VARIABLES
c
c     EFFNCY      :  Coagulation Efficiency
c     F       :  Parameter = log (Re)
c     RE      :  Reynolds number (based on particle i diameter
c             and difference of velocities
c     RK      :  Stokes number based on particle size k and
c             collector diameter = DPI
c     RKO :  Parameter = a0 + a1*F + a2*F**2
c     YC      :  Parameter
c
c-----------------------------------------------------------------
c
      FUNCTION EFFNCY (DPI, DPK, UDEL)
      IMPLICIT DOUBLE PRECISION (A-H, O-Z)
      EXTERNAL RLAM,VISC,RHO,C
      COMMON /A/ P, TK
      COMMON /B/ PI, RHP
c
      A0 = -0.1007
      A1 = -0.358
      A2 = 0.0261
      B0 = 0.1465
      B1 = 1.302
      B2 = -0.607
      B3 = 0.293
c
      RE  = RHP * UDEL * DPI / VISC(TK)
      F   = DLOG (RE)
      RK0 = DEXP (A0 + A1*F +A2*F**2)
      RKNI = 2. * RLAM (P,TK) / DPK
      RK  = RHP * C(RKNI) * DPK**2 * UDEL/ (18.*VISC(TK)*DPI)
      Z   = DLOG (RK/RK0)
      H   = B0 + B1*Z + B2*Z**2 + B3*Z**3
      YC0 = DATAN (H) * 2. / PI
      IF  ( YC0.LT.0.0 ) YC0 = 0.0
      YC  = YC0 + (DPK/DPI)
      EFFNCY = (YC/(1.+DPK/DPI))**2
      RETURN
      END
```

```
C
C
C
C*****************************************************************
C
C
c  PROGRAM PROP.FOR
c
c  This has the subroutine PROPTY(PI,RHP,DJ,LJ) which
c  passes the values in the parameter list to the main program
c  via a common statement.
c  Also contains the function subprograms RHO, VISC, and RLAM
c  which compute the density of air and its viscosity; and calculates
c  the mean free path respectively.
c
c
      SUBROUTINE PROPTY (X)
      IMPLICIT DOUBLE PRECISION (A-H,O-Z)
      COMMON /B/ PI, RHP
      PI = 3.1412
c
c  Properties of the aerosol; Density = RHP (kg/m**3)
      RHP =  1.0D03
c
c  Nozzle parameters, throat length and diameter
c     LJ =                ! in mm
c     DJ =                ! in mm
c
c  Properties of air; negligible variation with temperature
c  in range of interest of 273 K to 800 K
      GAM = 1.4
      RAIR = 8.3143D03/29.0
      CP   = 1009.0
      RETURN
      END


c
C*****************************************************************
c
c  FUNCTION  RHO
c
c  This computes the density of the carrier gas at any given
c  pressure and temperature
c
c  Function subprogram RHO
      FUNCTION RHO (T,P)
      IMPLICIT DOUBLE PRECISION (A-H,O-Z)
      TREF = 298.0          ! Kelvin
      PREF = 1.0D05         ! N/m**2
      RHREF = 1.177         ! kg/m**3
      RHO = RHREF*(P*TREF)/(T*PREF)
      RETURN
      END
```

```
c
c
c**********************************************************************
c
c  FUNCTION  VISC
c
c  This computes the dynamic viscosity of the carrier gas at any
c  temperature T
c
c  Function subprogram VISC
      FUNCTION VISC (T)
      IMPLICIT DOUBLE PRECISION (A-H,O-Z)
      TREF   = 298.0
      VISREF = 1.843D-05
      VISC   = VISREF * (T/TREF)**0.7
      RETURN
      END
```

```
c
c
c**********************************************************************
c
c  FUNCTION  RLAM
c
c  This computes the mean free path of the carrier gas at any pressure
c  and temperature
c
c  Function subprogram RLAM
      FUNCTION RLAM(P,T)
      IMPLICIT DOUBLE PRECISION (A-H,O-Z)
      PREF  = 1.0D05              ! N/m**2
      TREF  = 298.0               ! Kelvin
      RLAM0 = 0.065D-06           ! Mean free path at TREF, PREF
      RLAM = RLAM0 * (PREF/P) * (T/TREF)**1.2
      RETURN
      END
```